KTH Numerical Analysis
and Computer Science

Department of Numerical Analysis and Computer Science

Evaluation of the Influence of Feature Detectors and Photometric Descriptors in Object Recognition

Fredrik Furesjö and Henrik I. Christensen

TRITA-NA-P0406

NADA is a co-operating departement between the
Royal Institute of Technology and Stockholm University

Fredrik Furesjö and Henrik I. Christensen
Evaluation of the Influence of Feature Detectors and Photometric Descriptors in Object Recognition

Report number: TRITA-NA-P0406
Publication date: June 2004
E-mail of author: {fredrikf, hic}@nada.kth.se

Reports can be ordered from:

Numerical Analysis and Computer Science (NADA)
Royal Institute of Technology (KTH)
SE-100 44 Stockholm
SWEDEN

telefax: +46 8 790 09 30
http://www.nada.kth.se/

Evaluation of the Influence of Feature Detectors and Photometric Descriptors in Object Recognition

Fredrik Furesjö and Henrik I. Christensen
CVAP - Computational Vision and Adaptive Perception
Department of Numerical Analysis and Computer Science
KTH - Royal Institute of Technology
SE-100 44 Stockholm, Sweden

June 29, 2004

Abstract

An evaluation of the influence different interest point detectors in combination with different local photometric descriptors and different matching metrics has on object identification is presented. The evaluation was conducted on the coil-20 database by measuring the ability of the different combinations to represent and identify the different objects. The following issues were explored: over how large part of the view-sphere does different representations generalize and is there any difference in the performance between objects and between different views of an object. We further explore the influence the metric used for matching the descriptors has on the performance. The results are then compared to the performance of two descriptors of different character, shape context and receptive field histograms, on the same data set.

1 Introduction and Overview

Local photometric descriptors computed at interest points have shown great potential for successful object recognition, e.g. (Rao & Ballard 1995) (Schmidt & Mohr 1997) (Lowe 1999*a*). Several similar approaches have been developed with variations in how the different steps are performed, the fundamental steps can be dissected into the steps described in figure 1.

Position(x,y)	Scale	Orientation	Descriptor	Matching
Harris	Max Laplacian	Average Orientation	Jet	SSD Ratio
Extrema in DOG		Peak in Ori. Hist.	SIFT keys	SSD

Figure 1: The different steps that are common for approaches with local photometric descriptors computed at interest points for object recognition and examples of different suggestions

In this work we will investigate wherein the success of these approaches lie by combining different parts of the approaches and comparing the results. Further we want to answer the following questions: How many samples must be taken of an object to properly represent it for recognition from the full view-sphere and are there any views which represent the object better then other views? In addition: Are there any difference in the performance of the different combinations for the different objects? We will then compare the results to two other types of representations: local shape descriptor (Belongie, Malik & Puzicha 2002) and high dimensional receptive field histograms (Linde & Lindeberg 2004).

1.1 Related Work

In (Mikolajczyk & Schmid 2003) an extensive study with Harris-Laplace (Mikolajczyk & Schmid 2001), Difference-of-Gaussians (Lowe 1999*b*), and Harris-Affine (Mikolajczyk 2002) interest point detectors in combination with six different descriptors: normalized pixel patches, SIFT keys (Lowe 1999*b*), Gaussian derivatives as steerable filters(Freeman & Adelson 1991) and differential invariants, a.k.a. "local jets",(Koenderink & van Doorn 1987), complex filters (Schaffalitzky & Zisserman 2002), and moment invariants (Tuytelaars & Gool 2000) is presented. The evaluation was performed on a test set containing images of different scenes and using the different descriptor to index into a database containing 1000 images. Each detector/descriptor pair was tested for image rotation, scale, view-point, and illumination change. Three different metrics was used for matching the different descriptors: Euclidean for SIFT keys, normalized cross-correlation for pixel patches, and Mahalanobis distance for the all others. An evaluation of the repeatability and the information content, measured by the entropy of "local jets", of different interest point detectors was presented in (Schmid, Mohr & Bauckhage 2000). In (Lowe 2004) several evaluations, considering the repeatability respectively the distinctiveness, of the different parameters used for determining the local extrema points of the Difference-of-Gaussian function and the SIFT key descriptor was performed. (Leibe & Schiele 2003) have performed a comparison of color(Swain & Ballard 1991), texture(Schiele & Crowley 2000), local(Belongie et al. 2002) and global(Murase & Nayar 1995) shape features on the task of classifying objects into "basic level" categories. The best overall performance for all categories was achieved with the local contour descriptor, however, it is noteworthy that it was not the best feature for each single category, suggesting a need for a multiple cue approach.

1.2 Interest point detection and Scale Selection

The idea of using 'interest points' for solving the correspondence problem between two images can be traced back to (Moravec 1980), were the minimum of four directional variances, in horizontal, vertical and two diagonals direction, was used as the interest measure. In this context a point is considered 'interesting' if it is a local maximum.

1.2.1 Extremal in a Difference of Gaussian Pyramid

The principal for determining characteristic scale by determining local maximum of some combination of normalized derivatives was proposed in (Crowley & Parker 1989) and explored for different features in (Lindeberg 1998), e.g. the Laplacian. In (Lowe 1999*b*) this approach was adopted to efficiently detect stable point locations in scale space by selecting extremal points in a Difference-of-Gaussian function

$$D(x, y, \sigma) = (G(x, y, k\sigma) - G(x, y, \sigma)) * I(x, y) \tag{1}$$

where $G(x, y, \sigma) = \frac{1}{2\pi\sigma^2} e^{\frac{-(x^2+y^2)}{2*\sigma^2}}$ and $I(x, y)$ is the image. The choice is motivated by the computational efficiency and the similarity to scale-normalized Laplacian of Gaussian, $\sigma^2(L_{xx} + L_{yy})$, which was used by (Lindeberg 1998). In recent work, (Lowe 2004) have determined that a good value for k in equation 1 is $2^{\frac{1}{3}}$. Further (Lowe 2004) suggest to suppress points located on edges with high curvature in only one direction since those points are known to be unstable. It was suggested the ratio of the eigenvalues of the Hessian matrix

$$\mathbf{H} = \begin{bmatrix} D_{xx} & D_{xy} \\ D_{xy} & D_{yy} \end{bmatrix} \tag{2}$$

should be larger then 10. By determining the interpolated maximum of the 3D quadratic function given by the Taylor expansion around an interest point (Brown & Lowe 2002) has shown that this will increase the accuracy in matching.

1.2.2 Harris and Maximum of Difference of Gaussian

The interest point detector (Harris & Stephens 1988) is defined as when the auto-correlation matrix

$$C = \begin{pmatrix} G_x^2 & G_x G_y \\ G_x G_y & G_y^2 \end{pmatrix} \tag{3}$$

,where $G_x = -\frac{x}{2\pi\sigma^4} * exp^{\frac{-(x^2+y^2)}{2*\sigma^2}}$, has two large eigenvalues, thereby locating regions which have large intensity changes in two directions. The scale selection is done by maximizing the Difference-of-Gaussian over scales at the interest point.

1.3 Orientation

After location of scale and position a distinct orientation of each descriptor is assigned to make the descriptors invariant to rotations in the image plane. This can be done by computing the gradient direction at the point. However, there are more robust ways. (Lowe 2004) uses peaks in a low-pass filtered histogram of the gradient direction wighted by the gradient magnitude and a Gaussian-weighted window around each interest point. An alternative is computing an Gaussian- and magnitude-weighted average of the gradient orientation around the point.

1.4 Descriptors

1.4.1 Normalized Pixel Patches

The most straight forward way of describing a local neighborhood around a point is by representing it with the pixel values in a region. To make the descriptor robust against linear intensity transformations, $I'(p) = aI(p)+b$, the pixel patch r can be normalize to $r_{norm} = \frac{1}{\sigma_r}(r - \overline{r})$, where σ_r is the standard deviation and $\overline{r}$ is the mean. For this experiments we used a 11x11 pixel patch creating a 121 dimensional vector sampled at the selected scale and orientation by bilinear interpolation.

1.4.2 Gaussian derivatives

This descriptor is defined by the a vector of Gaussian derivatives steered (Freeman & Adelson 1991) in the assigned orientation and scale of the point. We here omitted the normalization constants for convenience since the discrete kernels were all normalized to one. Here we use a Gaussian derivatives up to the fourth order resulting in a 13 element long feature vector:

$$G_x = -x * exp^{\frac{-(x^2+y^2)}{2*\sigma^2}}$$
$$G_y = -y * exp^{\frac{-(x^2+y^2)}{2*\sigma^2}}$$
$$G_{xx} = (x^2 - \sigma^2) * exp^{\frac{-(x^2+y^2)}{2*\sigma^2}}$$
$$G_{xy} = xy * exp^{\frac{-(x^2+y^2)}{2*\sigma^2}}$$
$$G_{yy} = (y^2 - \sigma^2) * exp^{\frac{-(x^2+y^2)}{2*\sigma^2}}$$
$$G_{xxx} = (-x^3 + 3x\sigma^2) * exp^{\frac{-(x^2+y^2)}{2*\sigma^2}}$$
$$G_{xxy} = (-x^2y + y\sigma^2) * exp^{\frac{-(x^2+y^2)}{2*\sigma^2}}$$
$$G_{xyy} = (-xy^2 + x\sigma^2) * exp^{\frac{-(x^2+y^2)}{2*\sigma^2}}$$
$$G_{yyy} = (-y^3 + 3y\sigma^2) * exp^{\frac{-(x^2+y^2)}{2*\sigma^2}}$$
$$G_{xxxx} = (x^4 - 6x^2\sigma^2 + 3\sigma^4) * exp^{\frac{-(x^2+y^2)}{2*\sigma^2}}$$
$$G_{xxxy} = (x^3y - 3\sigma^2) * exp^{\frac{-(x^2+y^2)}{2*\sigma^2}}$$
$$G_{xxyy} = (x^2y^2 - x^2\sigma^2 - y^2\sigma^2 + \sigma^4) * exp^{\frac{-(x^2+y^2)}{2*\sigma^2}}$$
$$G_{xyyy} = (xy^3 - 3\sigma^2) * exp^{\frac{-(x^2+y^2)}{2*\sigma^2}}$$
$$G_{yyyy} = (y^4 - 6y^2\sigma^2 + 3\sigma^4) * exp^{\frac{-(x^2+y^2)}{2*\sigma^2}}$$

1.4.3 SIFT key

The Scale Invariant Feature Transform is a local photometric descriptor computed at interest points. It was introduced in (Lowe 1999*a*). The descriptor is a histogram of the gradient orientations, sampled over a 4-by-4 grid around the extremal point, with eight orientation bins at each point in the grid, producing a 128 dimensional vector. The orientation is computed relative to the dominant direction around the local extreme point to cancel out effects from image rotation.

1.5 Matching

In this comparative study we use two different matching metrics for all the different features. The first metric is the sum of square differences between two descriptors, d^a and d^b, of the same sort is defined as:

$$\mathbf{SSD}(\mathbf{d^a}, \mathbf{d^b}) = \sum_{i=0}^{n} (d_i^a - d_i^b)^2 \tag{4}$$

The second metric for matching we use, as proposed by (Lowe 2004), is the quotient of the SSD measure of the best match and the second best match.

1.6 Contour matching

The approach used for contour matching here is Shape Context (Belongie et al. 2002) which describes edge points, here found by a Canny edge detector, by their relations to other edge points in a log-polar histogram of the relative coordinates of the other edge point. To find two corresponding points between two shapes the two histograms characterizing the points, h_i and h_j, are matched via the χ_2 measure:

$$C_{i,j} = \frac{1}{2} \sum_{k=1}^{K} \frac{(h_i(k) - h_j(k))^2}{h_i(k) + h_j(k)} \tag{5}$$

1.7 Receptive Field Histograms

Histograms of filter responses were used for object recognition in (Schiele & Crowley 2000), using up to six dimensional histograms of filter responses for Gaussian derivatives and for Laplacian and gradient magnitude. Recently (Linde & Lindeberg 2004) demonstrated better results using higher dimensional histograms with up to 14 dimensions, combining filter responses and color information. To make it feasible to store the histograms a sparse representation of the histograms was used, only storing the non-zero bins. In this experiment a representation of three rotation invariant differentials, the gradient magnitude, the Laplacian, and the determinant of the Hessian computed at three different scales are used, creating a nine dimensional histogram. To match the histograms the χ_2 measure is used.

2 Experiments

The experiments were conducted on the coil-20-unproc database(S. A. Nene & Murase 1996), examples can be seen in figure 2. The database contains images of five objects taken five degrees apart along a small circle of the upper view-sphere, making a total of 72 images of each object. In this experiments we have considered six combinations of detectors/descriptors with two different matching criterion, SSD and ratio of best and second best match, were the ratio threshold was set to four. The six combinations of detector/descriptor were:

- SIFT keys computed at Difference-of-Gaussian local extreme points.
- Jets computed at Difference-of-Gaussian local extreme points.
- Pixel patches computed at Difference-of-Gaussian local extreme points.
- SIFT keys computed at Harris/Difference-of-Gaussian points.
- Jets computed at Harris/Difference-of-Gaussian points.
- Pixel patches computed at Harris/Difference-of-Gaussian points.

The performance of the different combinations of detectors/descriptors was estimated by matching all views of each object against the views of the same object taken from +/- 5-60 degrees, with five degrees intervals. First ROC curves were plotted, using the quotient of the best and second best matching as metric for matching, for different angles of the same object compared to random views of the other objects in the dataset to visualize the performance of all the different combinations of detectors and descriptors to find which feature has the overall best performance for all objects. Next the same measure was done for all objects separately to investigate if there were any difference in performance between the objects. To further visualize the performance on the different objects the average and standard deviation of the number of matches after the object had been turned different degrees was estimated. In order to analyze the influence of the metric, ROC curves using SSD as the metric were also plotted. The threshold for each feature was determined by the break point were the increase of the cumulative sum of matches for false matches became higher than that of the positive matches. Further to find out which view of each object that generalize the best and the worst the degree that the object could be rotated before the matching passes below the level which corresponds to one percent false positives were estimated. Finally the ROC curves for each object using shape context and receptive field histograms were plotted as a reference.

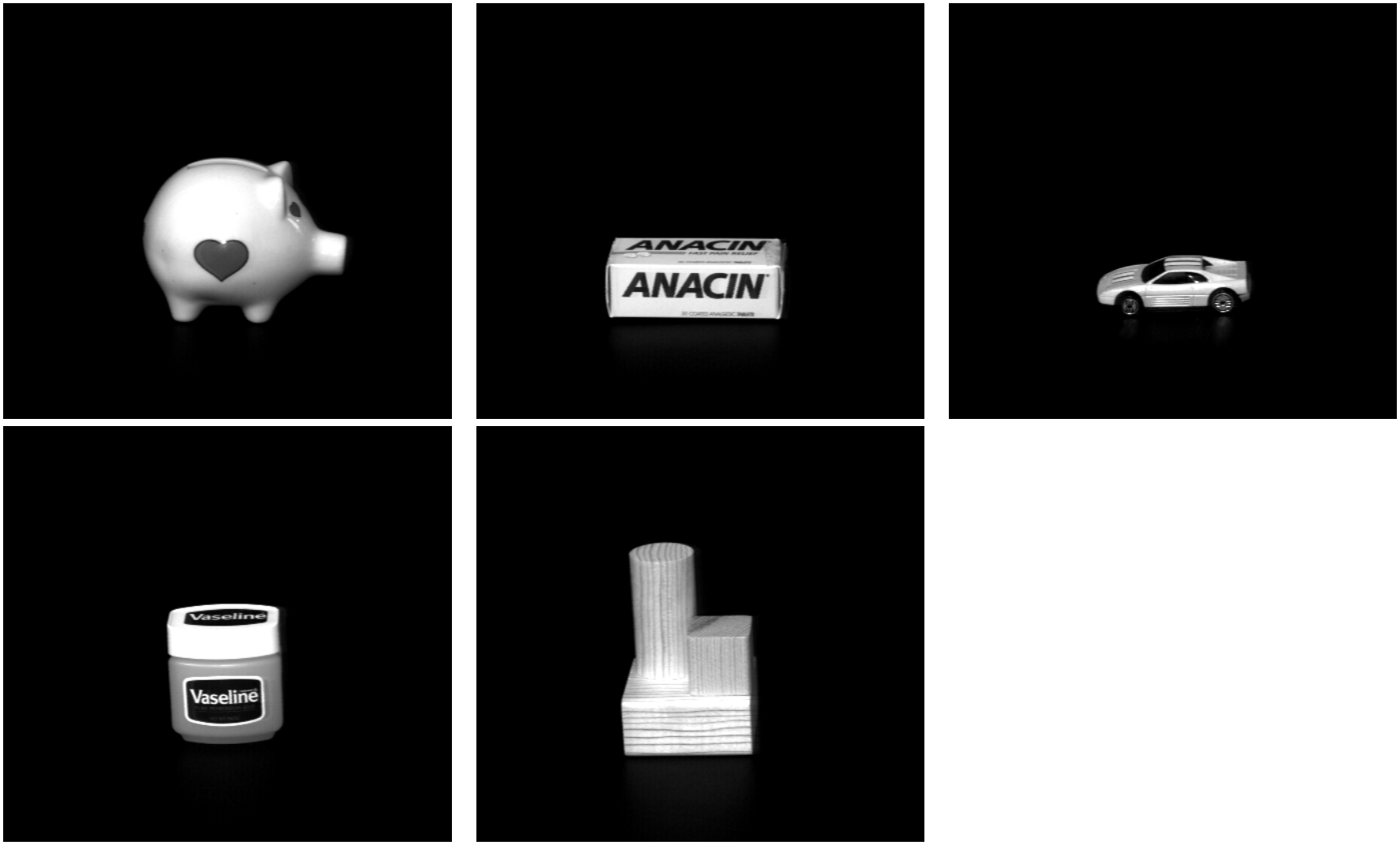

Figure 2: Coil-20 database examples

3 Result

Figures 3 and 4 show the ROC curves across all objects, when a rotation of 25 and 55 degrees, respectively, is performed between the images. The ROC curves are presented for the different detector/descriptor combinations. The figures illustrate that the combination of computing SIFT keys at Difference-of-Gaussian extrema produce the best result for the objects when they have been turned, however, if the rotation is as high as 55 degrees the combination of computing a local feature jet at Difference-of-Gaussian extrema performs slightly better. However, the performance is rather poor for such large rotation and indicates that the objects need to be sampled more densely for reliable detection. The results for all rotation angles, 5-55 degrees, can be found in appendix A, were it can be seen that the detection performance is good for most features until the object have been turned more than 20-25 degree revealing that the appearance of the objects need to be sampled at least every 45 degrees for successful detection.

In figure 5 to 9 the matches of the different combinations of detectors and descriptors for the different objects is shown using the ratio metric. The corresponding ROC curves can be found in the appendix A. The results show that the performance is pretty similar for all objects, with a slightly better performance for objects with many feature points like object 5, with SIFT key and local feature jets computed at Difference-of-Gaussian extrema offering the best results.

The performance with the ratio measurement outperforms the simple SSD metric, which can be seen in figure 10 to 17. Especially for the patch and jet feature descriptors computed at Difference-of-Gaussians the performance with SSD was really poor, this is due to the fact that some extrema are found in the black background due to noise. These features generate that many false positives are found when SSD is used as metric, which is avoided by using the quotient of the best and second best match.

In figure 18 the number of degrees each view can be turned before the number of matches becomes lower than the number that corresponds to one percent false positives. This gives a good indication of over how large portion of the view sphere a representation generalize using DOG/SIFTkey combination and matching with the ratio metric. In figure 19 the views that generalize the best respectively the worst are shown. Not surprisingly the views that contains the least information, fewest interest points, is the ones that performs the worst for object 3 and 4. However it is noteworthy that the views that are usually consider as canonical views for object 2 and 5 performs the worst.

Finally to compare the performance of the approach with local feature point descriptors to other methods, ROC curves were plotted for shape context and for high dimensional receptive field histograms. Both these descriptors show great variation between the objects. Showing great results for objects with not so much texture. Especially receptive field histograms show great generalization over large rotation, in all other cases the local methods show a similar performance or better. The results are presented in figures 121 to 132 in appendix A.

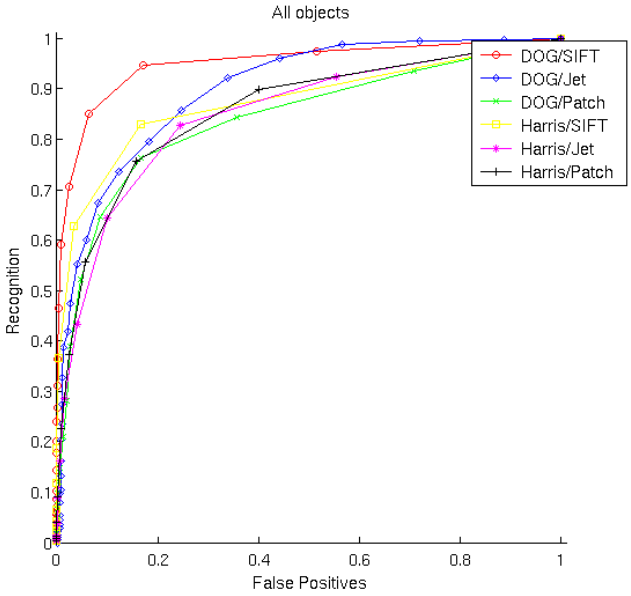

Figure 3: ROC for all objects when the objects has been turned 25 degrees. The ratio between the best and the second best match was used for finding correspondences.

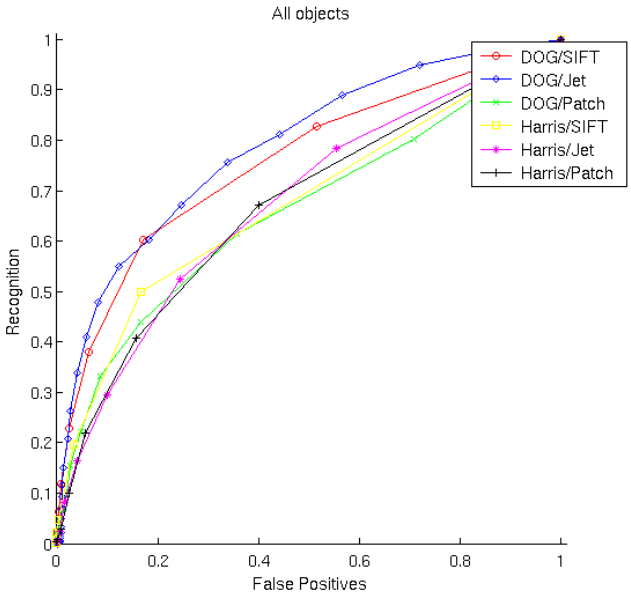

Figure 4: ROC for all objects when the objects has been turned 55 degrees. The ratio between the best and the second best match was used for finding correspondences.

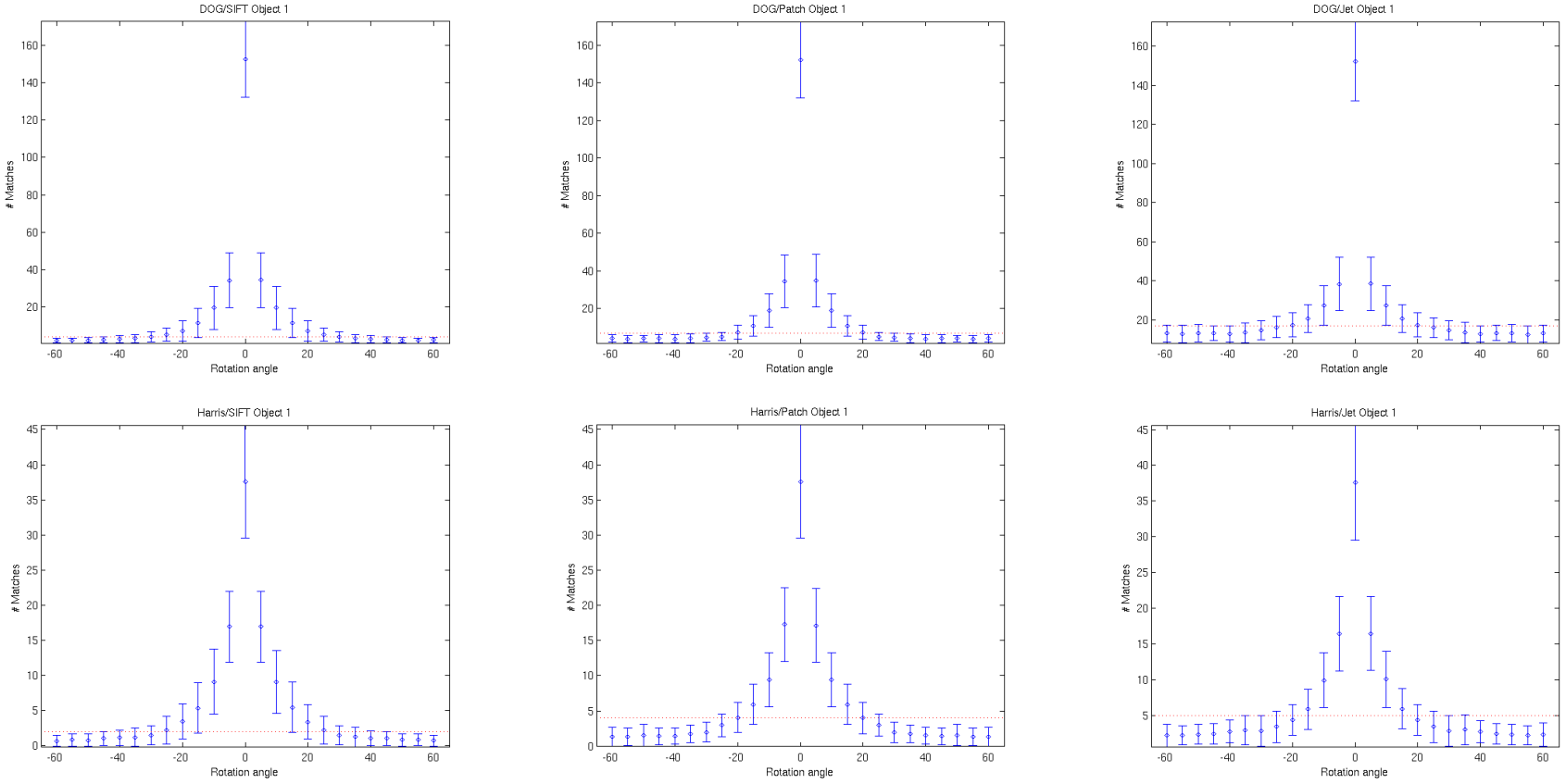

Figure 5: Result for object 1 showing the number of matches, the middle point is the mean and the bars are the standard deviation, for the different combinations of detectors and descriptors. The dotted line shows the limit for one percent false positives.

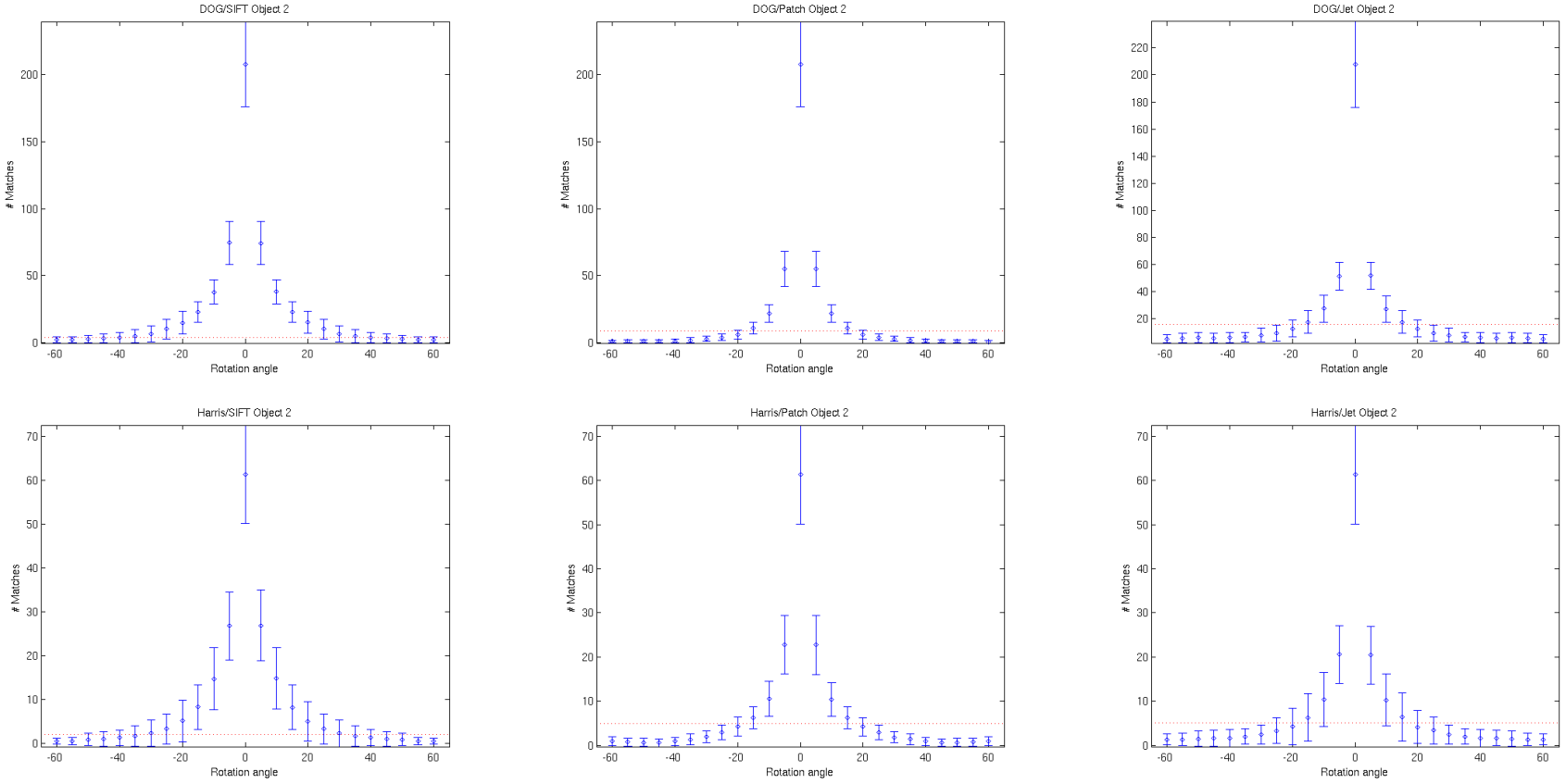

Figure 6: Result for object 2 showing the number of matches, the middle point is the mean and the bars are the standard deviation, for the different combinations of detectors and descriptors. The dotted line shows the limit for one percent false positives.

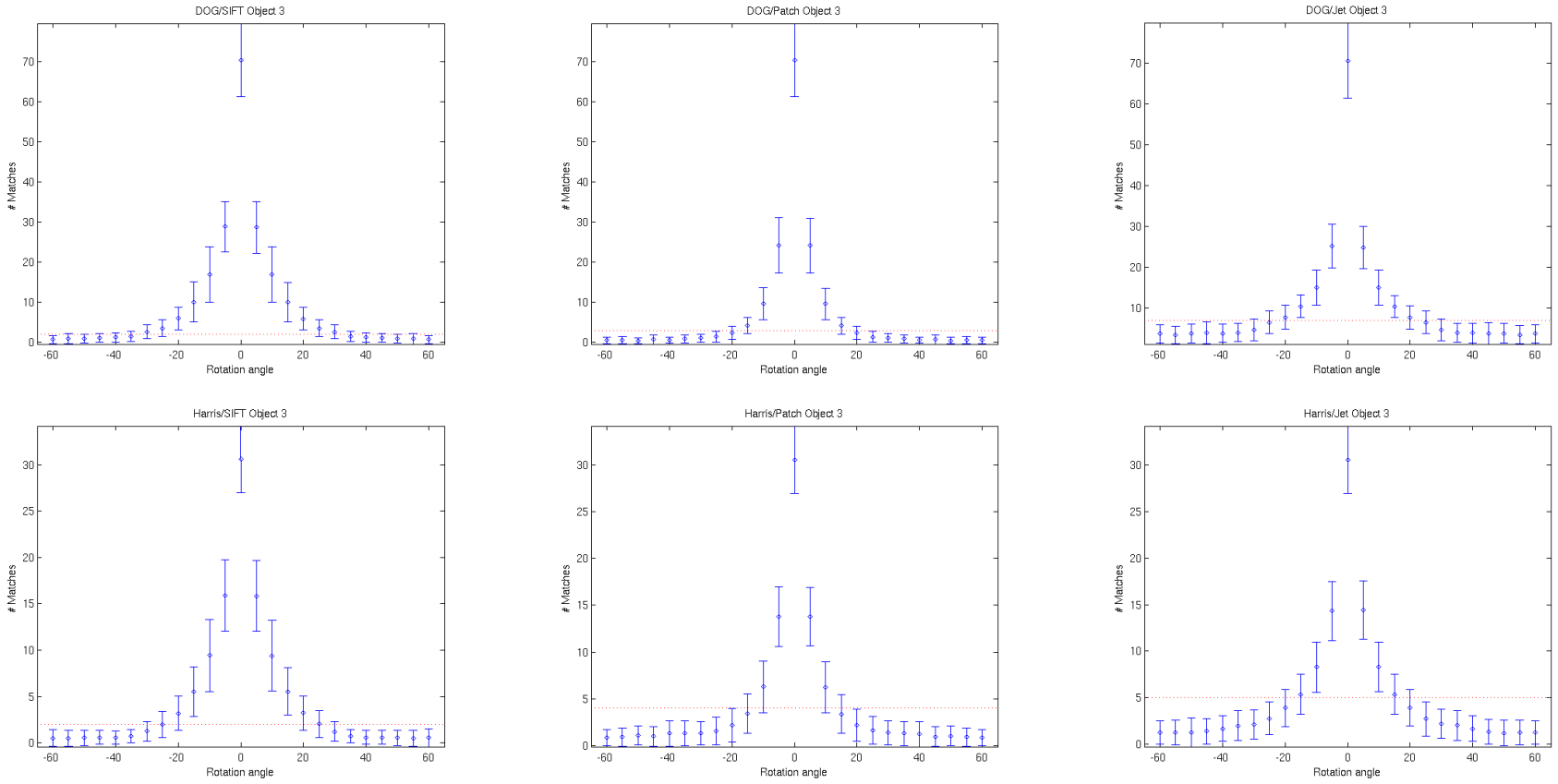

Figure 7: Result for object 3 showing the number of matches, the middle point is the mean and the bars are the standard deviation, for the different combinations of detectors and descriptors. The dotted line shows the limit for one percent false positives.

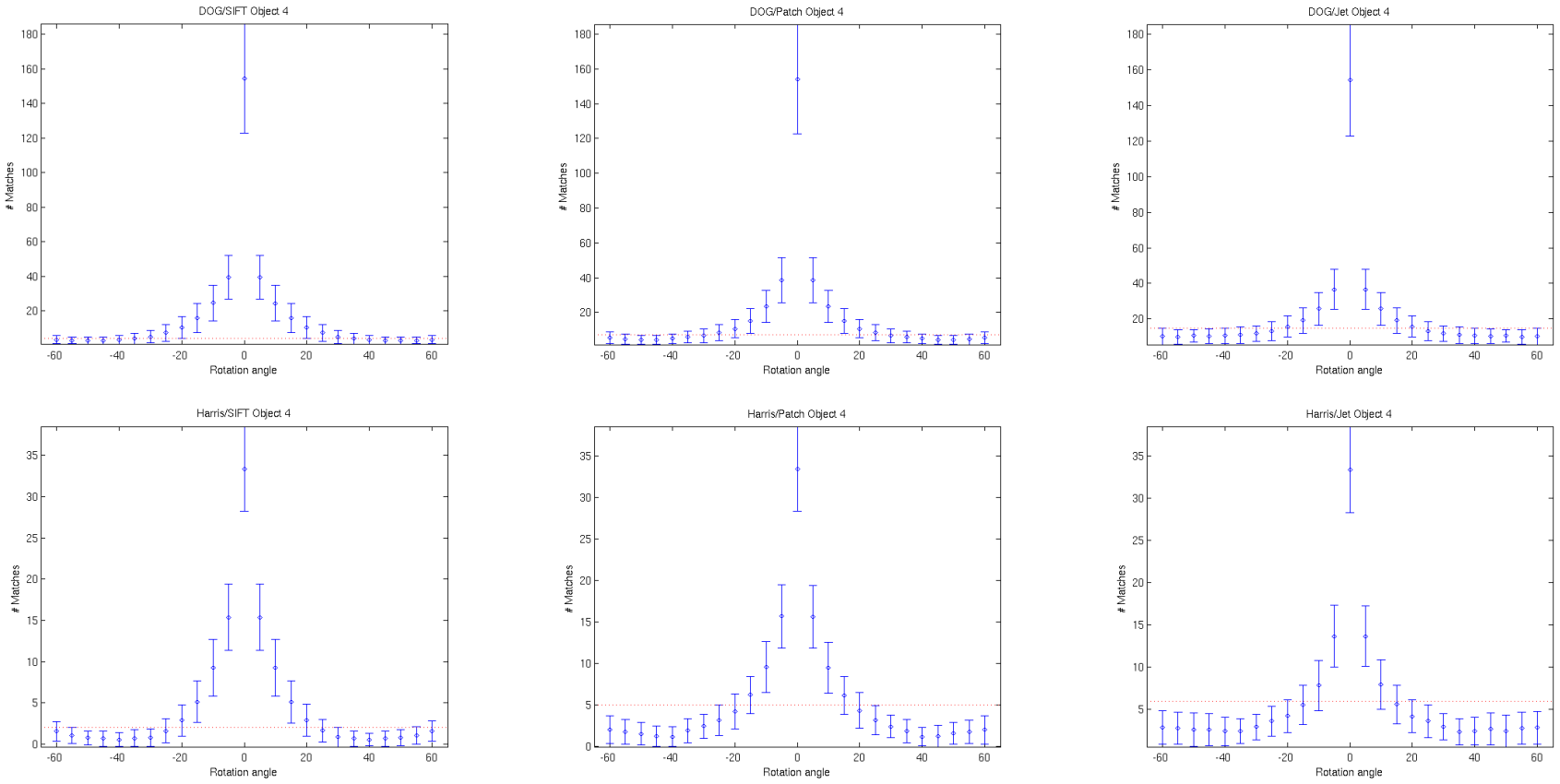

Figure 8: Result for object 4 showing the number of matches, the middle point is the mean and the bars are the standard deviation, for the different combinations of detectors and descriptors. The dotted line shows the limit for one percent false positives.

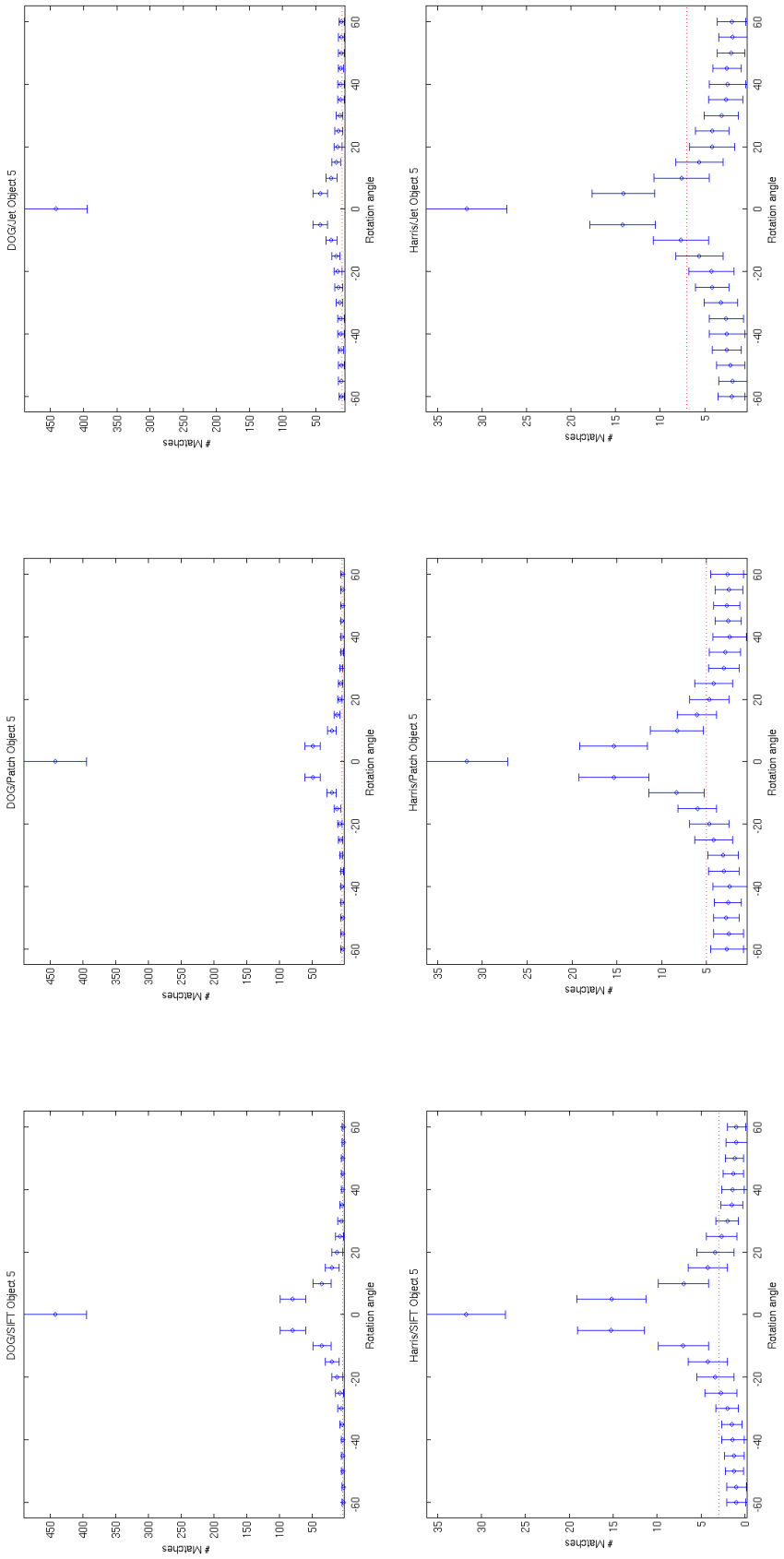

Figure 9: Result for object 5 showing the number of matches, the middle point is the mean and the bars are the standard deviation, for the different combinations of detectors and descriptors. The dotted line shows the limit for one percent false positives.

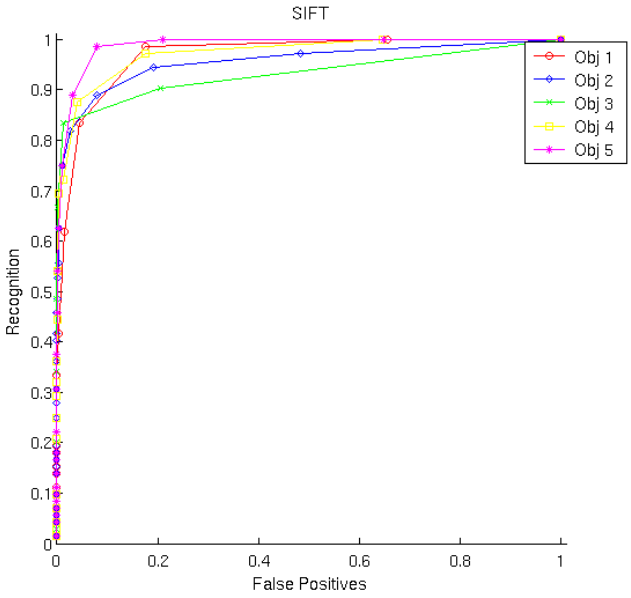

Figure 10: ROC for all objects when the object has been turned 25 degrees using DOG/SIFTkey combination and match with ratio metric.

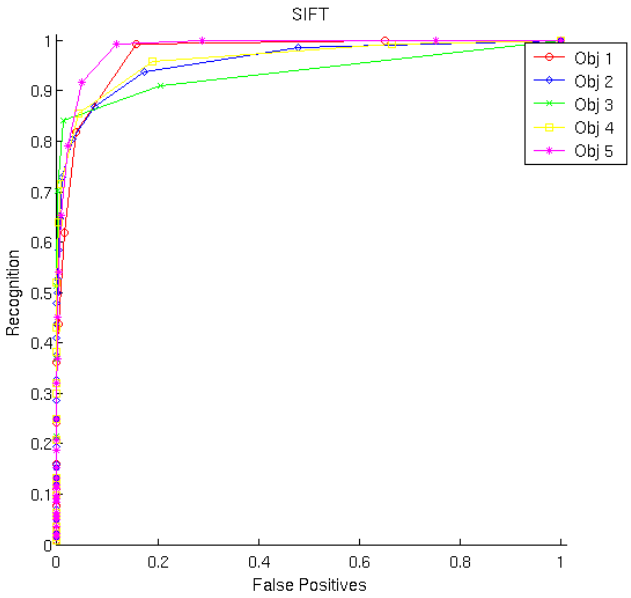

Figure 11: ROC for all objects when the object has been turned 25 degrees using DOG/SIFTkey combination and match with SSD as metric.

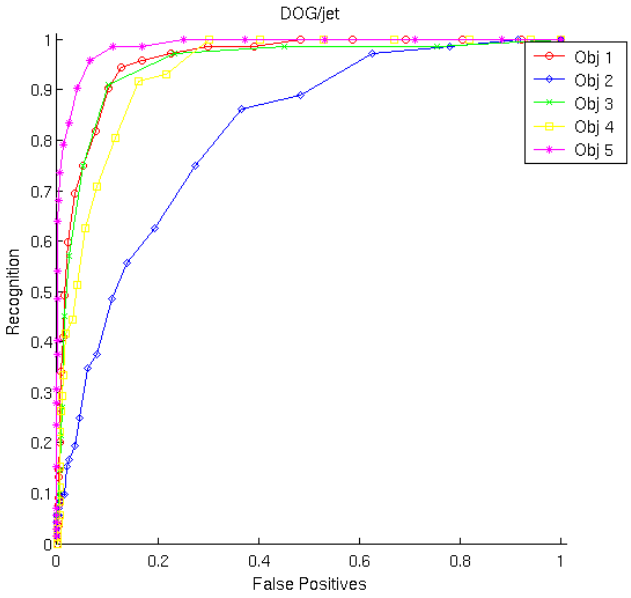

Figure 12: ROC for all objects when the object has been turned 25 degrees using DOG/jet combination and match with ratio metric.

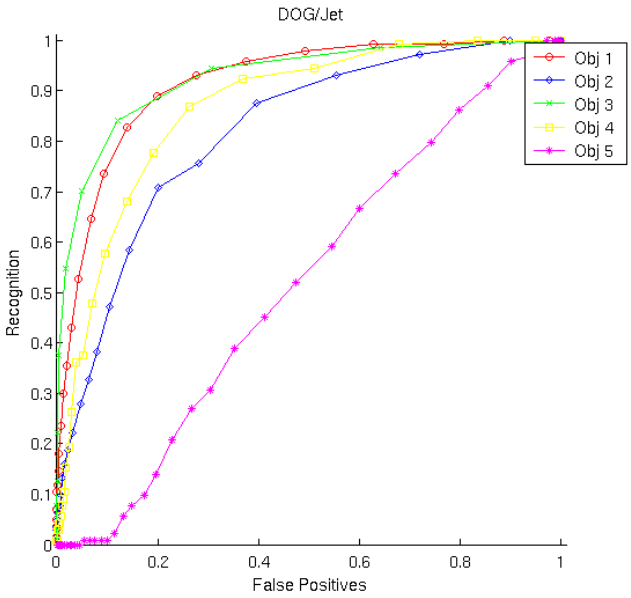

Figure 13: ROC for all objects when the object has been turned 25 degrees using DOG/jet combination and match with SSD as metric.

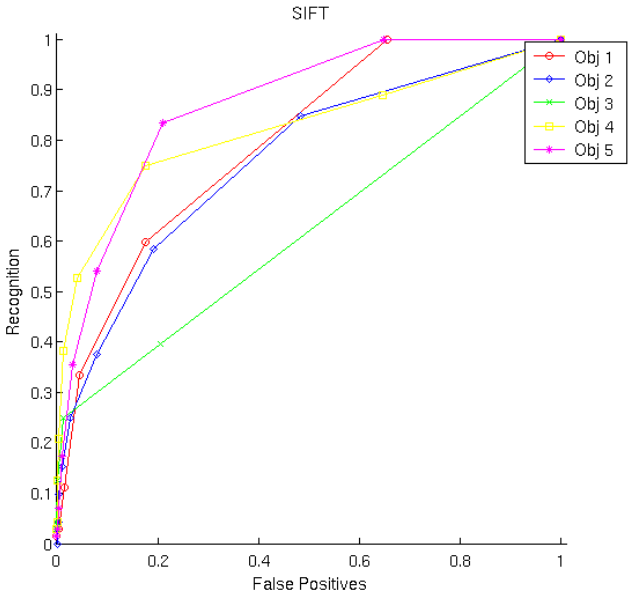

Figure 14: ROC for all objects when the object has been turned 55 degrees using DOG/SIFTkey combination and match with ratio metric.

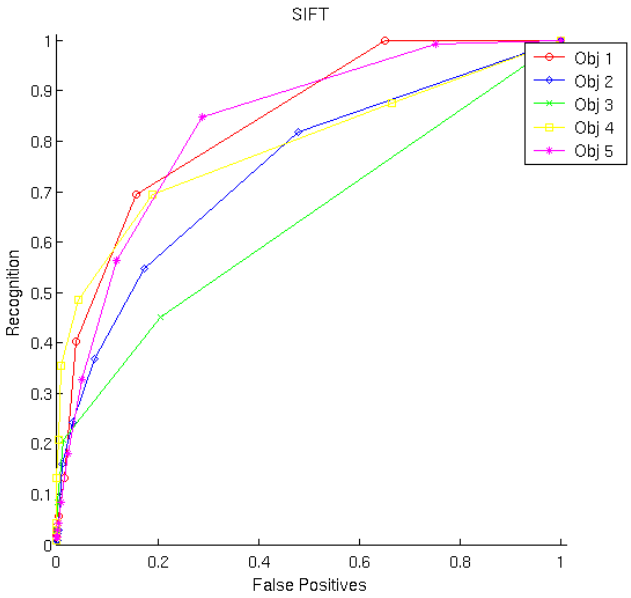

Figure 15: ROC for all objects when the object has been turned 55 degrees using DOG/SIFTkey combination and match with SSD as metric.

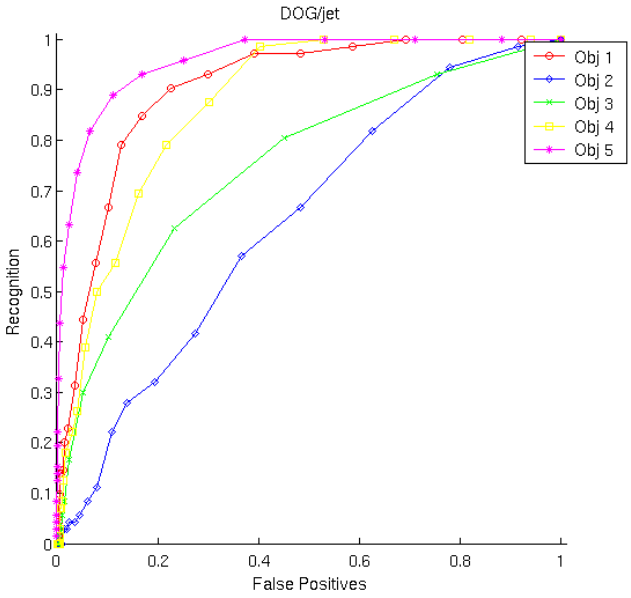

Figure 16: ROC for all objects when the object has been turned 55 degrees using DOG/jet combination and match with ratio metric.

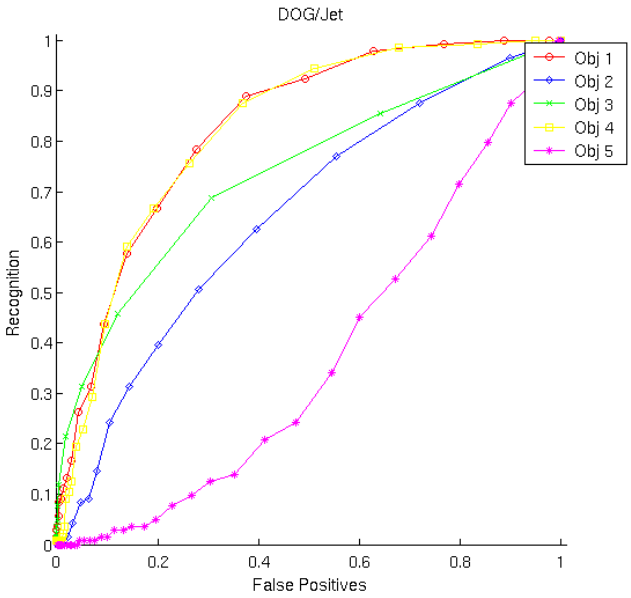

Figure 17: ROC for all objects when the object has been turned 55 degrees using DOG/jet combination and match with SSD as metric.

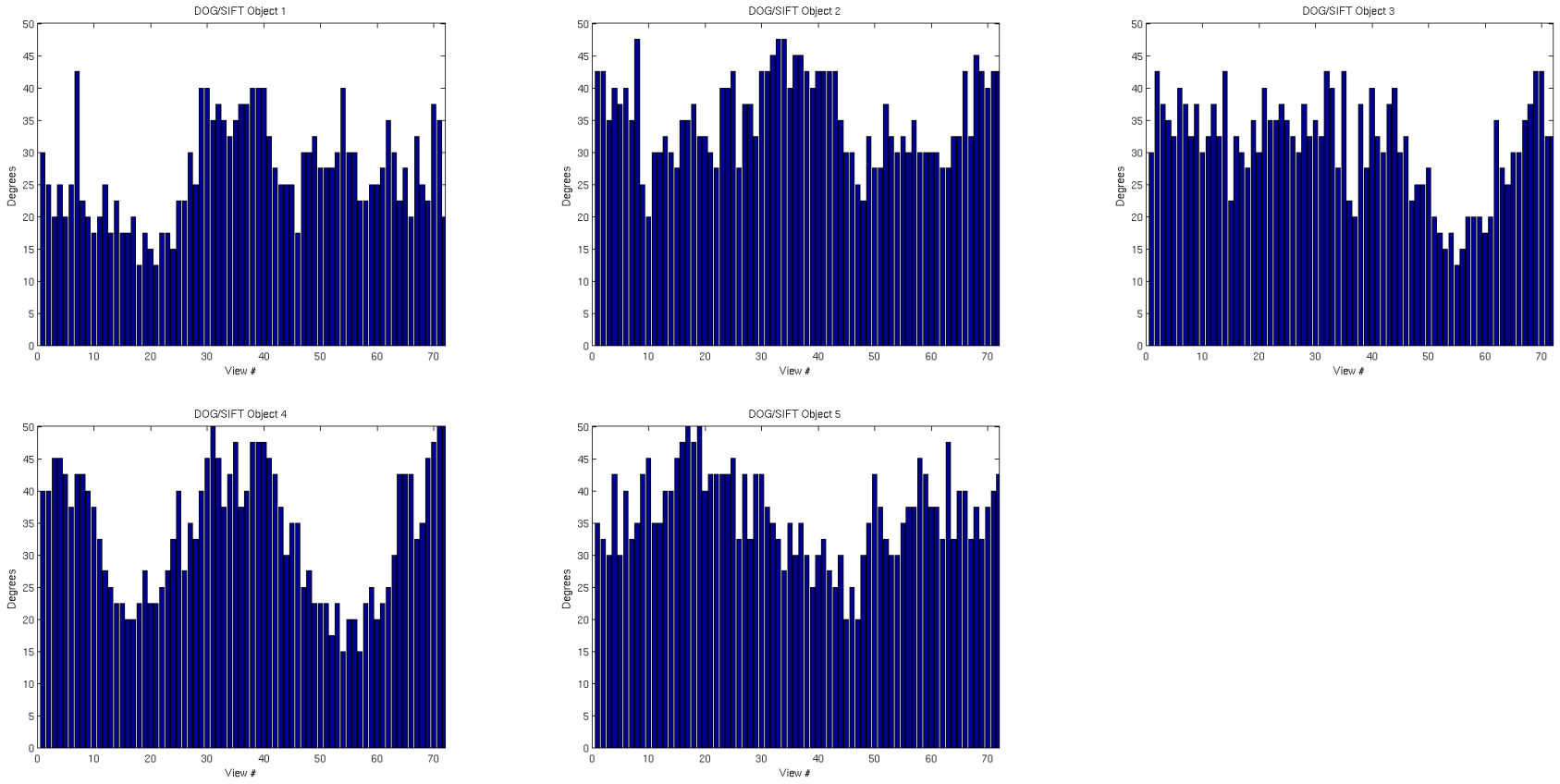

Figure 18: Results for over how many degrees each view of each object the number of matches is higher than a value resulting in 1 per mill false positives using DOG/SIFTkey. High values corresponds to views that generalize better than low values.

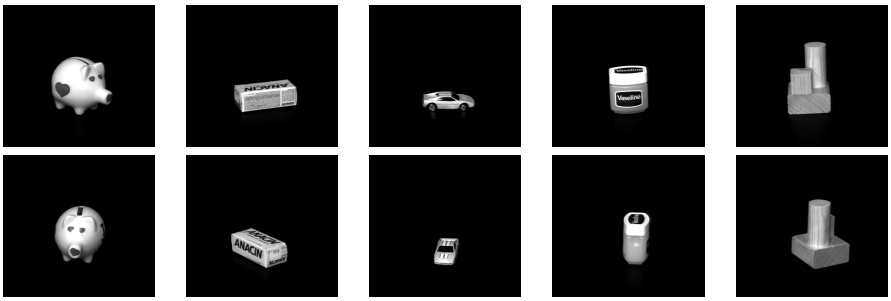

Figure 19: Results from the generalization of views: The upper images generalized the best and the lower generalized the worst.

4 Conclusions and Future Work

Results have been presented on the performance of different combination of feature point detectors and local descriptors and have been compared to the performance of a local shape descriptor and receptive field histogram for object identification. The best over all combination was SIFT keys computed at Difference-of-Gaussian extrema, which is in correlation with the results obtained in (Mikolajczyk & Schmid 2003). It was further shown that objects need to be sampled with at least every 45 degrees for successful recognition and that there is a great variation in the ability to generalize for different views of an object, were generally the views that produced many features performed the best. Indicating the weakness in these approaches that if few interest points are found the performance will go down, making the success for the approach highly object dependent. Further the performance of the local features were in parity with the performance of local shape context and receptive field histograms in general. Although the two later showed a large variability of their performance between objects. An interesting result is the indication, which can be seen by studying figures 10 and 129, that the global more shape based approaches and the local descriptors complements each other in the sense that the local features showed a better performance for objects with distinctive texture, and generate many descriptive features points (see figures 5 to 9), while the contour based and global descriptors performed better for objects with not so distinctive surface marks. This suggest that the two approaches might be suited for multiple cue integration due to their complementary nature.

Acknowledgement

This research was sponsored by the EU through its CogVis project (IST-2000-29375). The support is gratefully acknowledged.

References

Belongie, S., Malik, J. & Puzicha, J. (2002), 'Shape matching and object recognition using shape contexts', *PAMI* **24**(24), 509–522.

Brown, M. & Lowe, D. G. (2002), Invariant features from interest point groups, *in* 'British Machine Vision Conference', Cardiff, pp. 656–665.

Crowley, J. & Parker, A. (1989), 'A representation for shape based on peaks and ridges in difference of low-pass transform', *IEEE Trans. on PAMI* (6), 156–169.

Freeman, W. T. & Adelson, E. H. (1991), 'The design and use of steerable filters', *IEEE Transactions on Pattern Analysis and Machine Intelligence* **13**(9).

Harris, C. & Stephens, M. (1988), A combined corner and edge detector, *in* 'Proceedings of 4th Alvey Vision Conference', pp. 189–192.

Koenderink, J. J. & van Doorn, A. J. (1987), 'Representation of local geometry in the visual system', *Biological Cybernetics* **55**, 367–375.

Leibe, B. & Schiele, B. (2003), Analyzing contour and appearance based methods for object categorization, *in* 'Proceedings of International Conference on Computer Vision and Pattern Recognition'.

Linde, O. & Lindeberg, T. (2004), Object recognition using composed receptive field histograms of higher dimensionality, *in* 'ICPR'. to appear.

Lindeberg, T. (1998), 'Feature detection with automatic scale selection', *International Journal of Computer Vision* **30**(2), 77–116.

Lowe, D. G. (1999*a*), Object recognition from local scale-invariant features, *in* 'International Conference on Computer Vision', Corfu, Greece, pp. 1150–1157.

Lowe, D. G. (1999*b*), Object recognition from local scale-invariant features, *in* 'International Conference on Computer Vision', Corfu, Greece, pp. 1150–1157.

Lowe, D. G. (2004), 'Distinctive image features from scale-invariant keypoints', *International Journal of Computer Vision* . Preprint.

Mikolajczyk, K. (2002), Detection of local features invariant to affine transformations, PhD thesis, INPG Grenoble.

Mikolajczyk, K. & Schmid, C. (2001), Indexing based on scale invariant interest points, *in* 'Proceedings of the International Conference on Computer Vision', pp. 525–531.

Mikolajczyk, K. & Schmid, C. (2003), A performance evaluation of local descriptors, *in* 'IEEE Conference on Computer Vision and Pattern Recognition'.

Moravec, H. P. (1980), Obstacle Avoidance and Navigation in the Real World by a Seeing Robot Rover, PhD thesis, Stanford University.

Murase, H. & Nayar, S. K. (1995), 'Visual learning and recognition of 3-d objects from appearance', *International Journal of Computer Vision* **14**(1), 5–24.

Rao, R. P. N. & Ballard, D. H. (1995), Object indexing using an iconic sparse distributed memory, *in* 'Proceedings Fifth International Conference on Computer Vision', pp. 24 – 31.

S. A. Nene, S. K. N. & Murase, H. (1996), Columbia object image library (coil-20), Technical report, Colombia University.

Schaffalitzky, F. & Zisserman, A. (2002), Multi-view matching for unordered image sets, or "How do I organize my holiday snaps?", *in* 'Proceedings of the 7th European Conference on Computer Vision', Vol. 1, Copenhagen, pp. 414–431.

Schiele, B. & Crowley, J. L. (2000), 'Recognition without correspondence using multidimensional receptive field histograms', *International Journal of Computer Vision* **36**(1), 31–50.

Schmid, C., Mohr, R. & Bauckhage, C. (2000), 'Evaluation of interest point detectors', *International Journal of Computer Vision* **37**(2), 151–172.

Schmidt, C. & Mohr, R. (1997), 'Local grayvalue invariants for image retrieval', *IEEE Transaction on Pattern Analysis and Machine Intelligence* **19**(5), 530–535.

Swain, M. J. & Ballard, D. H. (1991), 'Color indexing', *International Journal of Computer Vision* **7**(1), 11–32.

Tuytelaars, T. & Gool, L. V. (2000), Wide baseline stereo matching based on local, affinely invariant regions, *in* 'British Machine Vision Conference', pp. 412–422.

A Appendix A

A.1 ROC for all objects using quotient as metric

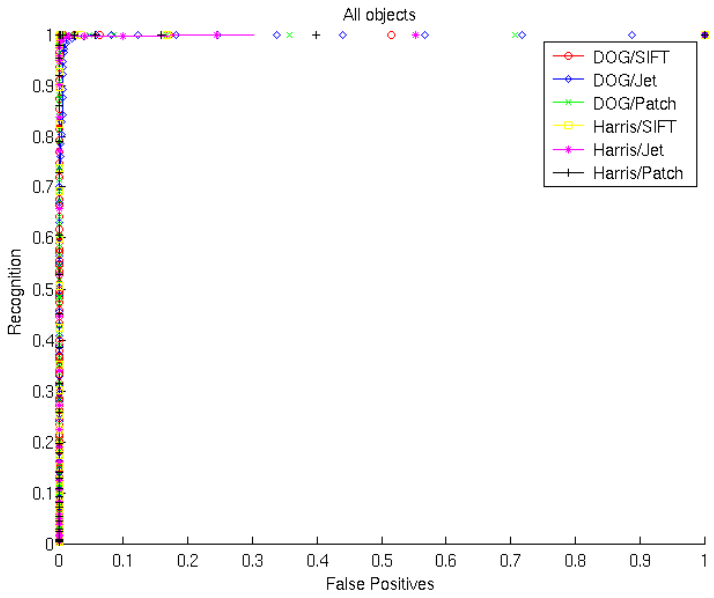

Figure 20: ROC for all objects when the objects have been turned 5 degrees.

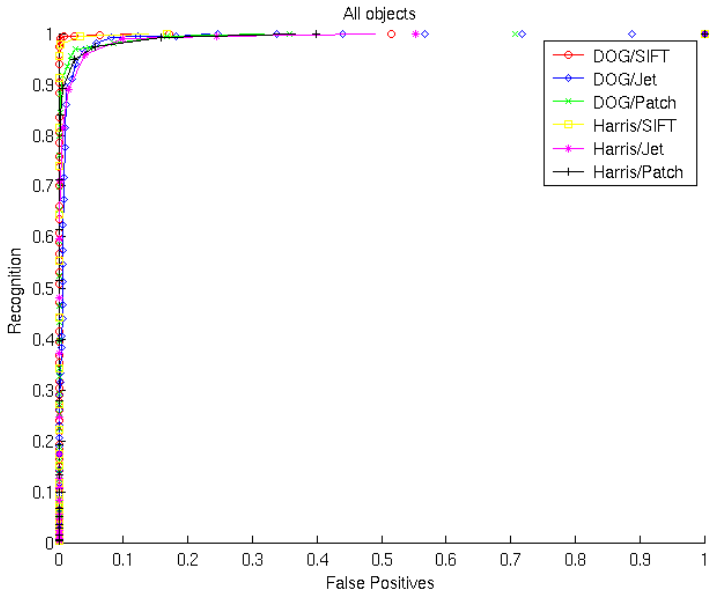

Figure 21: ROC for all objects when the objects have been turned 10 degrees.

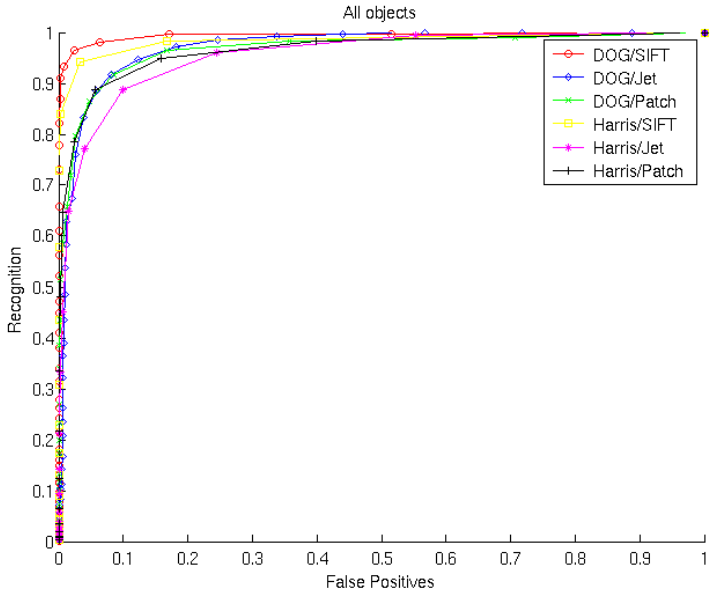

Figure 22: ROC for all objects when the objects have been turned 15 degrees.

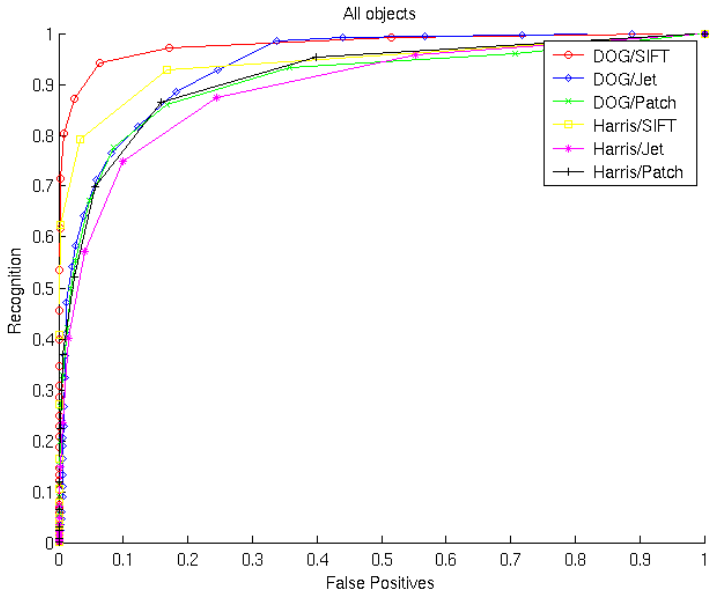

Figure 23: ROC for all objects when the objects have been turned 20 degrees.

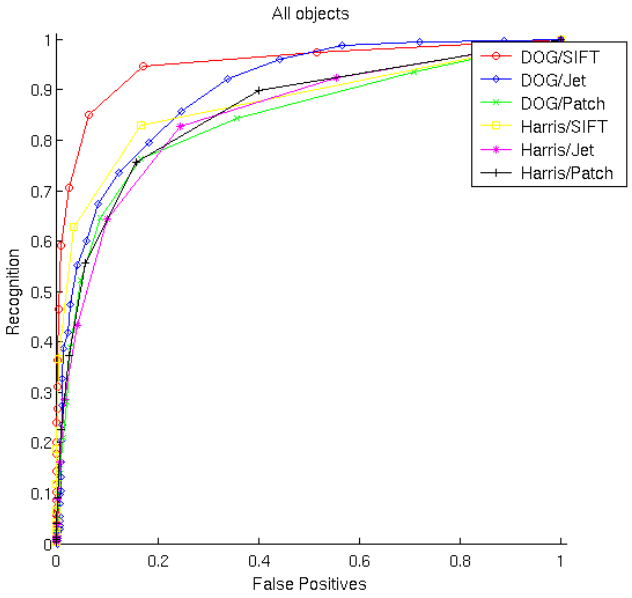

Figure 24: ROC for all objects when the objects have been turned 25 degrees.

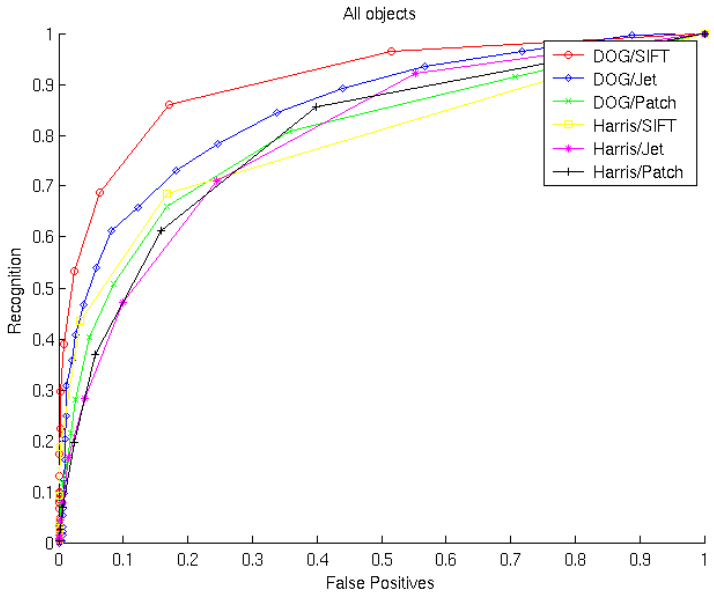

Figure 25: ROC for all objects when the objects have been turned 30 degrees.

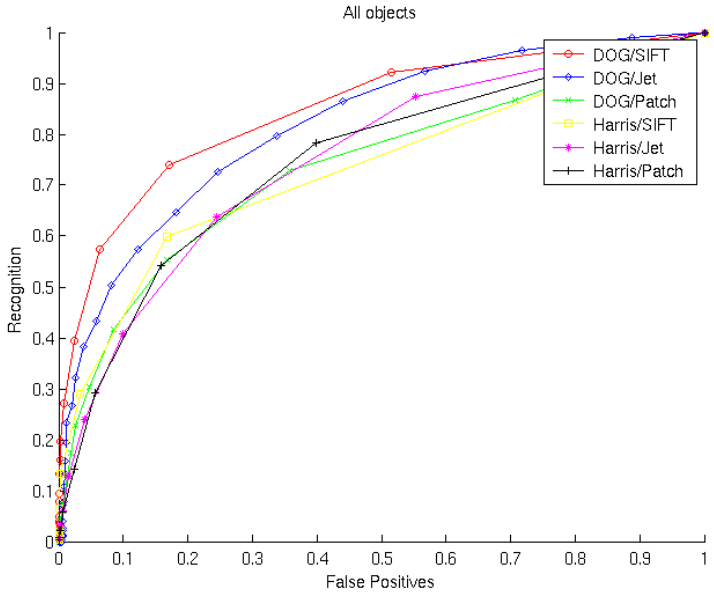

Figure 26: ROC for all objects when the objects have been turned 35 degrees.

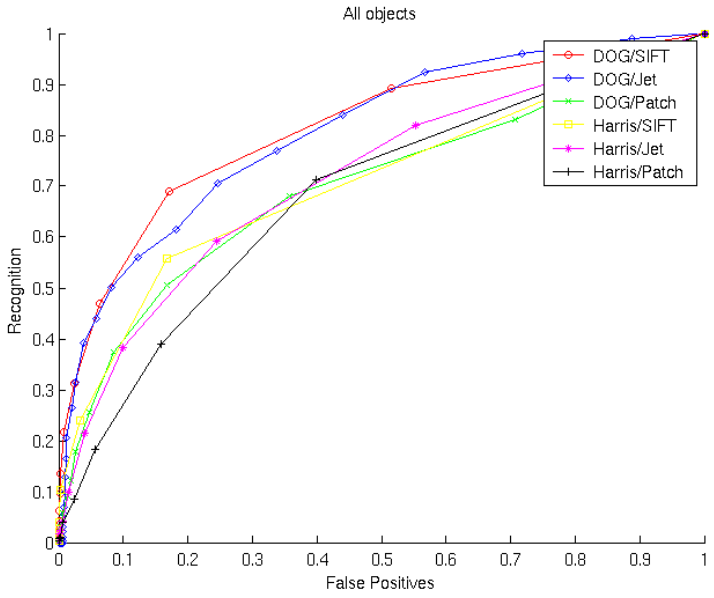

Figure 27: ROC for all objects when the objects have been turned 40 degrees.

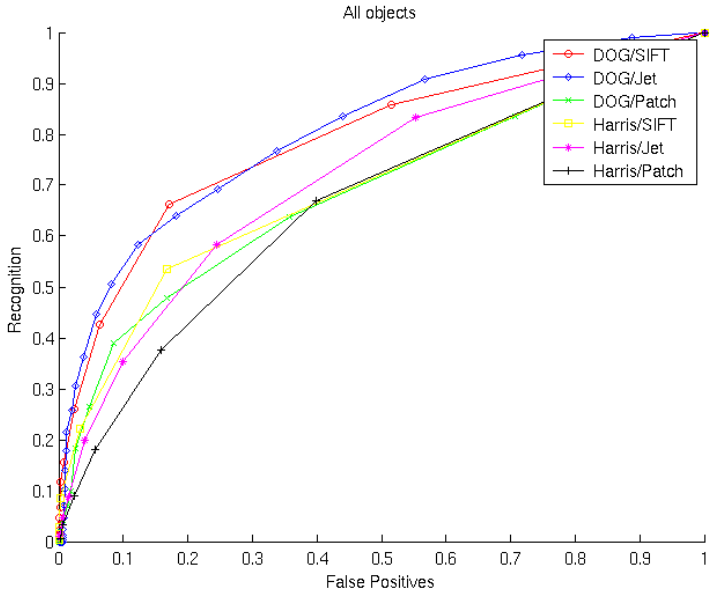

Figure 28: ROC for all objects when the objects have been turned 45 degrees.

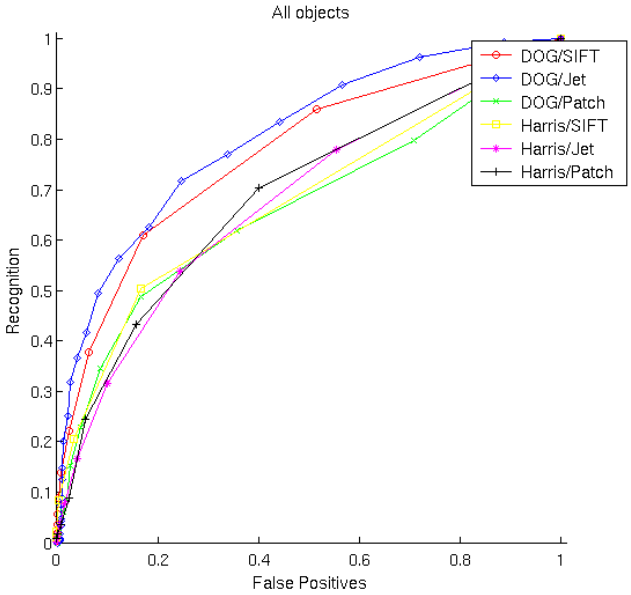

Figure 29: ROC for all objects when the objects have been turned 50 degrees.

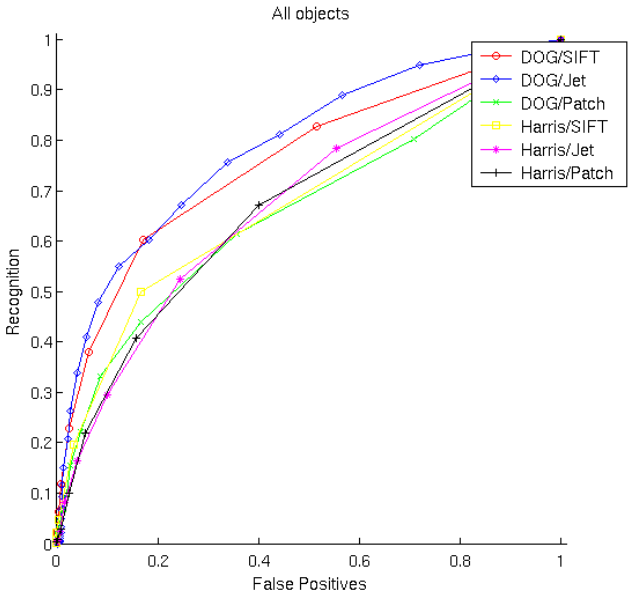

Figure 30: ROC for all objects when the objects have been turned 55 degrees.

A.2 Results for each individual object when matching with quotient

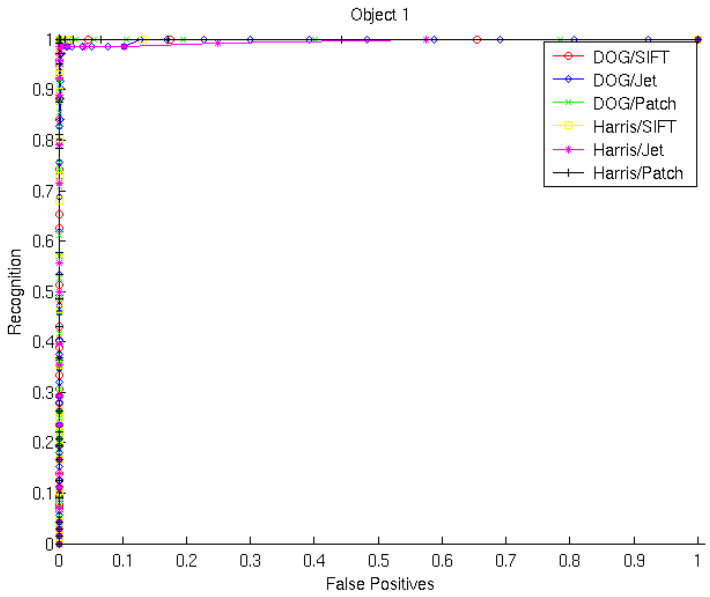

Figure 31: ROC for object 1 when the object has been turned 5 degrees.

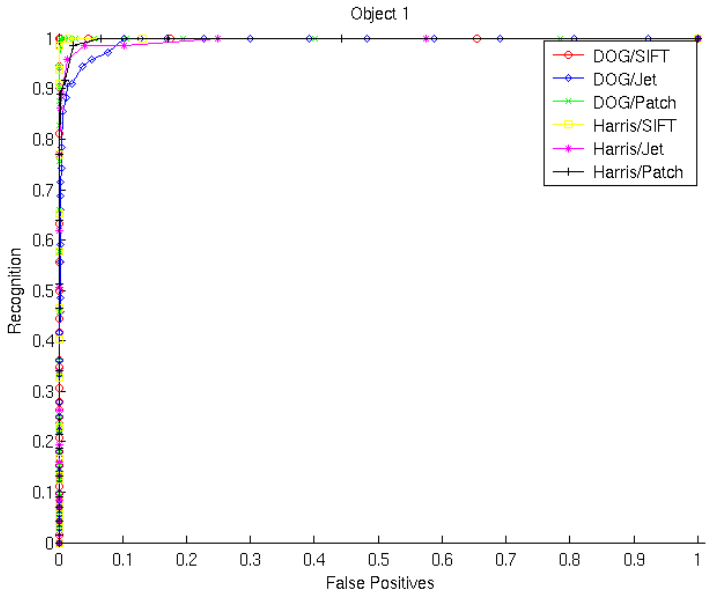

Figure 32: ROC for object 1 when the object has been turned 10 degrees.

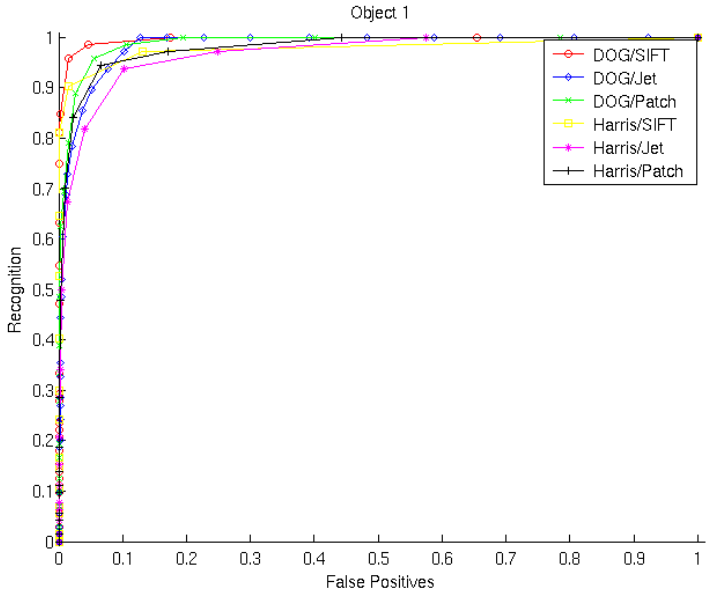

Figure 33: ROC for object 1 when the object has been turned 15 degrees.

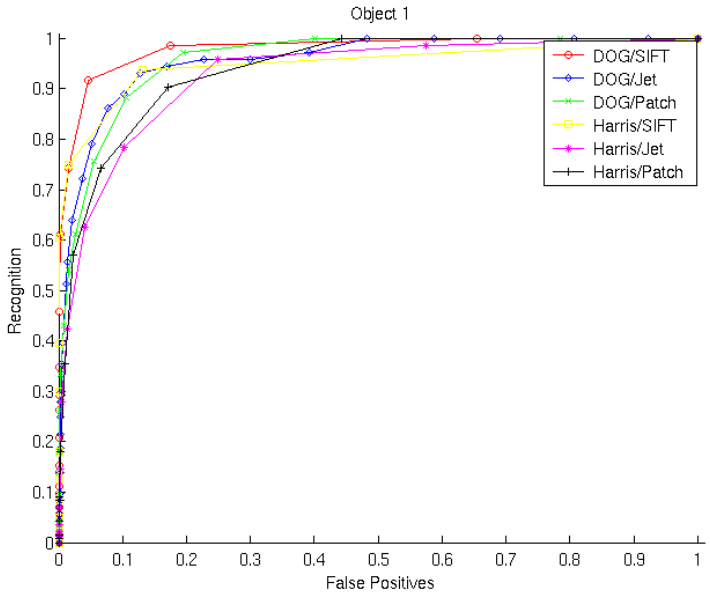

Figure 34: ROC for object 1 when the object has been turned 20 degrees.

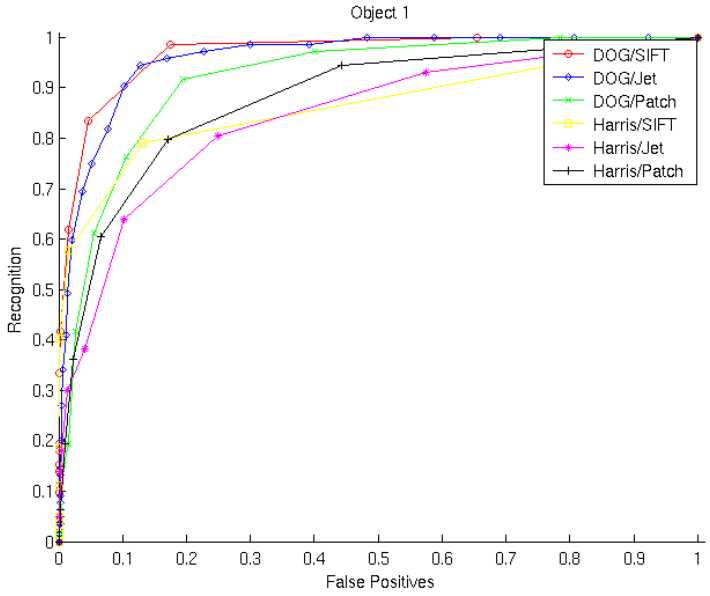

Figure 35: ROC for object 1 when the object has been turned 25 degrees.

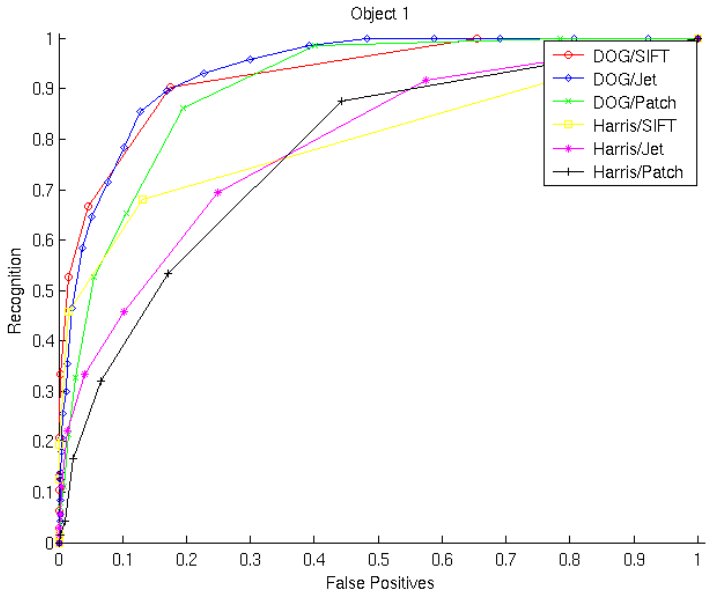

Figure 36: ROC for object 1 when the object has been turned 30 degrees.

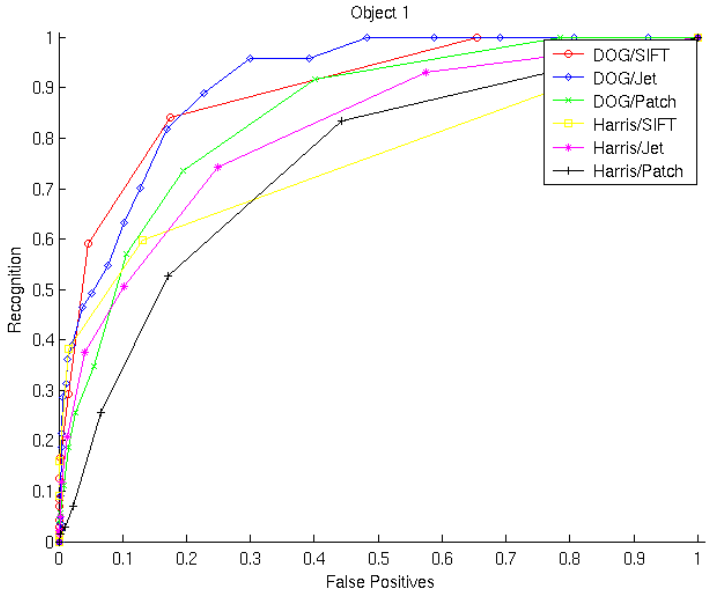

Figure 37: ROC for object 1 when the object has been turned 35 degrees.

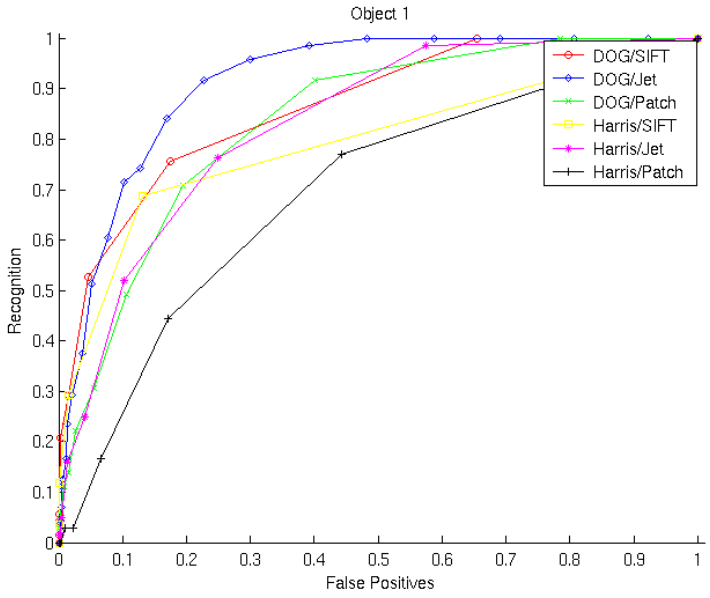

Figure 38: ROC for object 1 when the object has been turned 40 degrees.

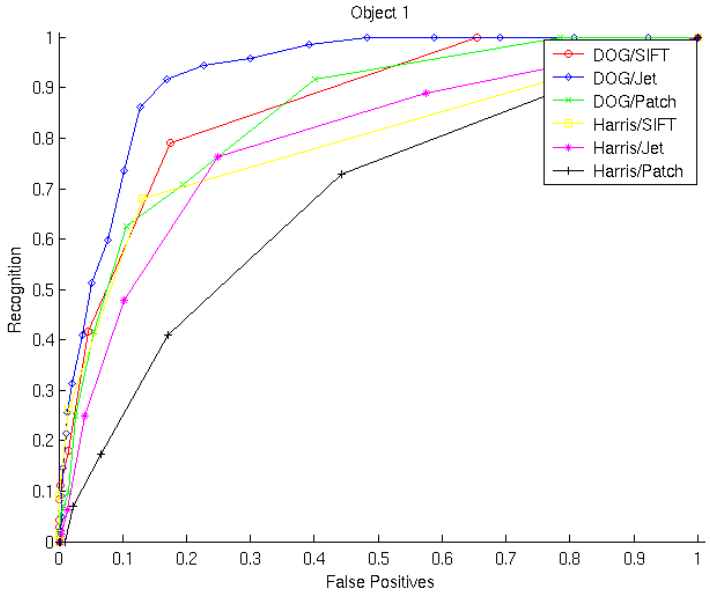

Figure 39: ROC for object 1 when the object has been turned 45 degrees.

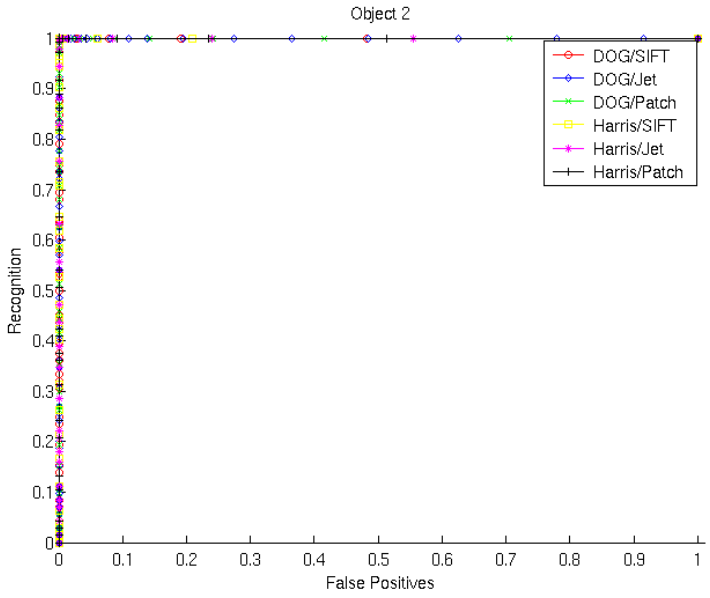

Figure 40: ROC for object 2 when the object has been turned 5 degrees.

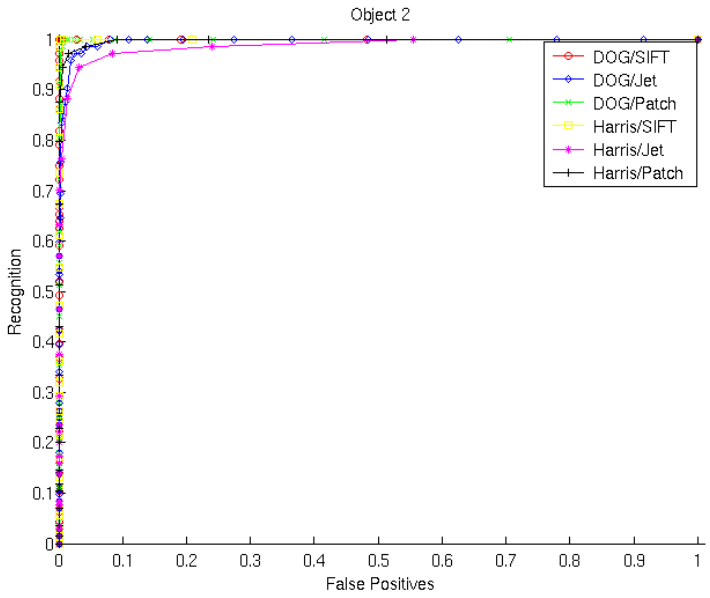

Figure 41: ROC for object 2 when the object has been turned 10 degrees.

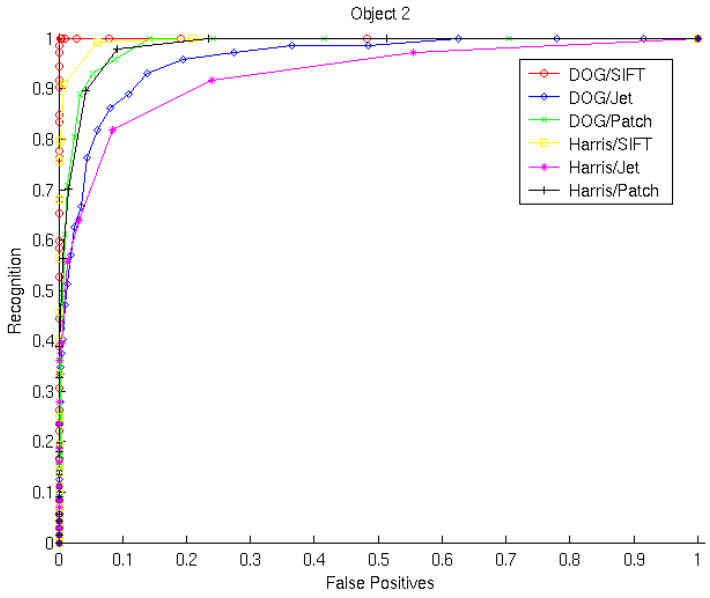

Figure 42: ROC for object 2 when the object has been turned 15 degrees.

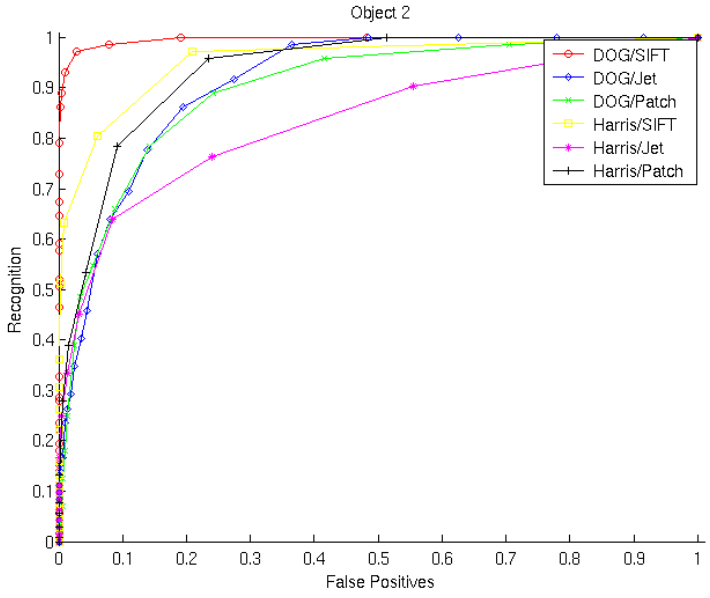

Figure 43: ROC for object 2 when the object has been turned 20 degrees.

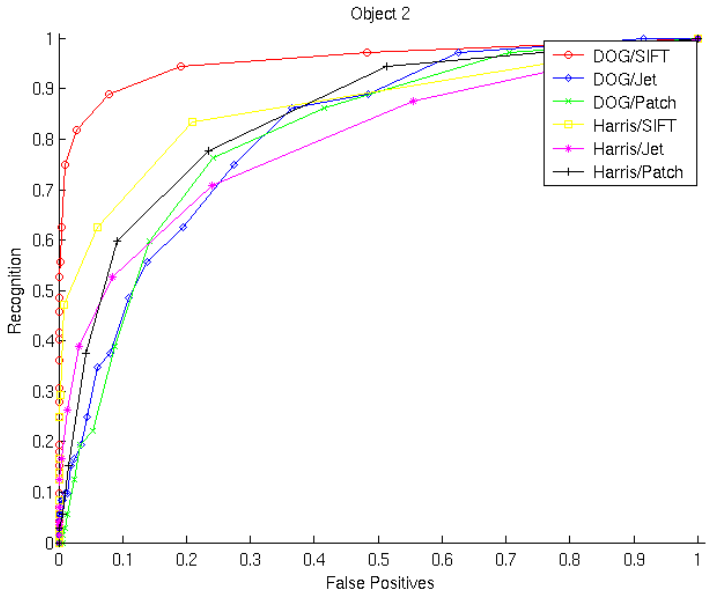

Figure 44: ROC for object 2 when the object has been turned 25 degrees.

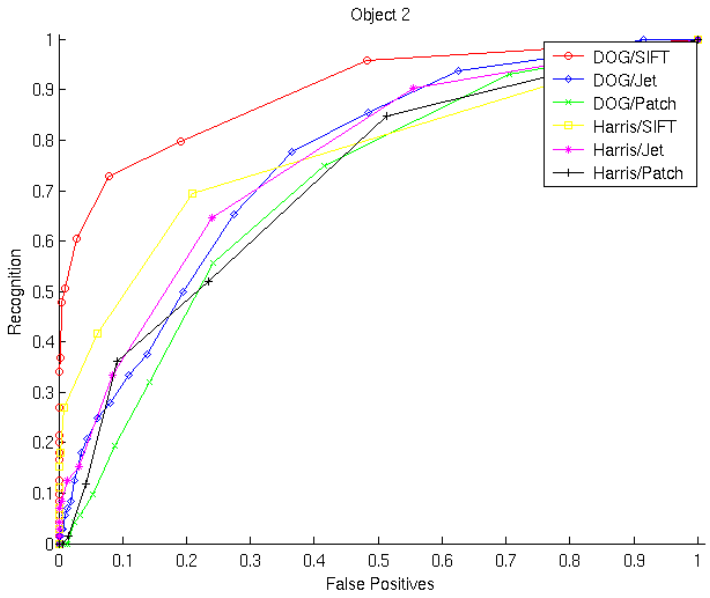

Figure 45: ROC for object 2 when the object has been turned 30 degrees.

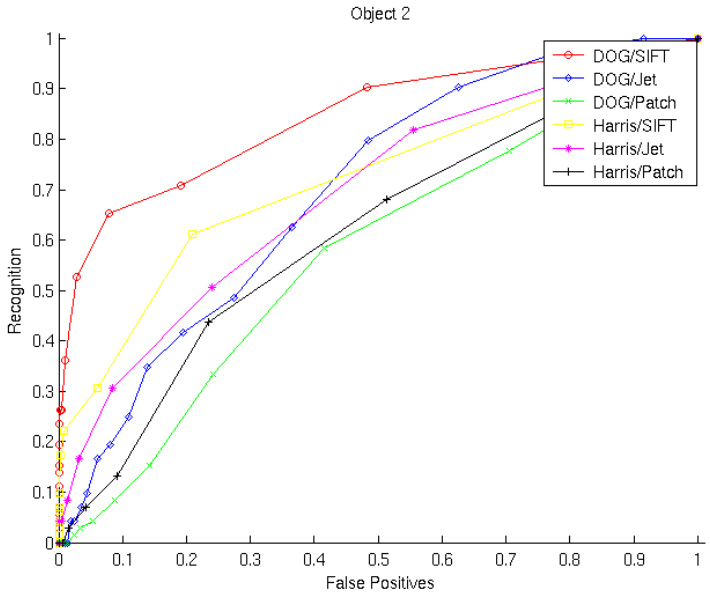

Figure 46: ROC for object 2 when the object has been turned 35 degrees.

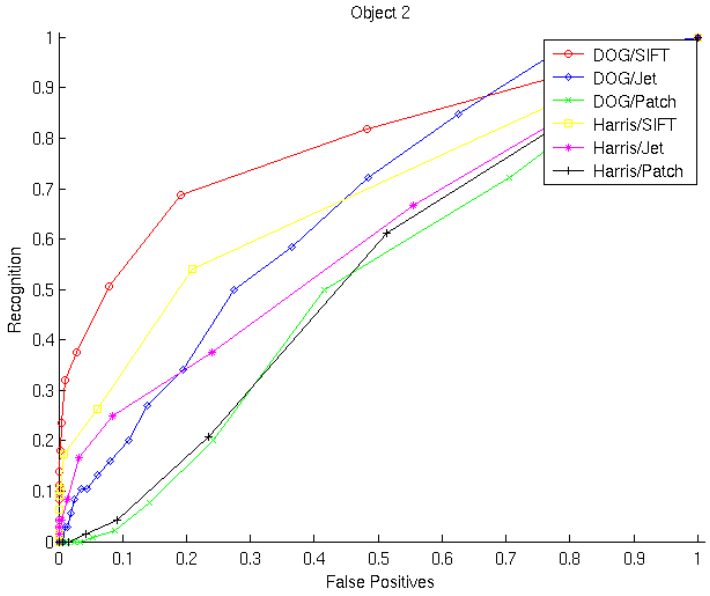

Figure 47: ROC for object 2 when the object has been turned 40 degrees.

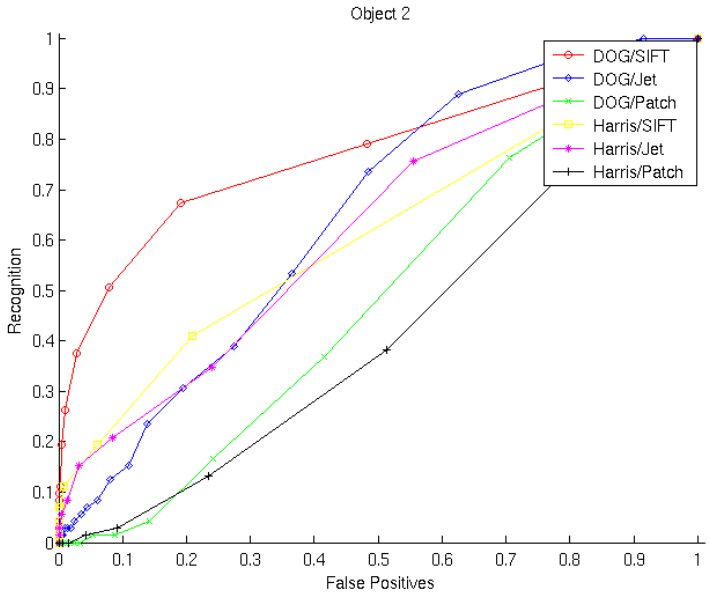

Figure 48: ROC for object 2 when the object has been turned 45 degrees.

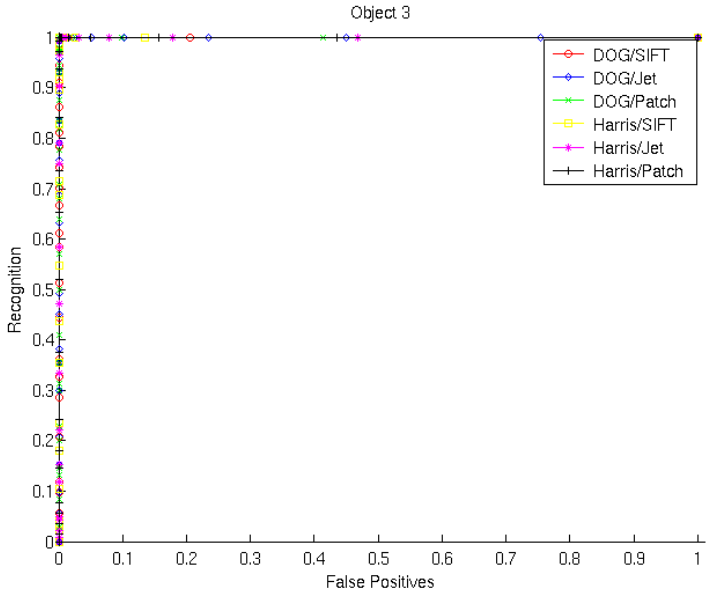

Figure 49: ROC for object 3 when the object has been turned 5 degrees.

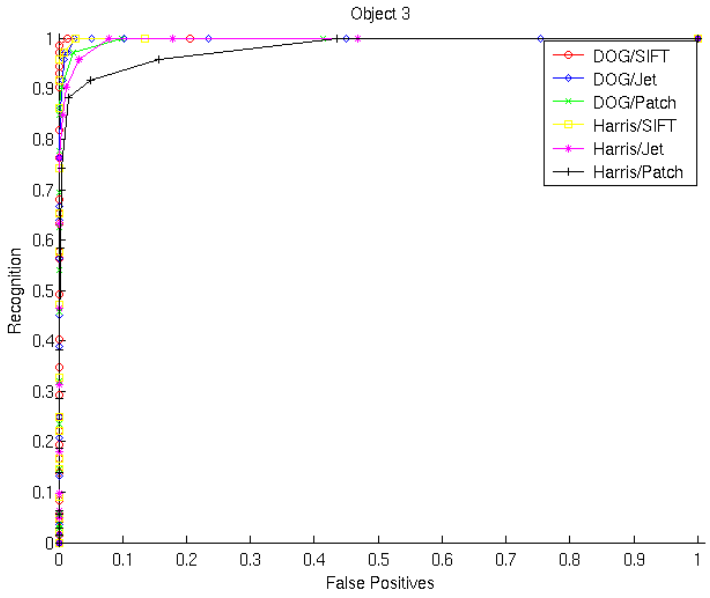

Figure 50: ROC for object 3 when the object has been turned 10 degrees.

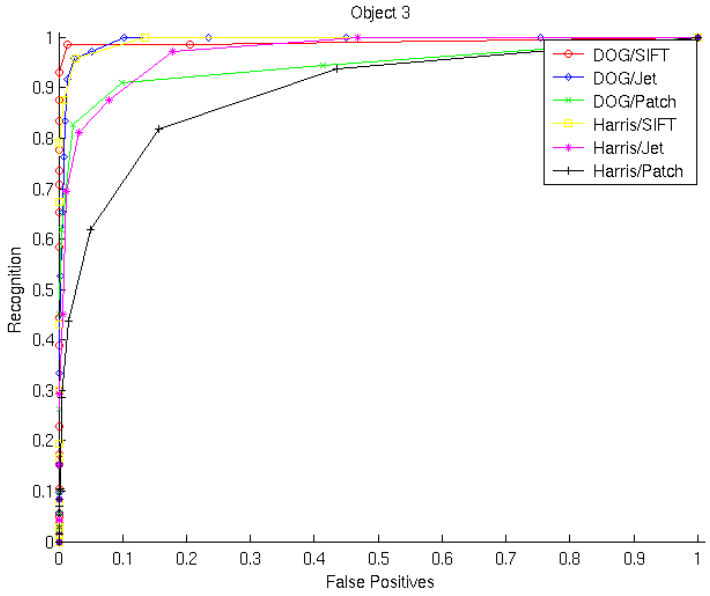

Figure 51: ROC for object 3 when the object has been turned 15 degrees.

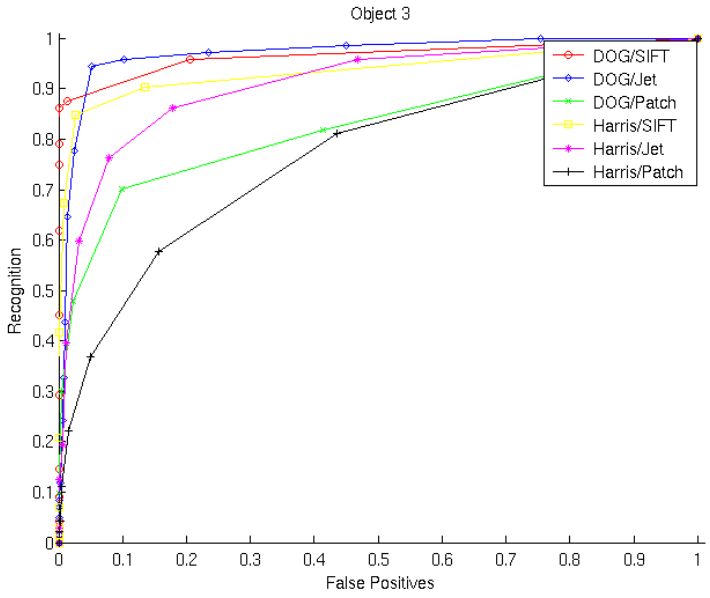

Figure 52: ROC for object 3 when the object has been turned 20 degrees.

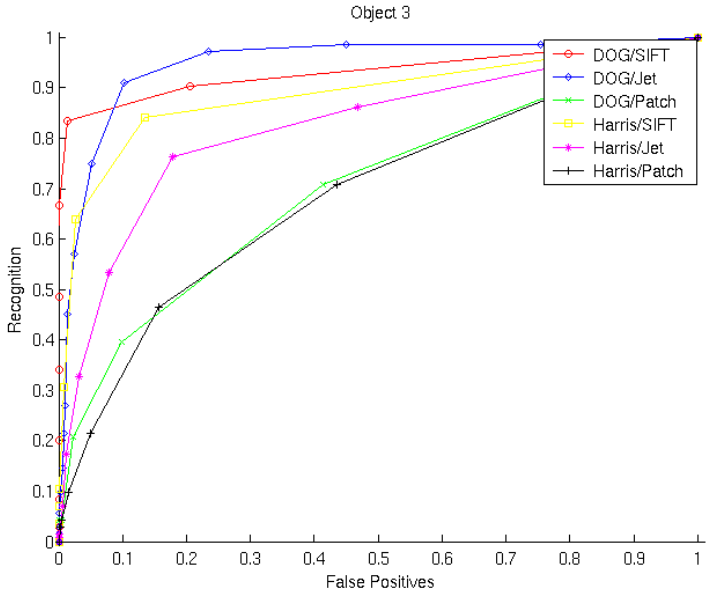

Figure 53: ROC for object 3 when the object has been turned 25 degrees.

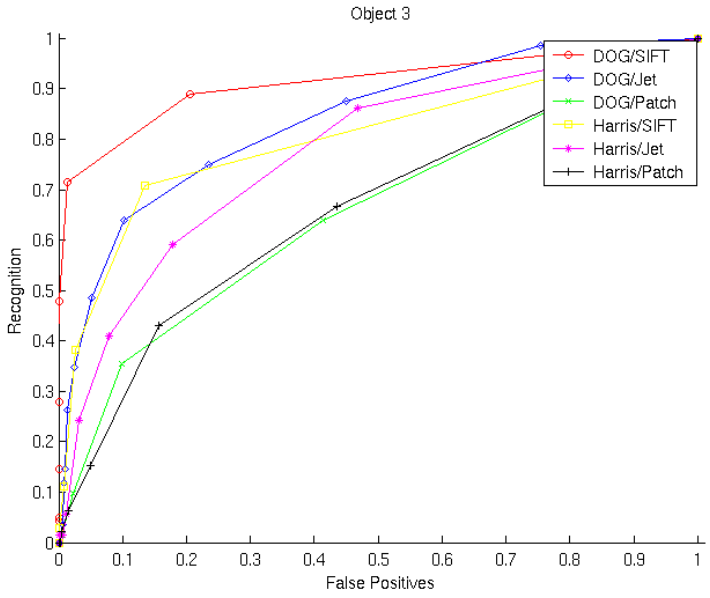

Figure 54: ROC for object 3 when the object has been turned 30 degrees.

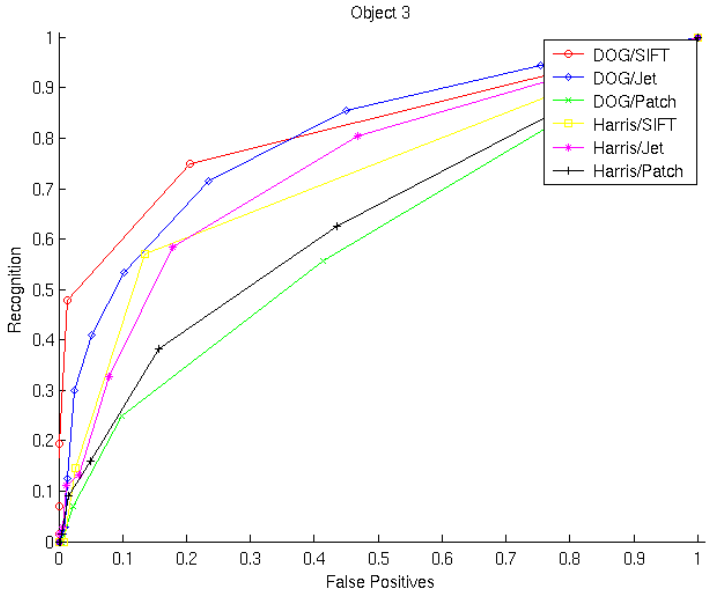

Figure 55: ROC for object 3 when the object has been turned 35 degrees.

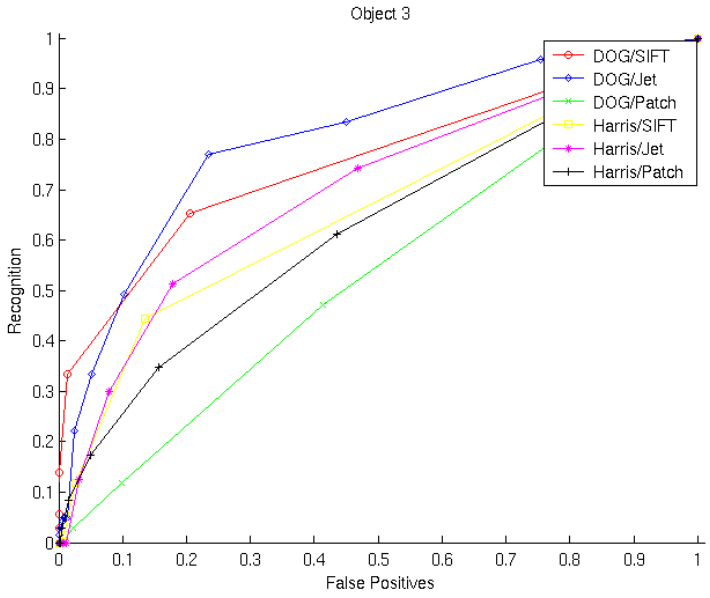

Figure 56: ROC for object 3 when the object has been turned 40 degrees.

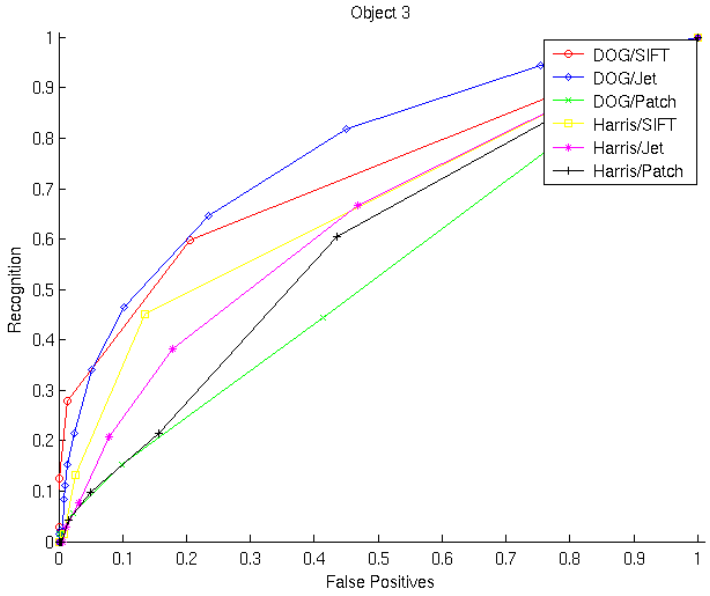

Figure 57: ROC for object 3 when the object has been turned 45 degrees.

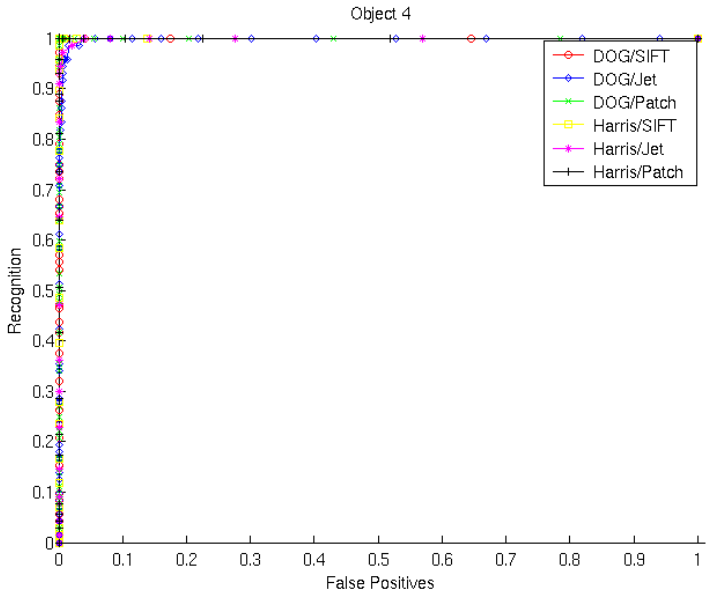

Figure 58: ROC for object 4 when the object has been turned 5 degrees.

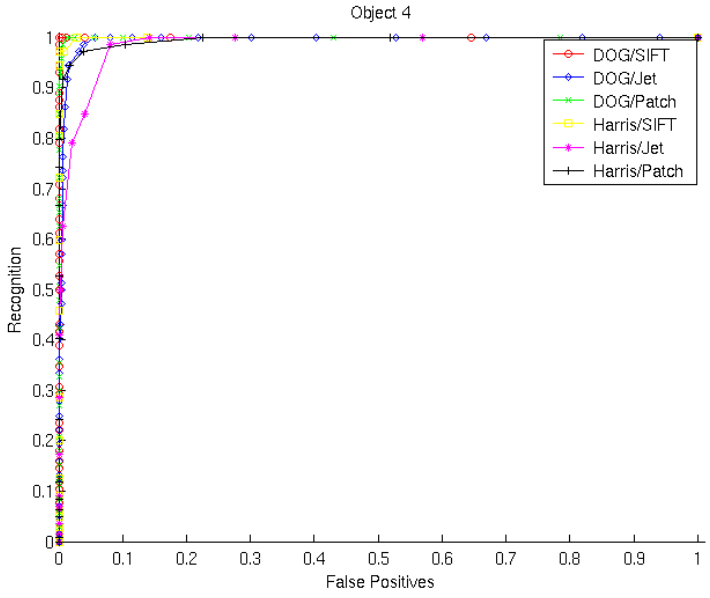

Figure 59: ROC for object 4 when the object has been turned 10 degrees.

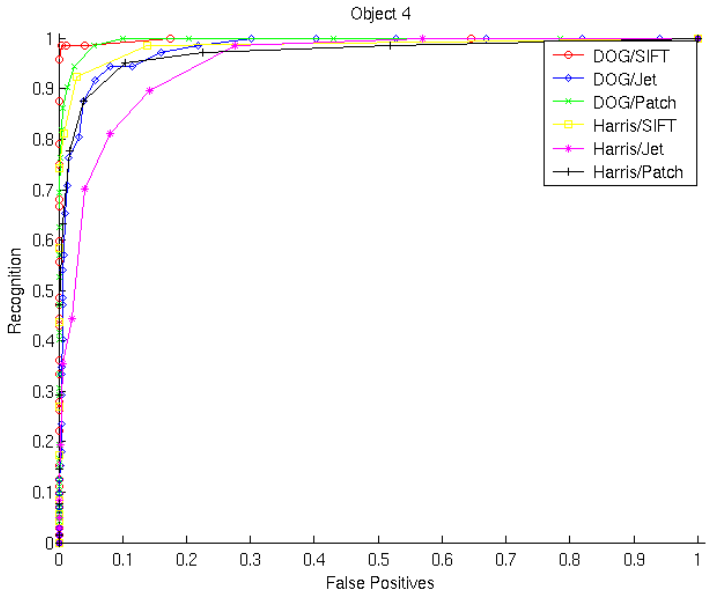

Figure 60: ROC for object 4 when the object has been turned 15 degrees.

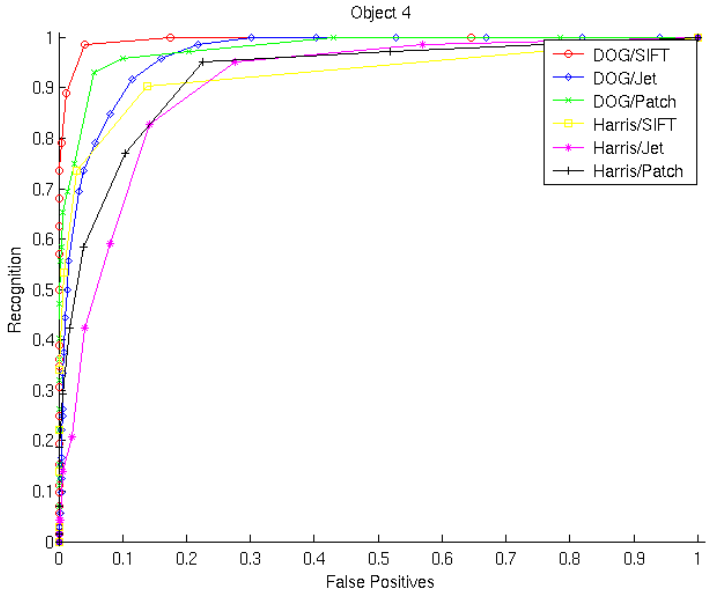

Figure 61: ROC for object 4 when the object has been turned 20 degrees.

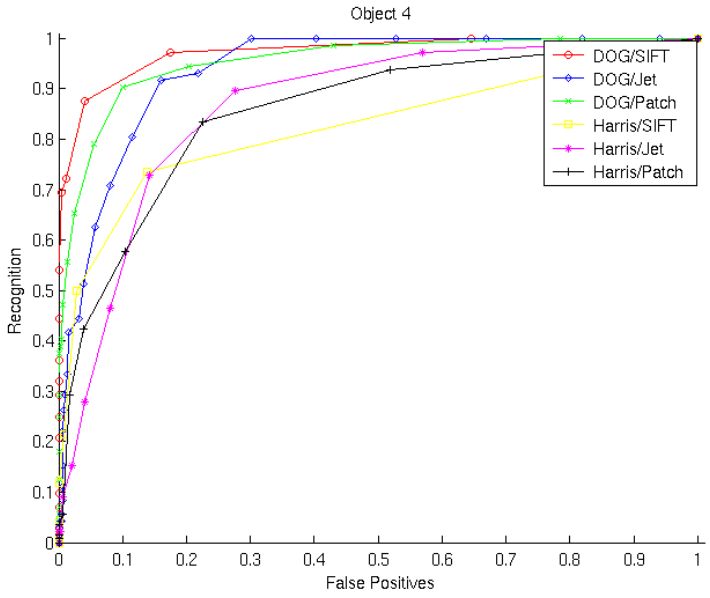

Figure 62: ROC for object 4 when the object has been turned 25 degrees.

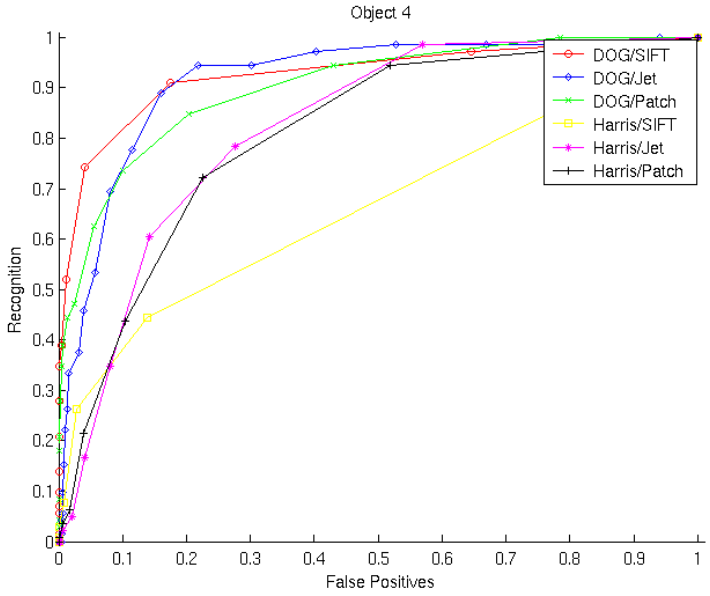

Figure 63: ROC for object 4 when the object has been turned 30 degrees.

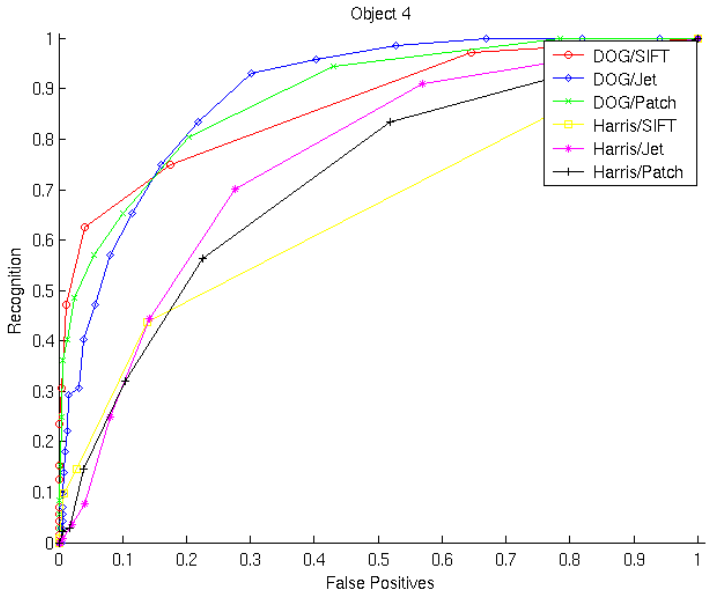

Figure 64: ROC for object 4 when the object has been turned 35 degrees.

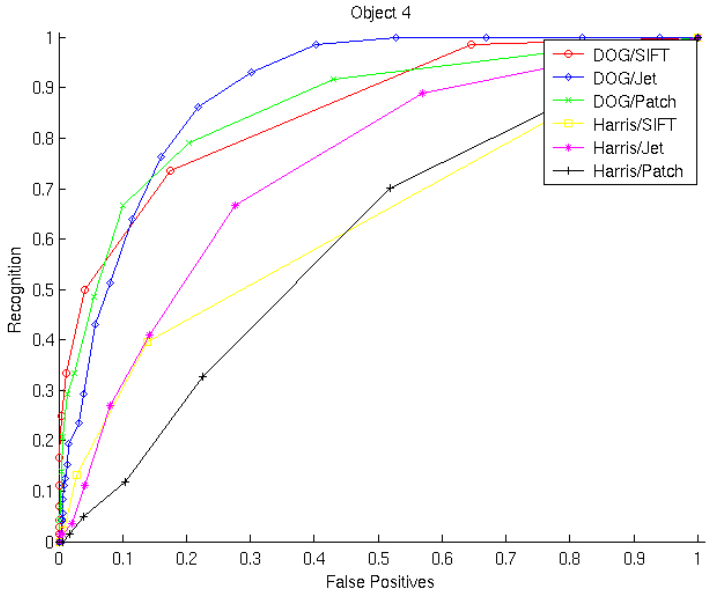

Figure 65: ROC for object 4 when the object has been turned 40 degrees.

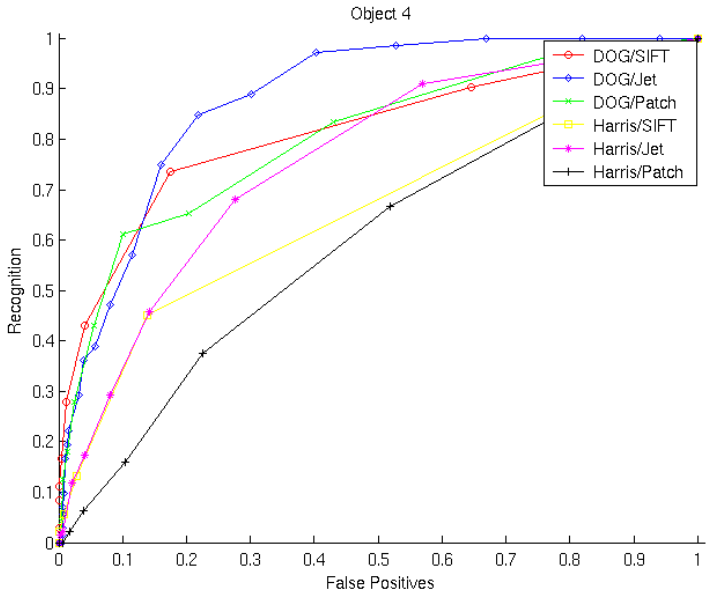

Figure 66: ROC for object 4 when the object has been turned 45 degrees.

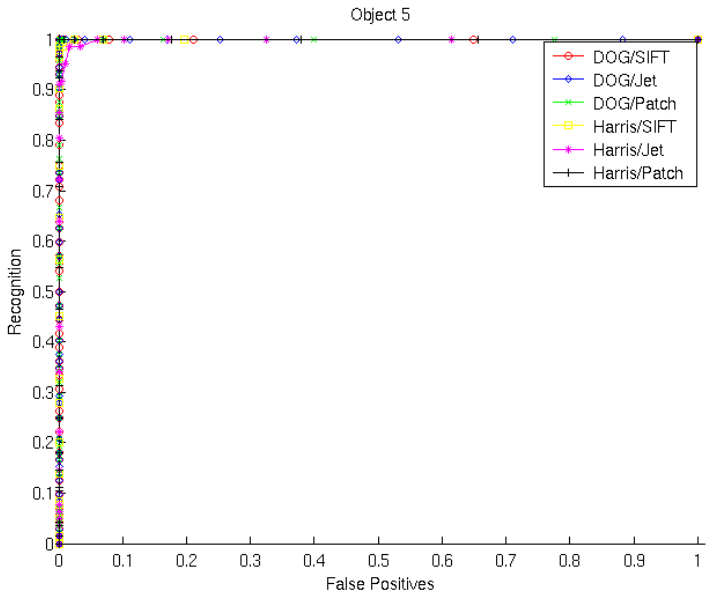

Figure 67: ROC for object 5 when the object has been turned 5 degrees.

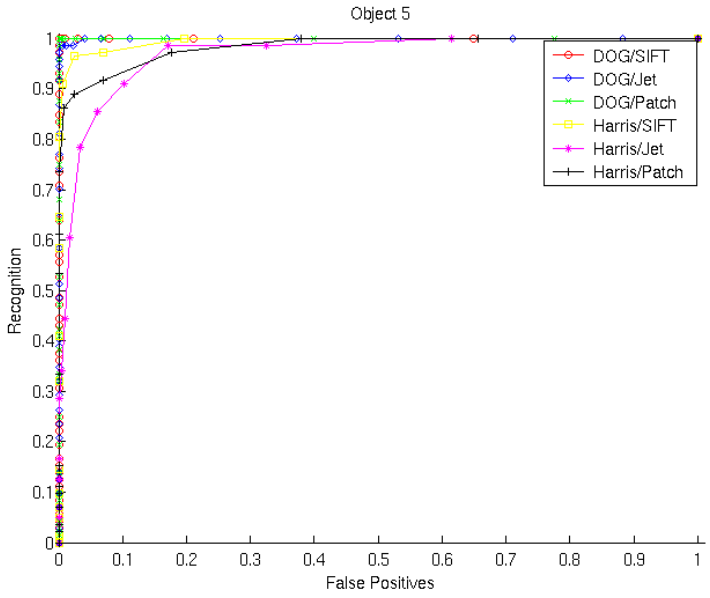

Figure 68: ROC for object 5 when the object has been turned 10 degrees.

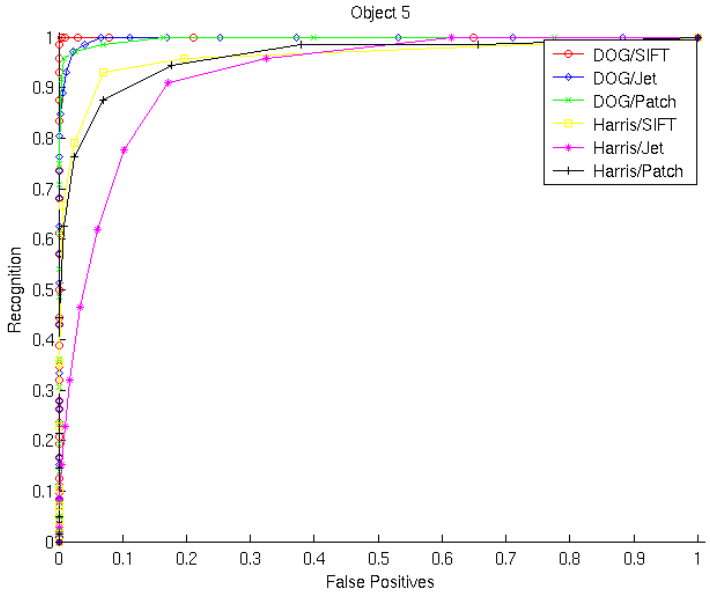

Figure 69: ROC for object 5 when the object has been turned 15 degrees.

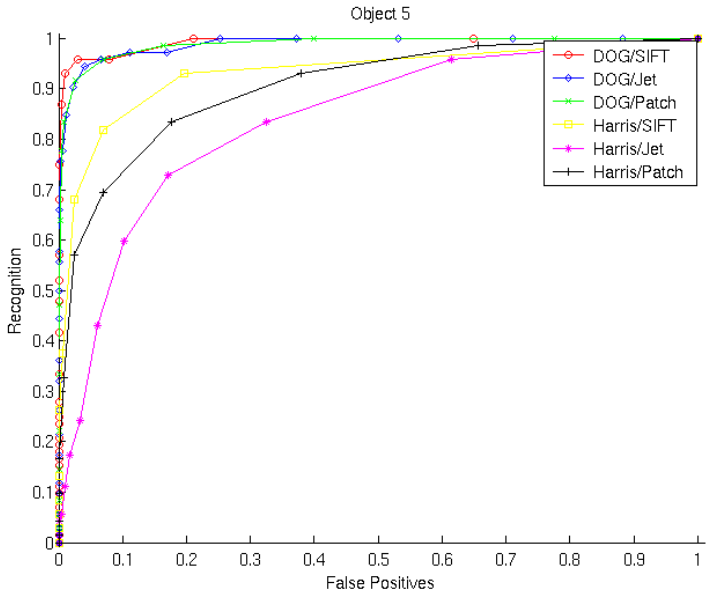

Figure 70: ROC for object 5 when the object has been turned 20 degrees.

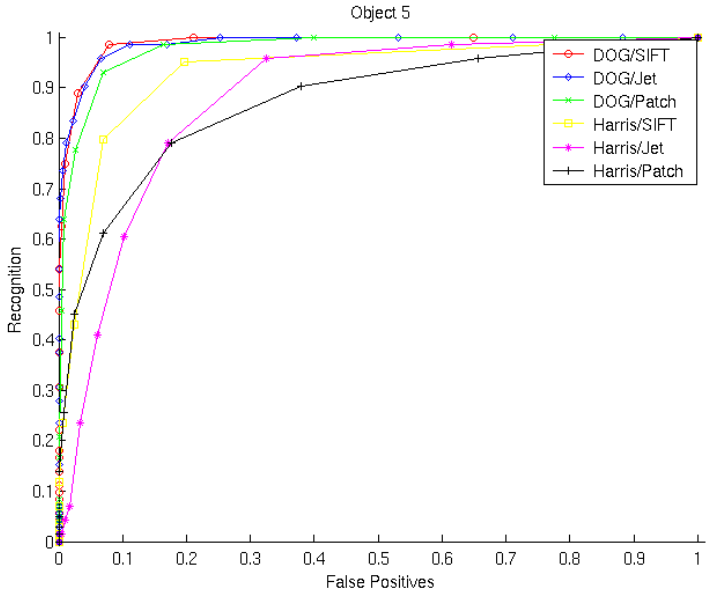

Figure 71: ROC for object 5 when the object has been turned 25 degrees.

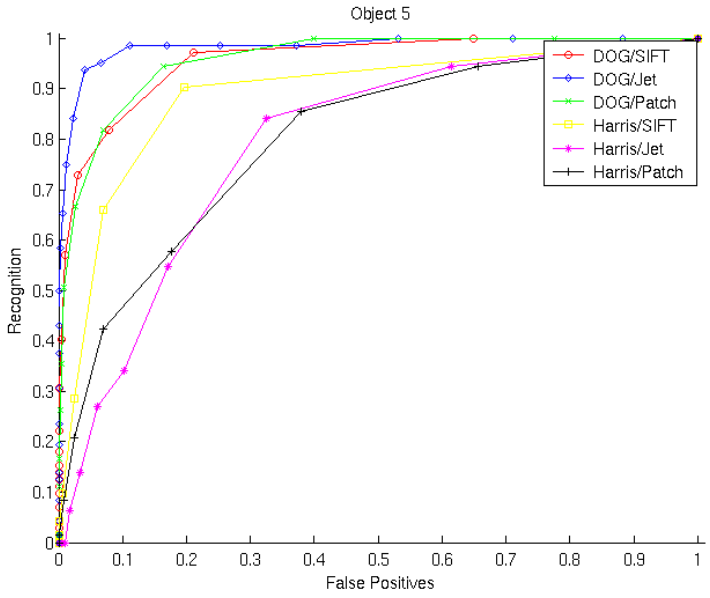

Figure 72: ROC for object 5 when the object has been turned 30 degrees.

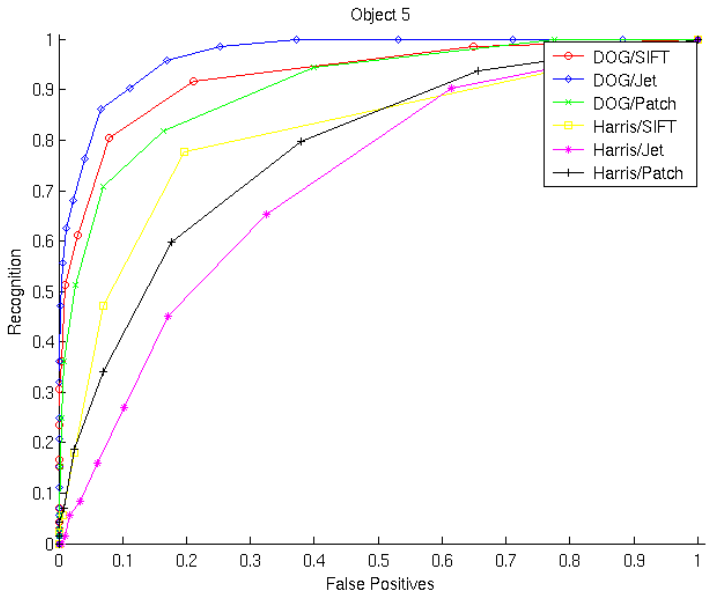

Figure 73: ROC for object 5 when the object has been turned 35 degrees.

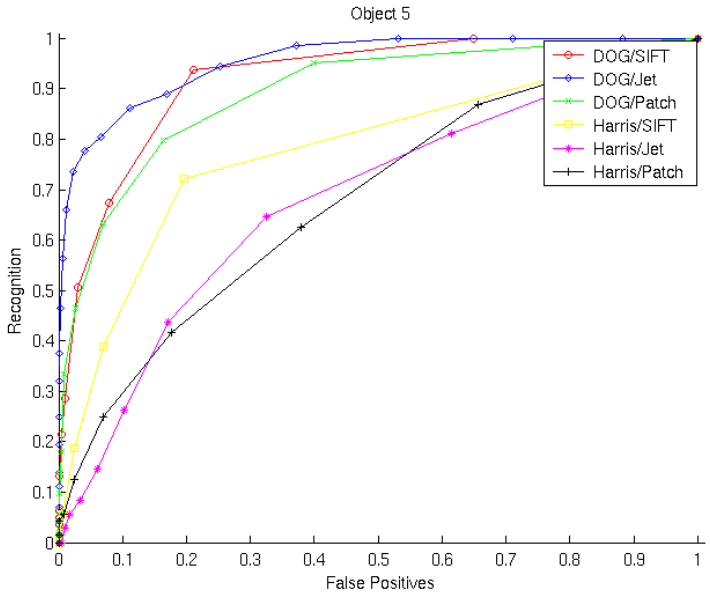

Figure 74: ROC for object 5 when the object has been turned 40 degrees.

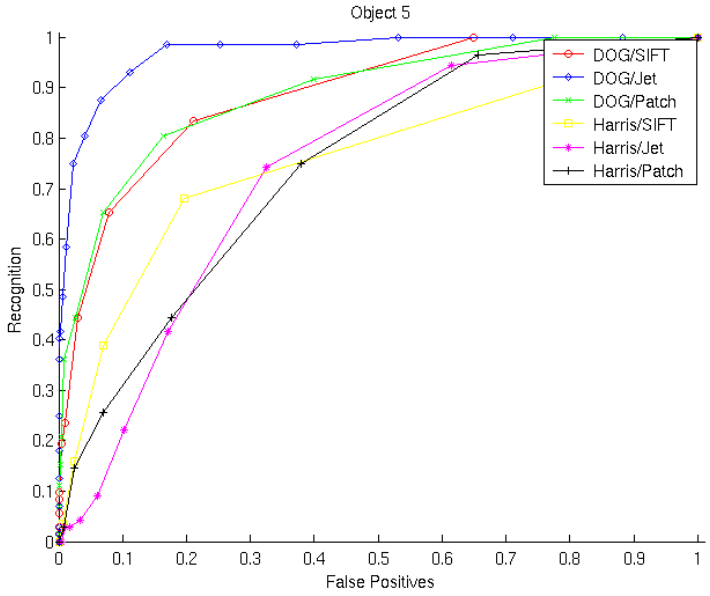

Figure 75: ROC for object 5 when the object has been turned 45 degrees.

A.3 Results for each individual object when matching with SSD

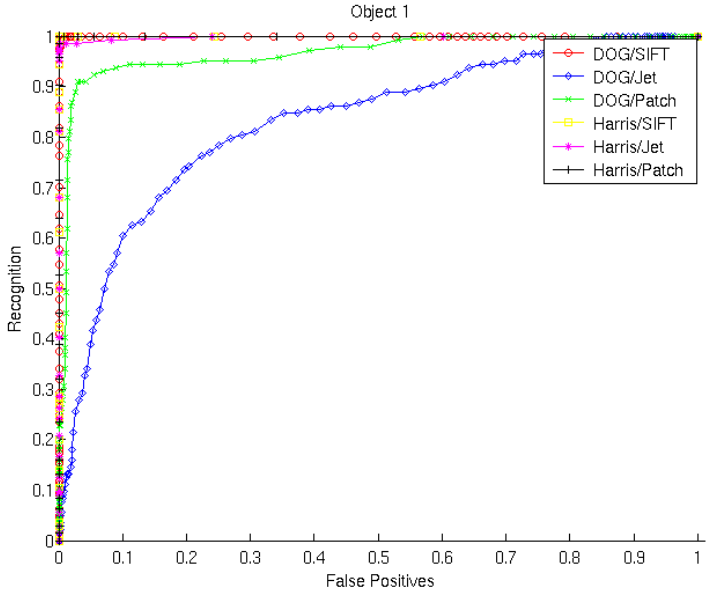

Figure 76: ROC for object 1 when the object has been turned 5 degrees.

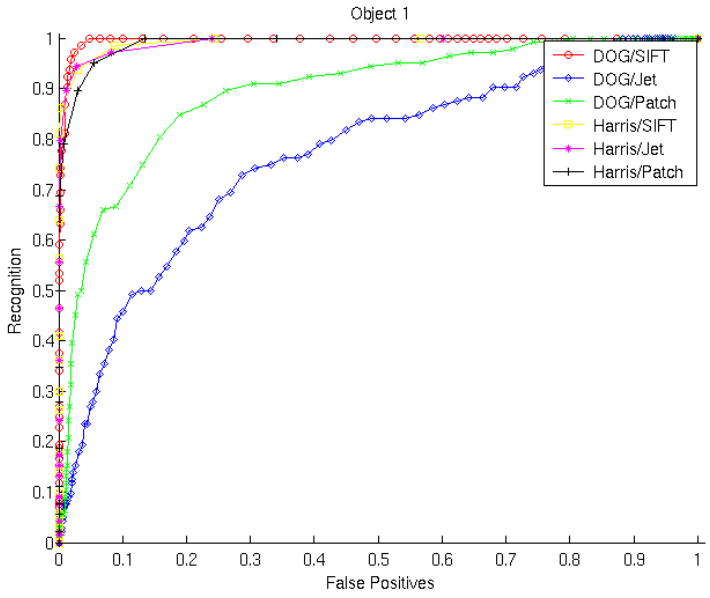

Figure 77: ROC for object 1 when the object has been turned 10 degrees.

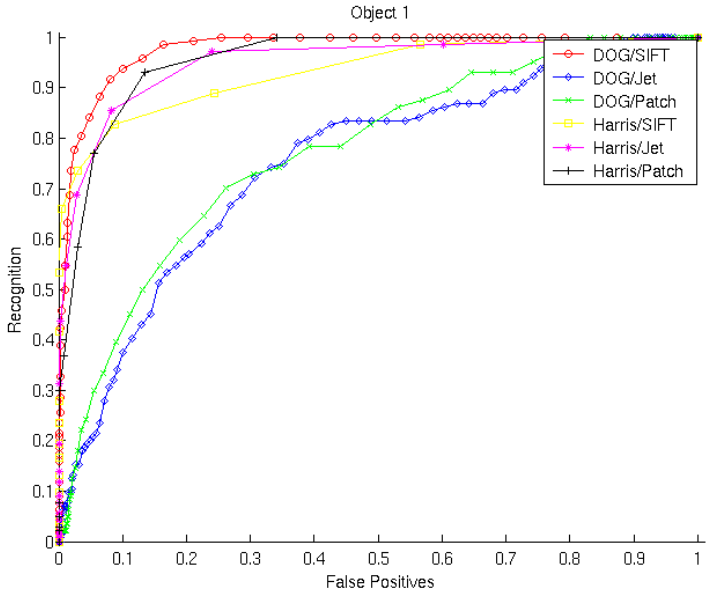

Figure 78: ROC for object 1 when the object has been turned 15 degrees.

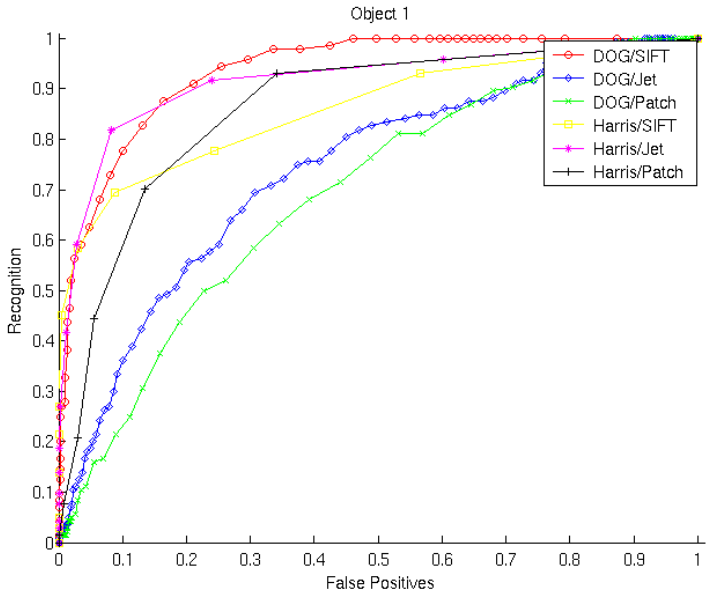

Figure 79: ROC for object 1 when the object has been turned 20 degrees.

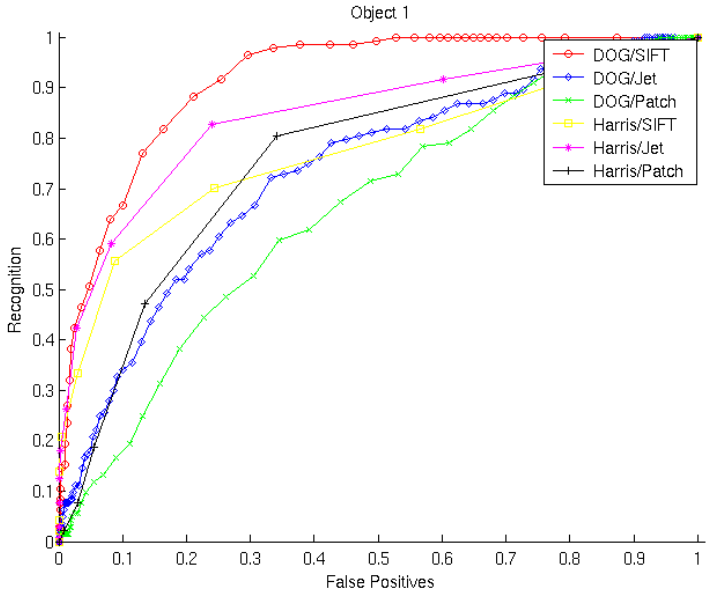

Figure 80: ROC for object 1 when the object has been turned 25 degrees.

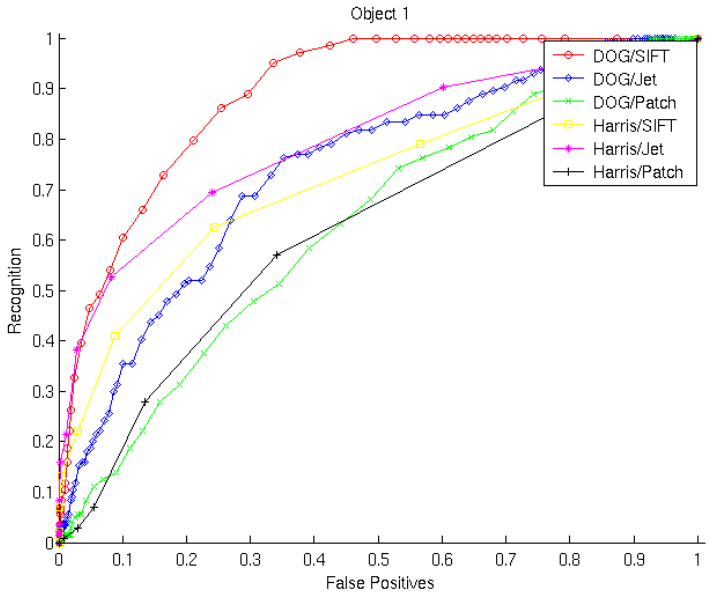

Figure 81: ROC for object 1 when the object has been turned 30 degrees.

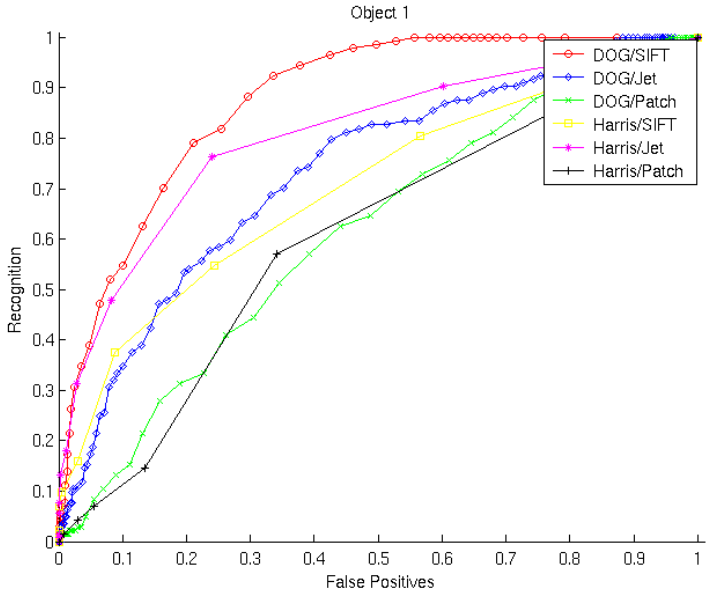

Figure 82: ROC for object 1 when the object has been turned 35 degrees.

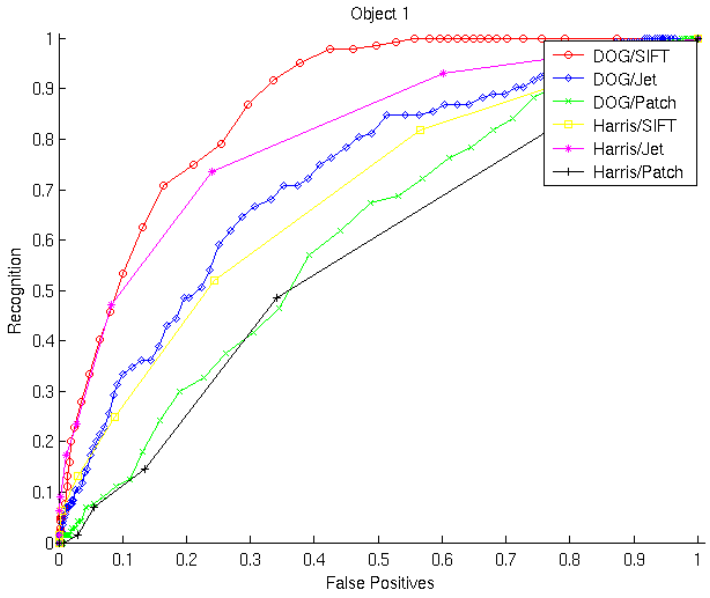

Figure 83: ROC for object 1 when the object has been turned 40 degrees.

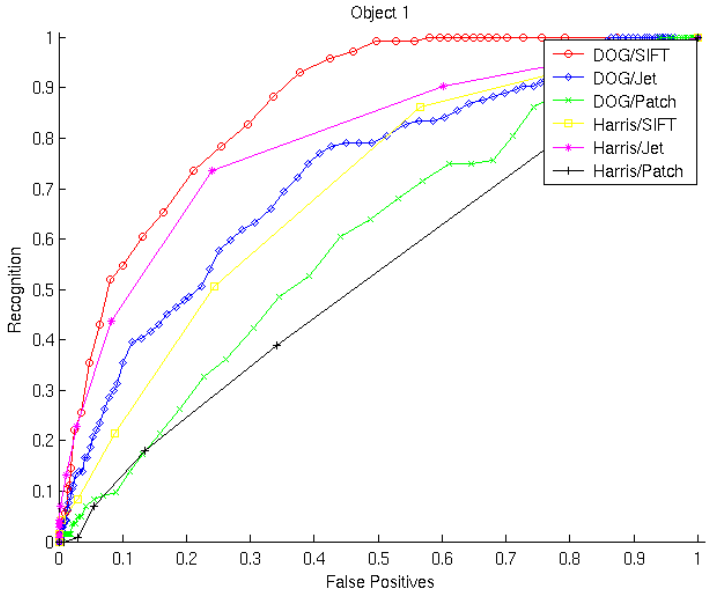

Figure 84: ROC for object 1 when the object has been turned 45 degrees.

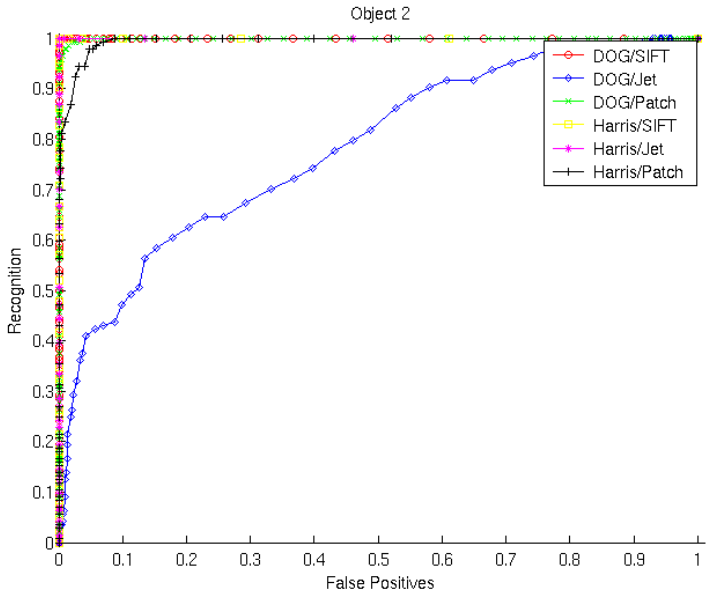

Figure 85: ROC for object 2 when the object has been turned 5 degrees.

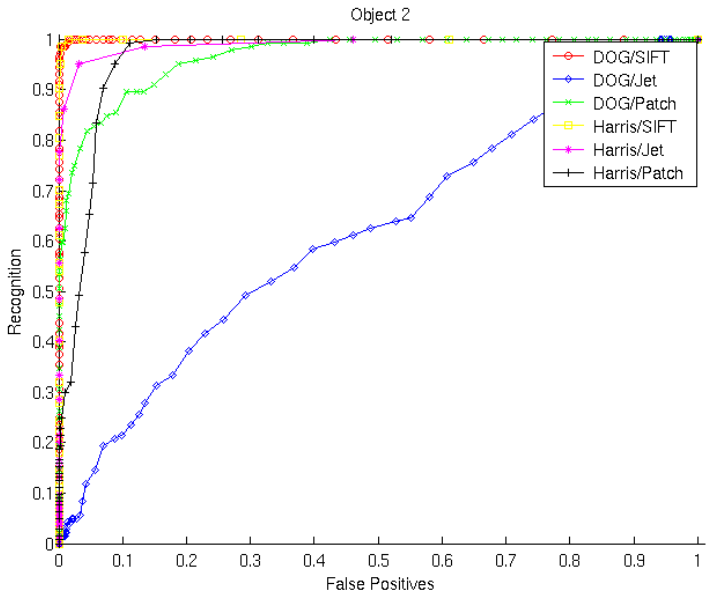

Figure 86: ROC for object 2 when the object has been turned 10 degrees.

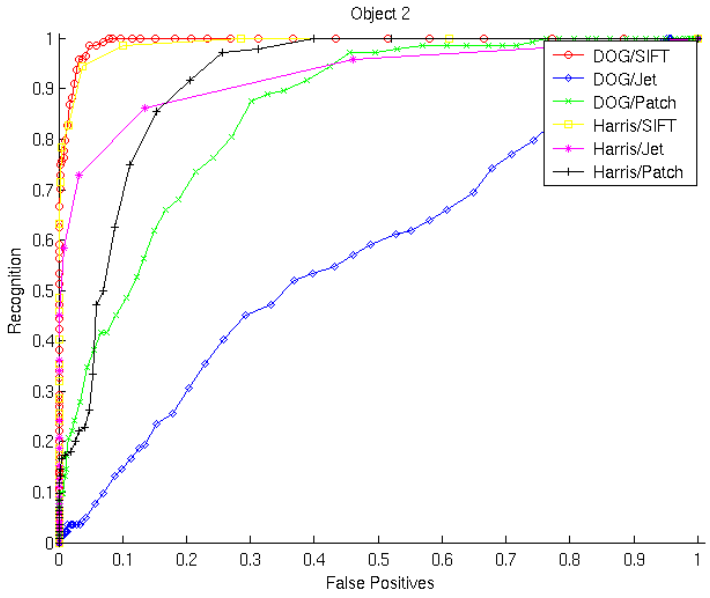

Figure 87: ROC for object 2 when the object has been turned 15 degrees.

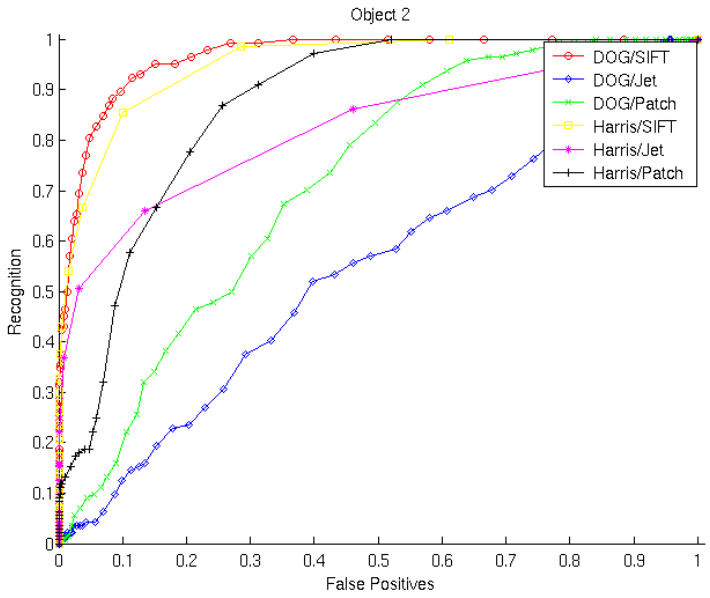

Figure 88: ROC for object 2 when the object has been turned 20 degrees.

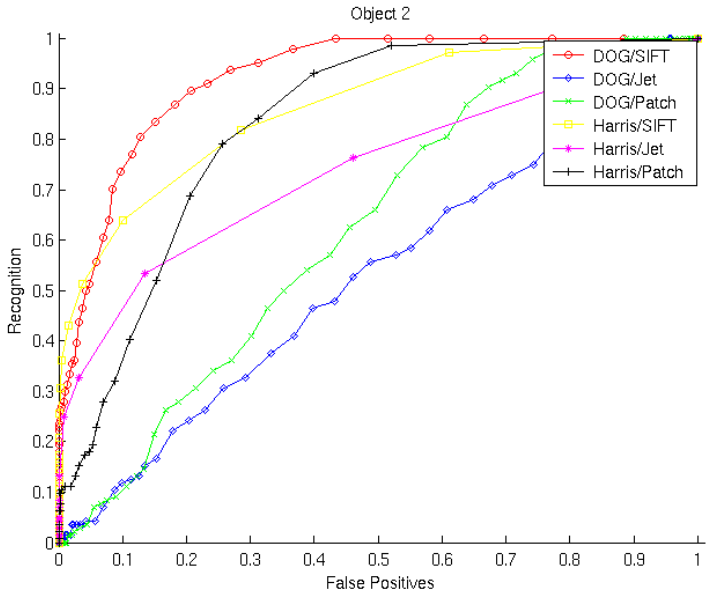

Figure 89: ROC for object 2 when the object has been turned 25 degrees.

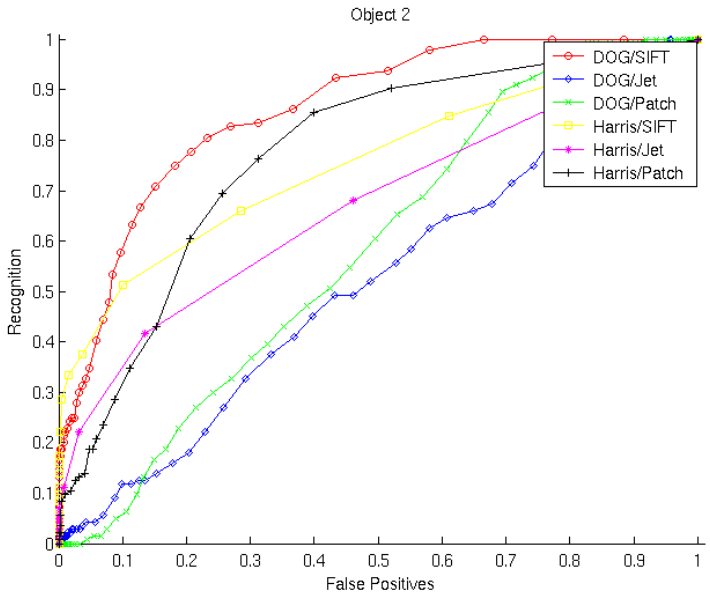

Figure 90: ROC for object 2 when the object has been turned 30 degrees.

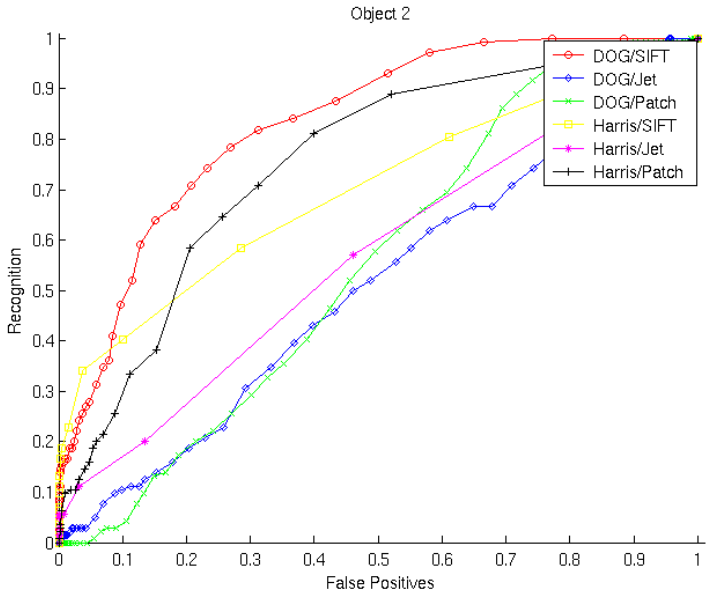

Figure 91: ROC for object 2 when the object has been turned 35 degrees.

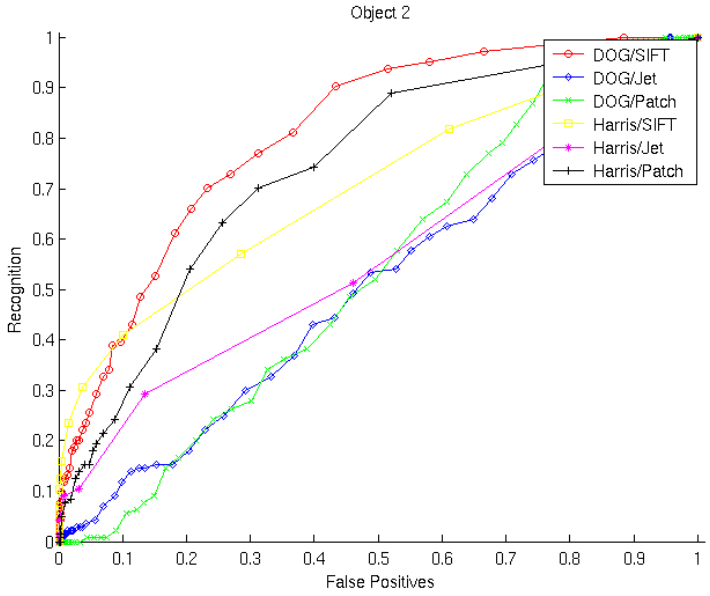

Figure 92: ROC for object 2 when the object has been turned 40 degrees.

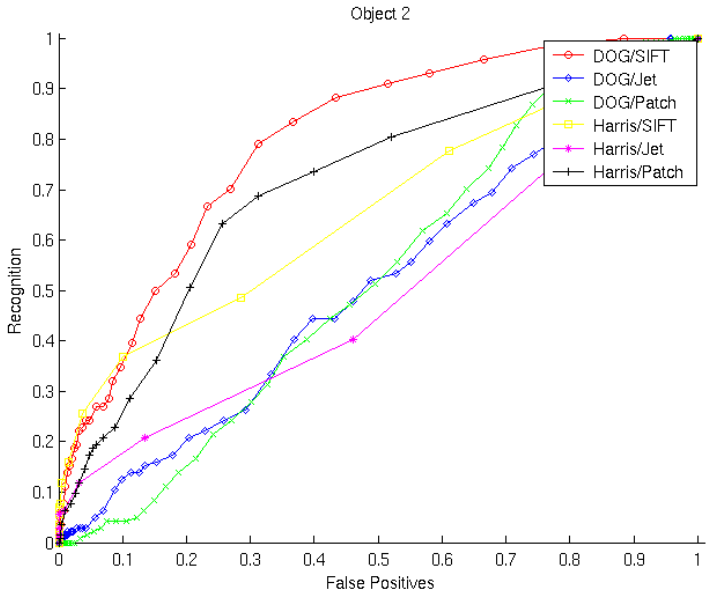

Figure 93: ROC for object 2 when the object has been turned 45 degrees.

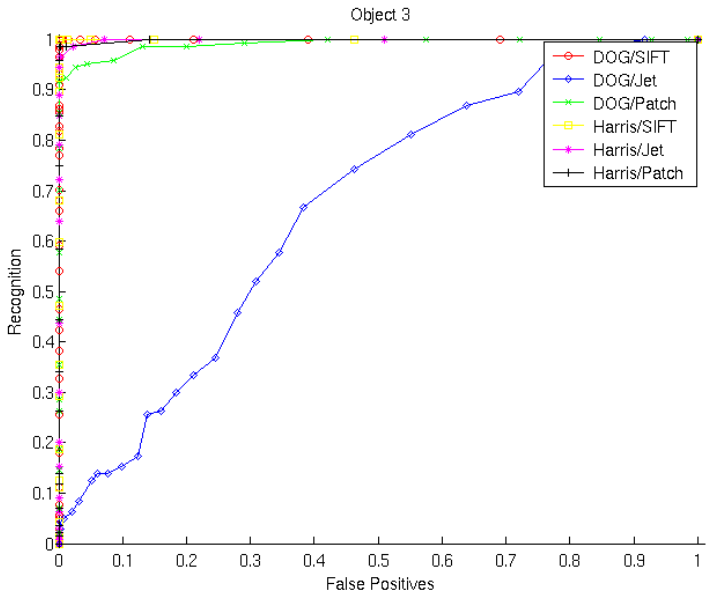

Figure 94: ROC for object 3 when the object has been turned 5 degrees.

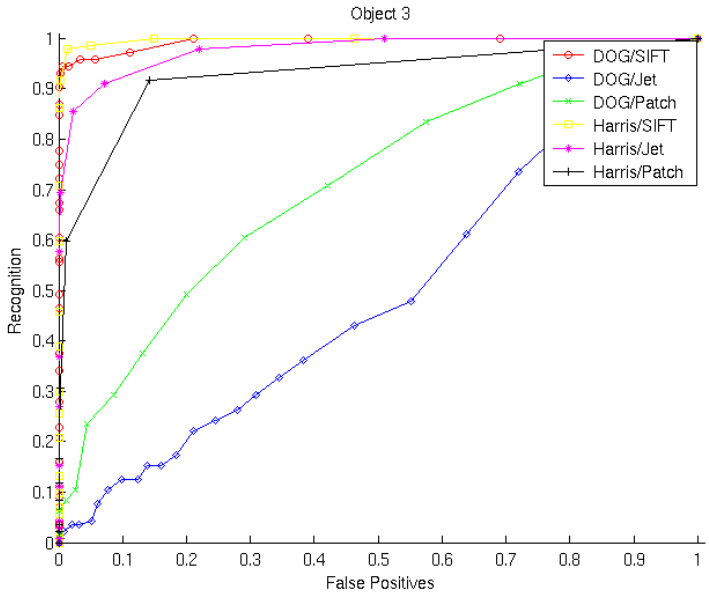

Figure 95: ROC for object 3 when the object has been turned 10 degrees.

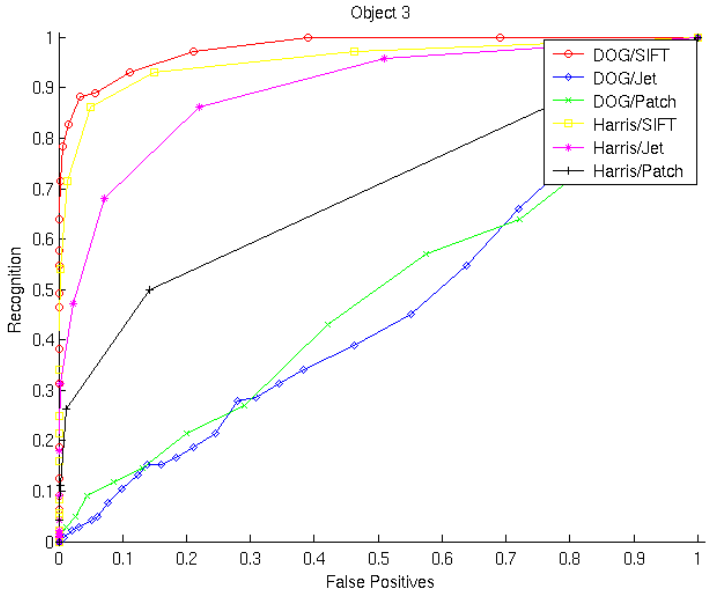

Figure 96: ROC for object 3 when the object has been turned 15 degrees.

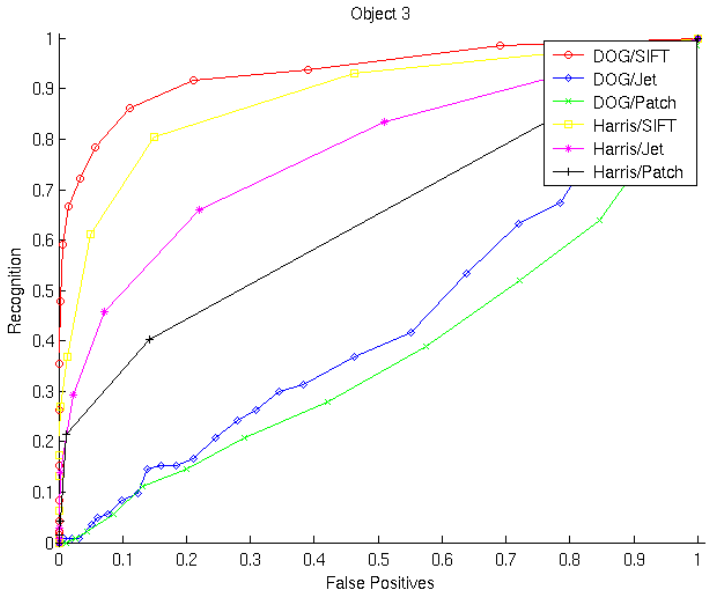

Figure 97: ROC for object 3 when the object has been turned 20 degrees.

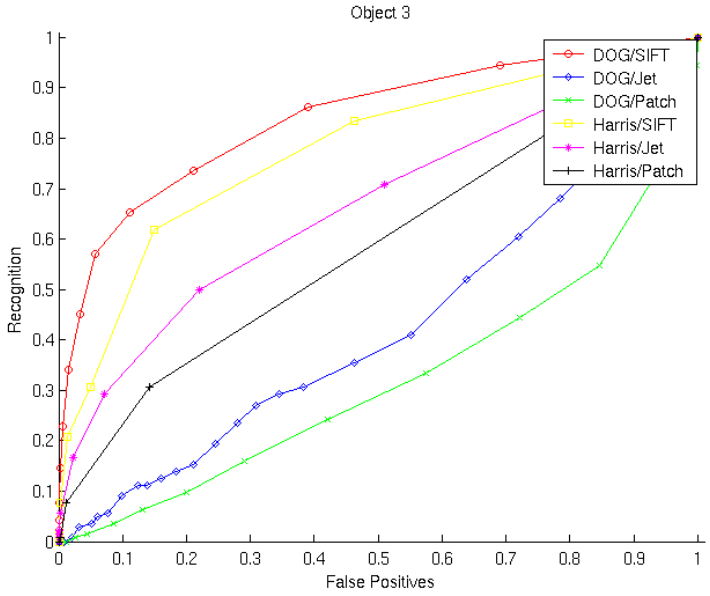

Figure 98: ROC for object 3 when the object has been turned 25 degrees.

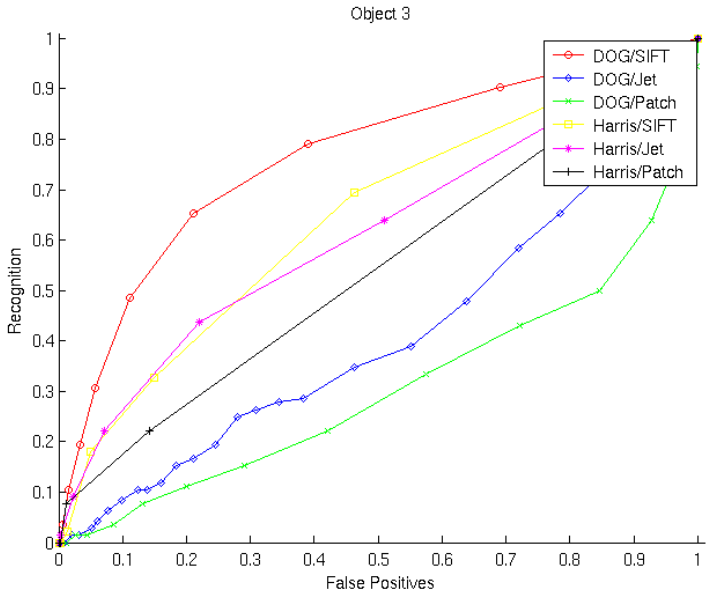

Figure 99: ROC for object 3 when the object has been turned 30 degrees.

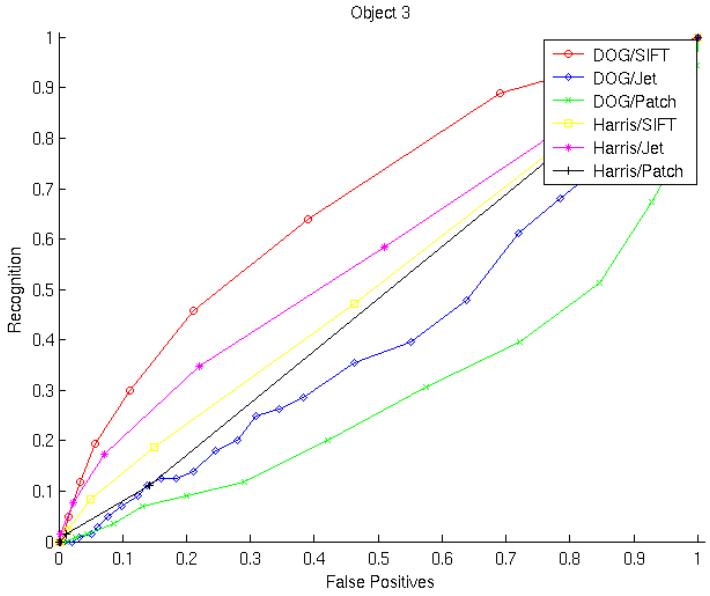

Figure 100: ROC for object 3 when the object has been turned 35 degrees.

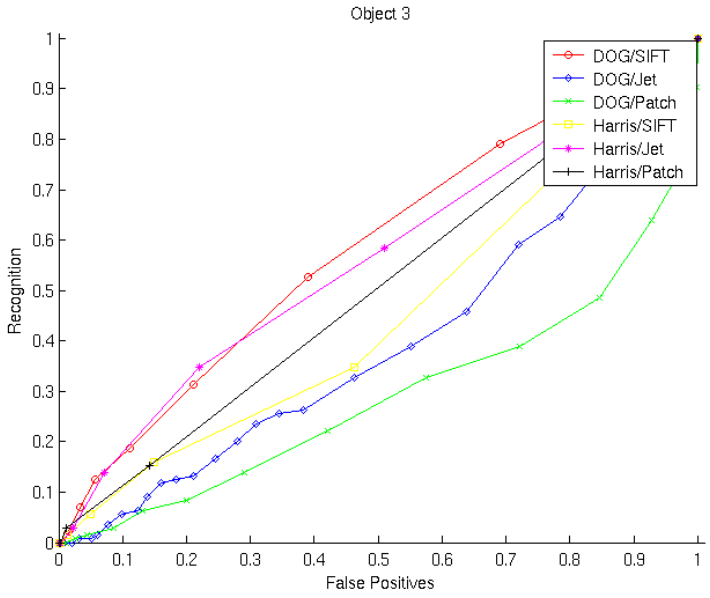

Figure 101: ROC for object 3 when the object has been turned 40 degrees.

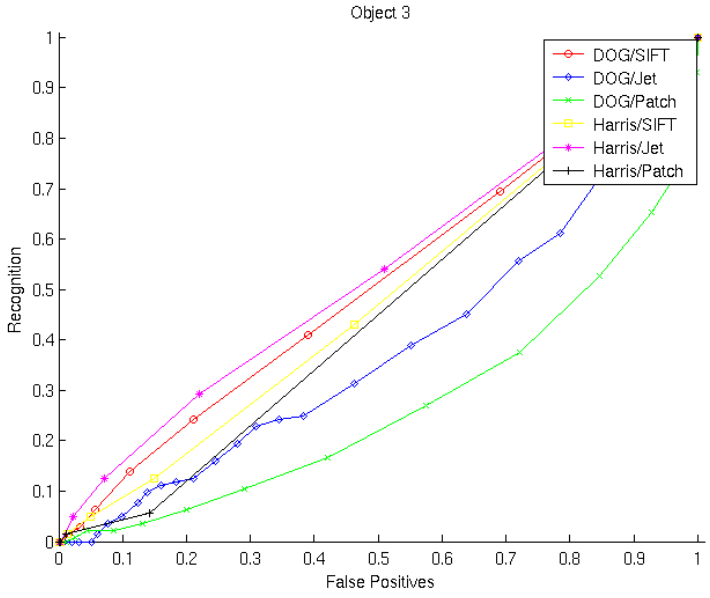

Figure 102: ROC for object 3 when the object has been turned 45 degrees.

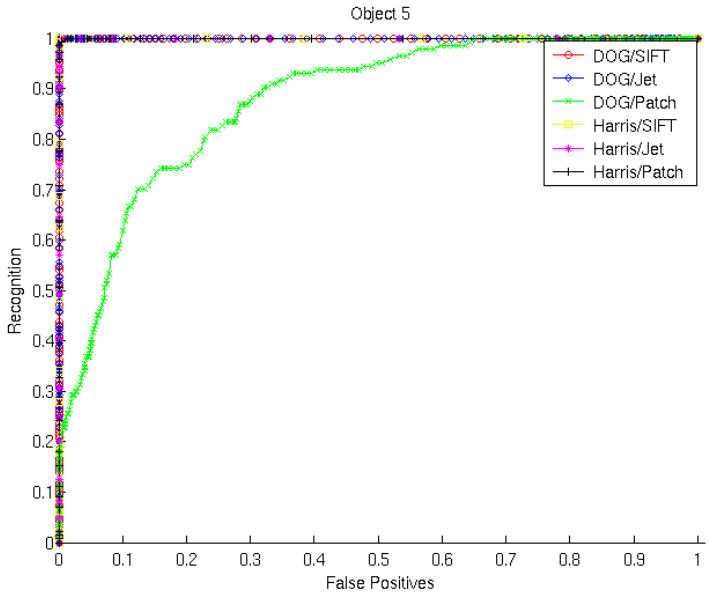

Figure 103: ROC for object 4 when the object has been turned 5 degrees.

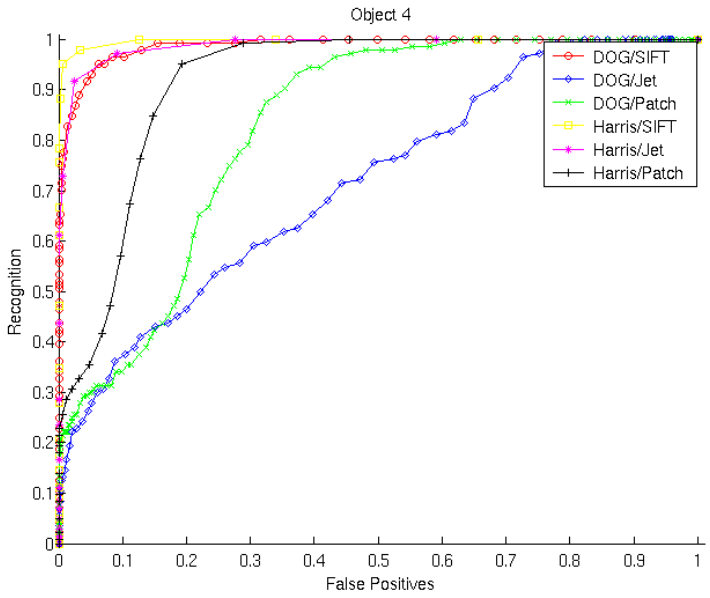

Figure 104: ROC for object 4 when the object has been turned 10 degrees.

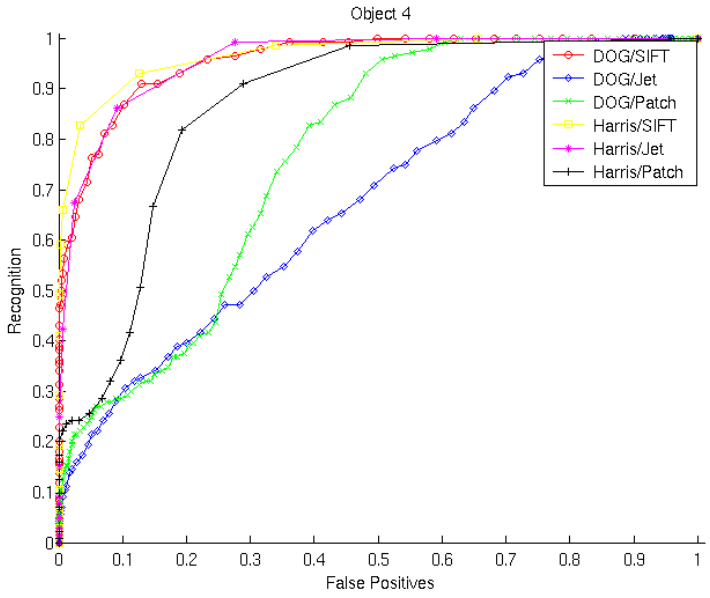

Figure 105: ROC for object 4 when the object has been turned 15 degrees.

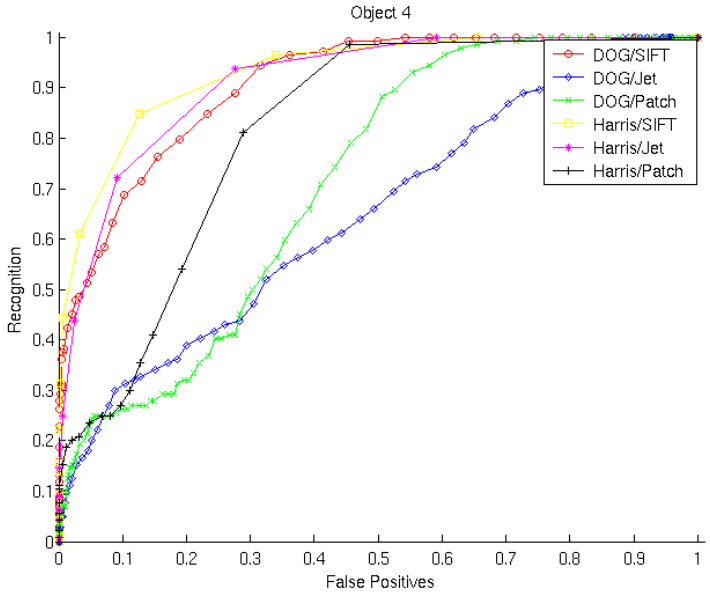

Figure 106: ROC for object 4 when the object has been turned 20 degrees.

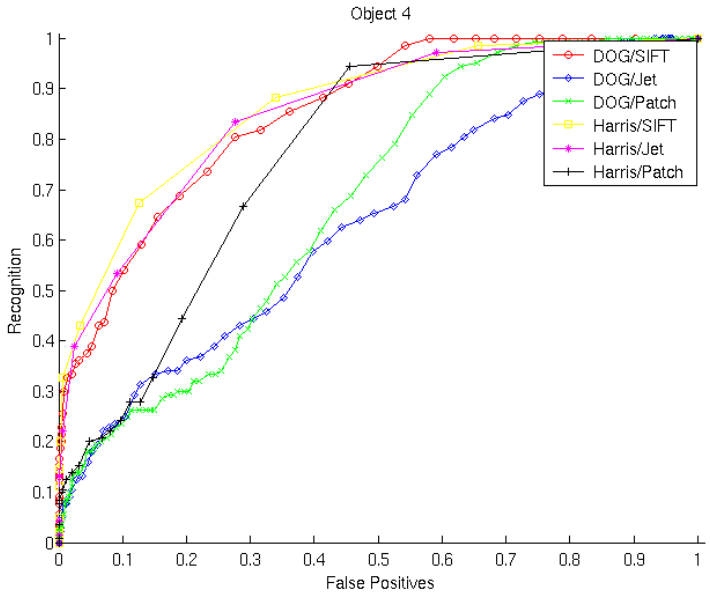

Figure 107: ROC for object 4 when the object has been turned 25 degrees.

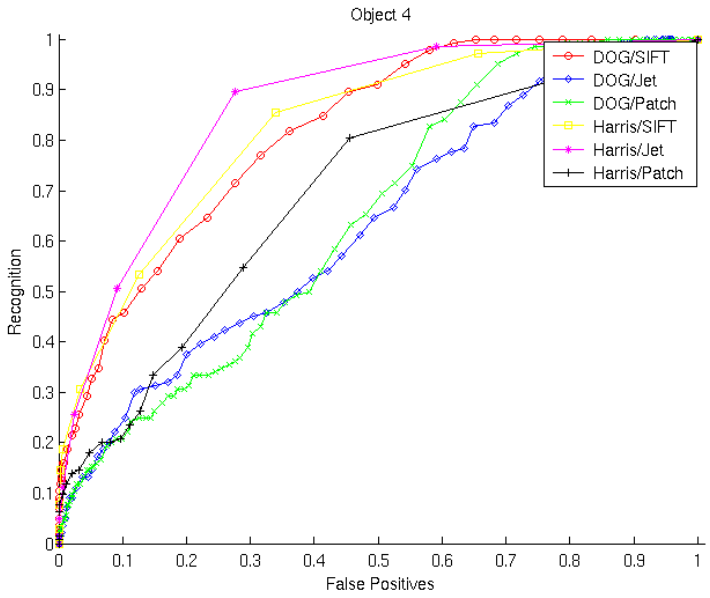

Figure 108: ROC for object 4 when the object has been turned 30 degrees.

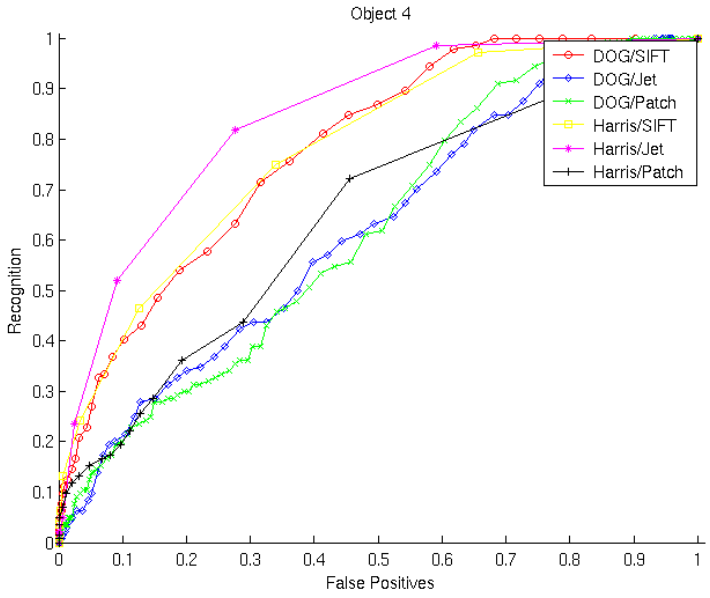

Figure 109: ROC for object 4 when the object has been turned 35 degrees.

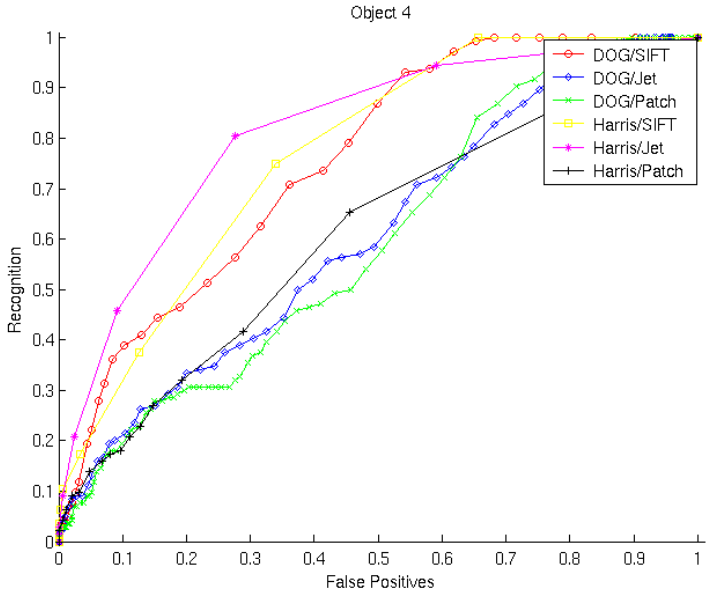

Figure 110: ROC for object 4 when the object has been turned 40 degrees.

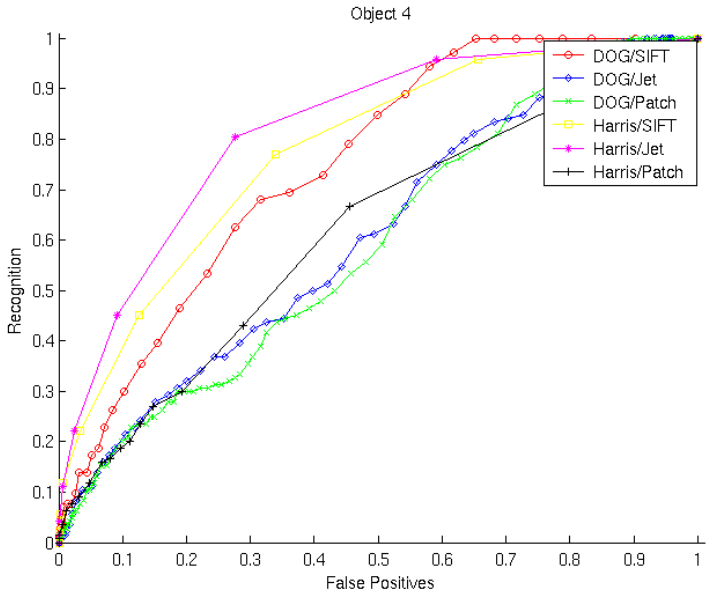

Figure 111: ROC for object 4 when the object has been turned 45 degrees.

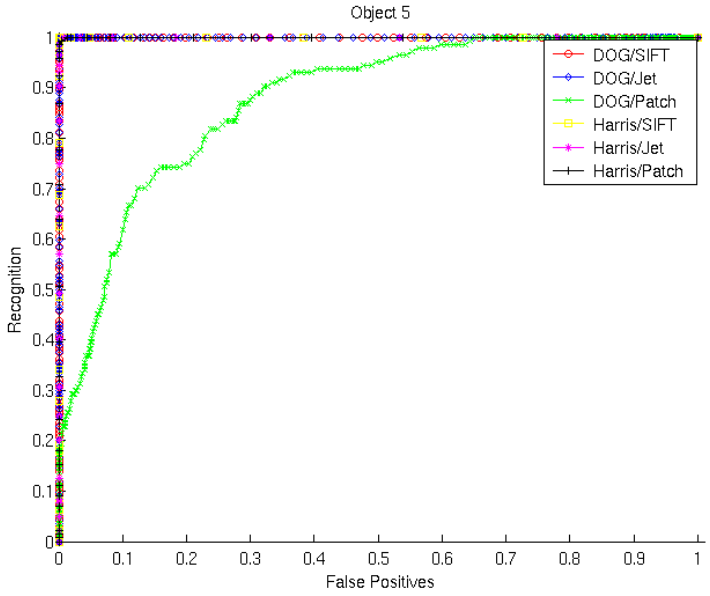

Figure 112: ROC for object 5 when the object has been turned 5 degrees.

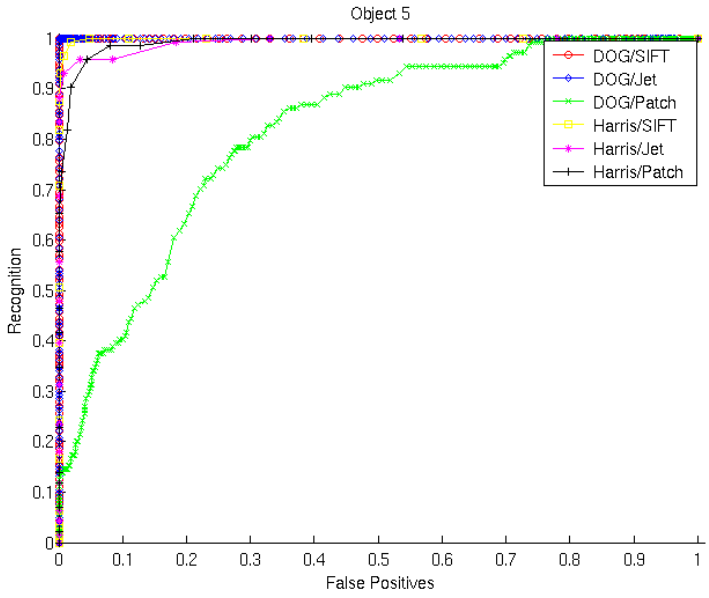

Figure 113: ROC for object 5 when the object has been turned 10 degrees.

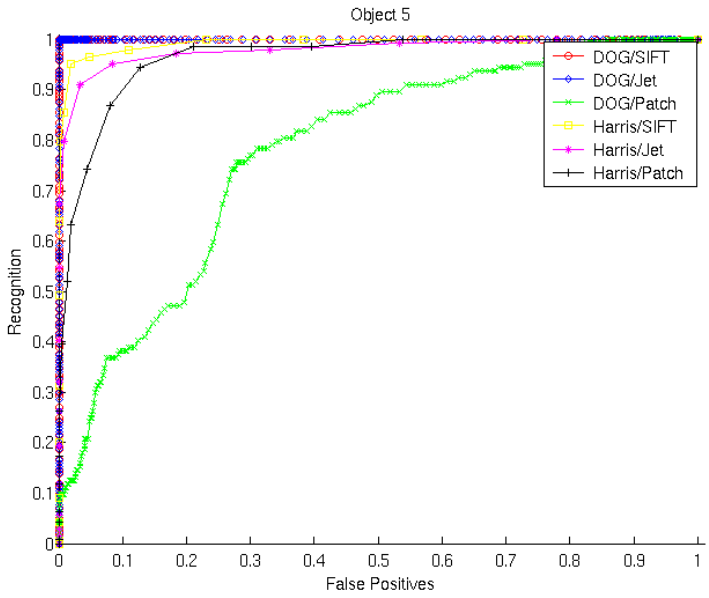

Figure 114: ROC for object 5 when the object has been turned 15 degrees.

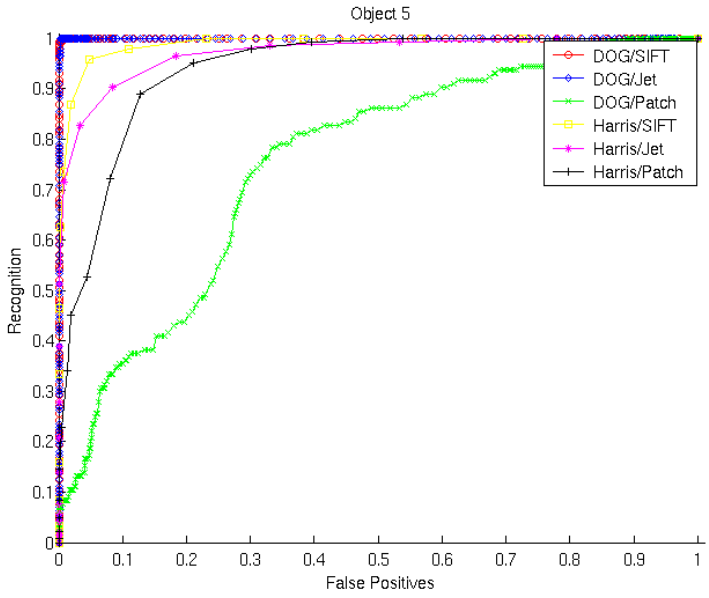

Figure 115: ROC for object 5 when the object has been turned 20 degrees.

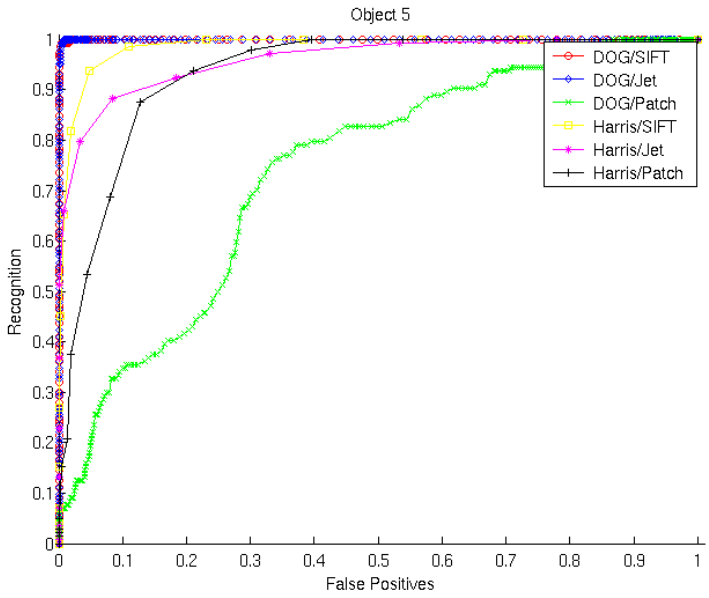

Figure 116: ROC for object 5 when the object has been turned 25 degrees.

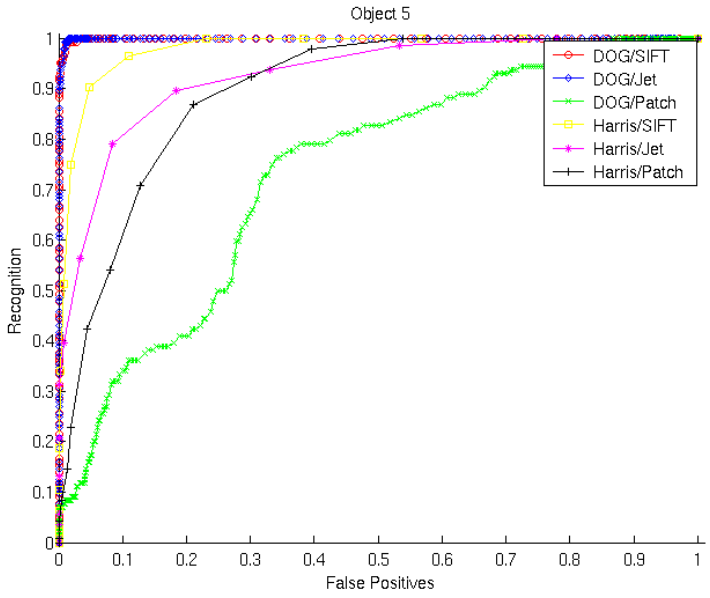

Figure 117: ROC for object 5 when the object has been turned 30 degrees.

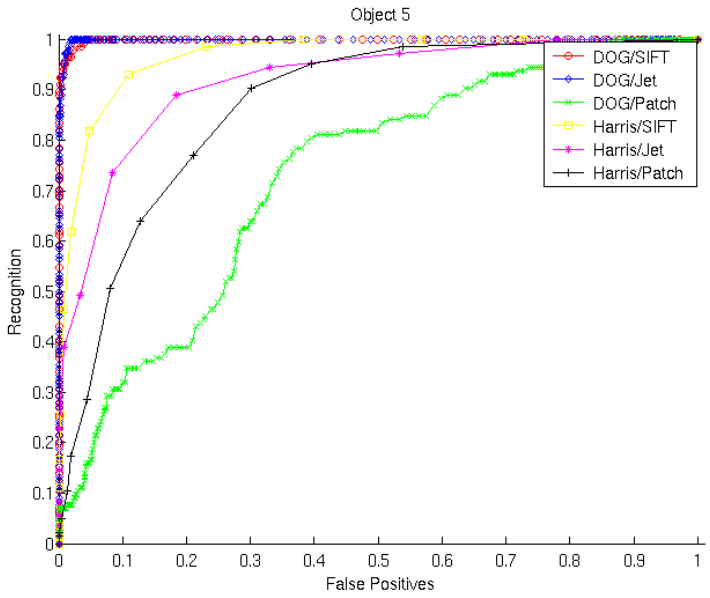

Figure 118: ROC for object 5 when the object has been turned 35 degrees.

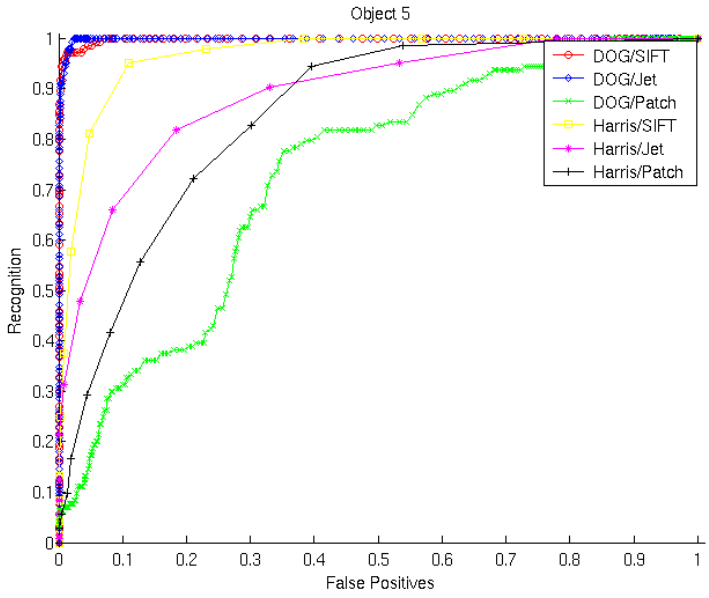

Figure 119: ROC for object 5 when the object has been turned 40 degrees.

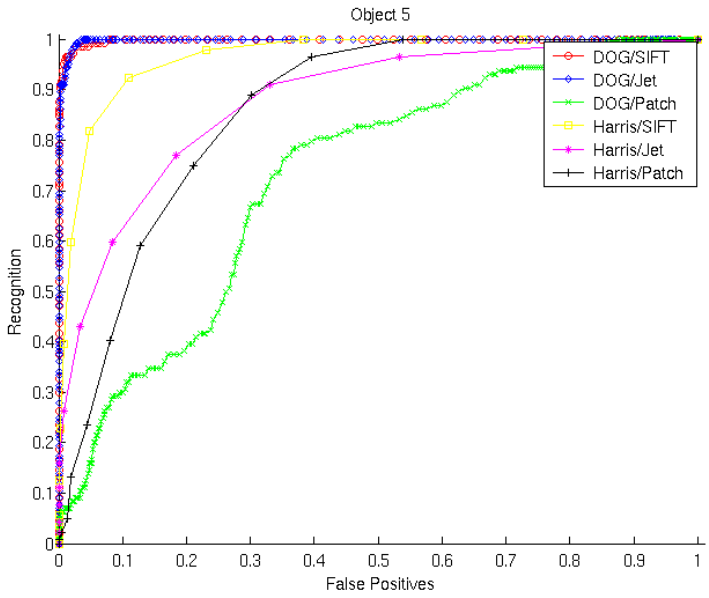

Figure 120: ROC for object 5 when the object has been turned 45 degrees.

A.4 Shape Context

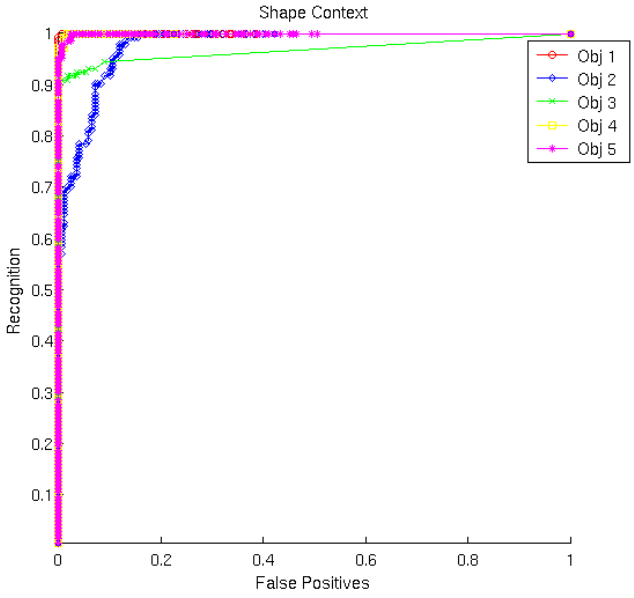

Figure 121: ROC for shape context when the objects have been turned 5 degrees.

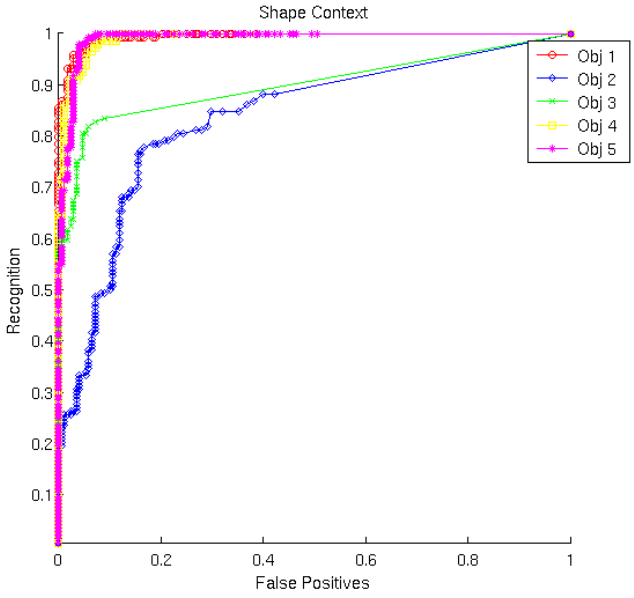

Figure 122: ROC for shape context when the objects have been turned 15 degrees.

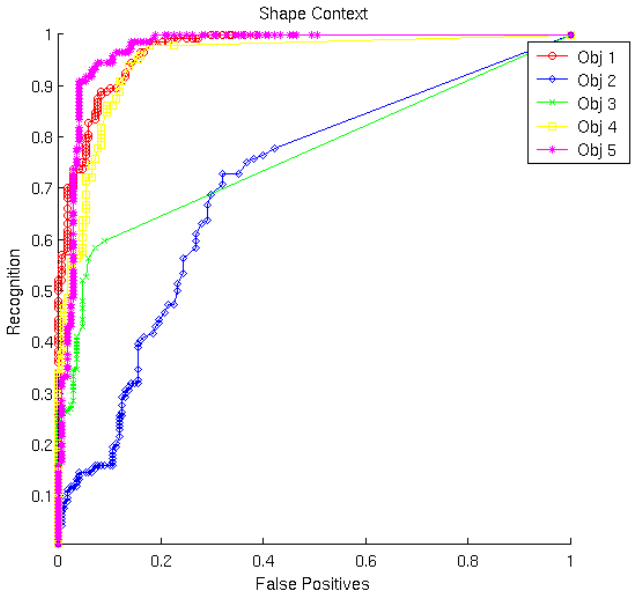

Figure 123: ROC for shape context when the objects have been turned 25 degrees.

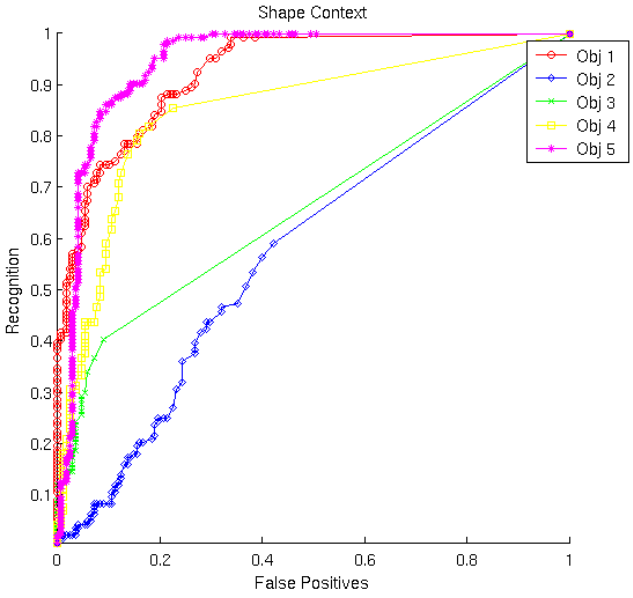

Figure 124: ROC for shape context when the objects have been turned 35 degrees.

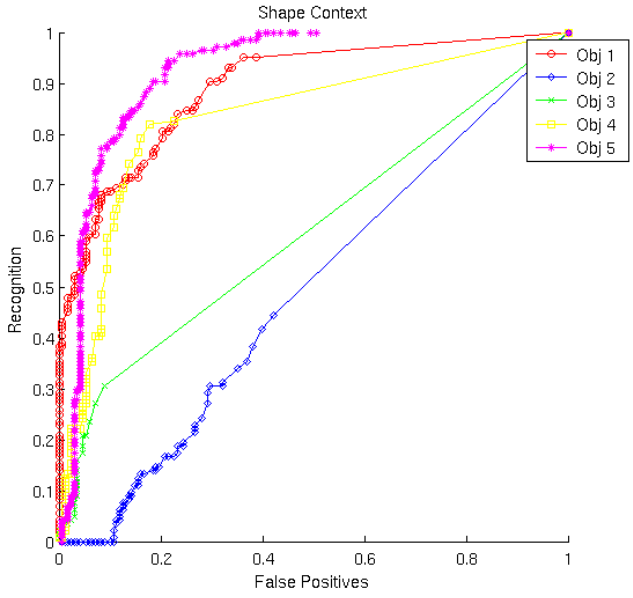

Figure 125: ROC for shape context when the objects have been turned 45 degrees.

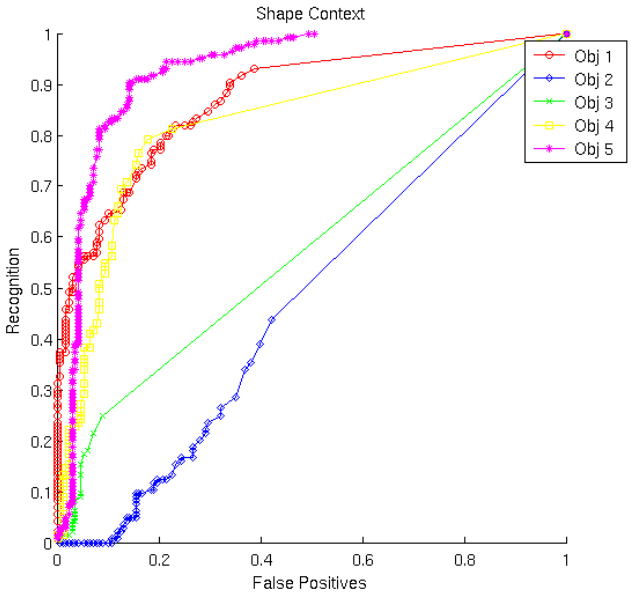

Figure 126: ROC for shape context when the objects have been turned 55 degrees.

A.5 Receptive Field Histogram

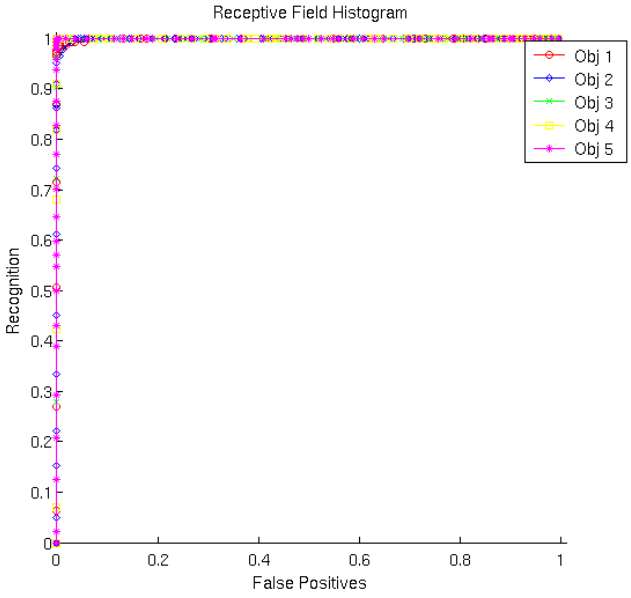

Figure 127: ROC for receptive field histograms when the objects have been turned 5 degrees.

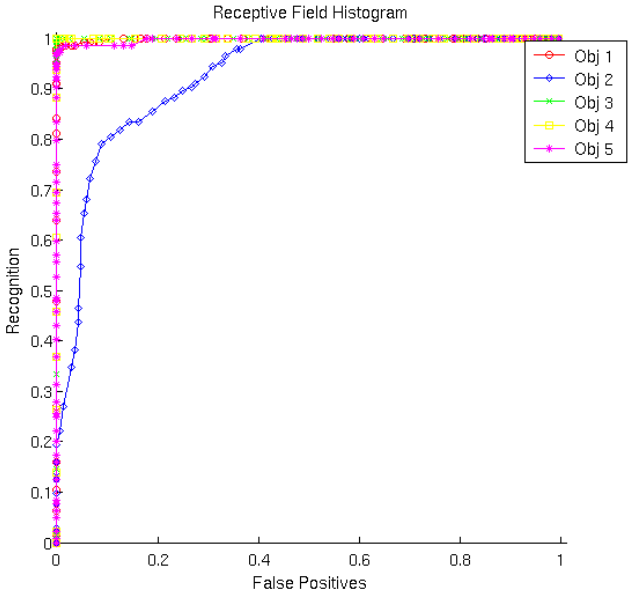

Figure 128: ROC for receptive field histograms when the objects have been turned 15 degrees.

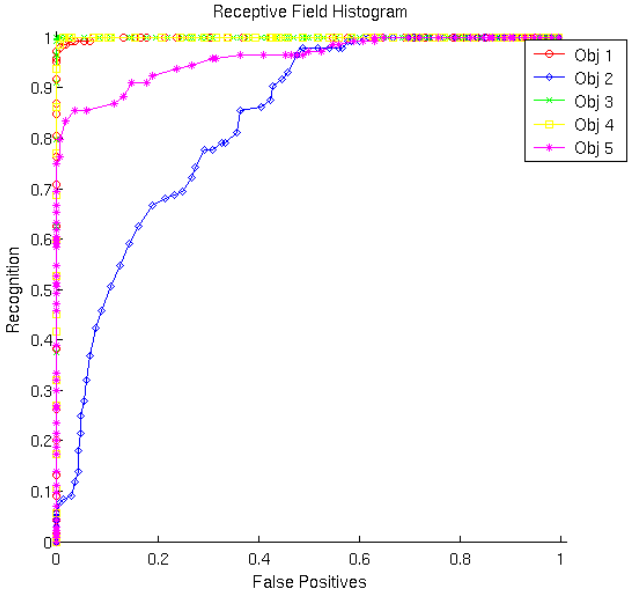

Figure 129: ROC for receptive field histograms when the objects have been turned 25 degrees.

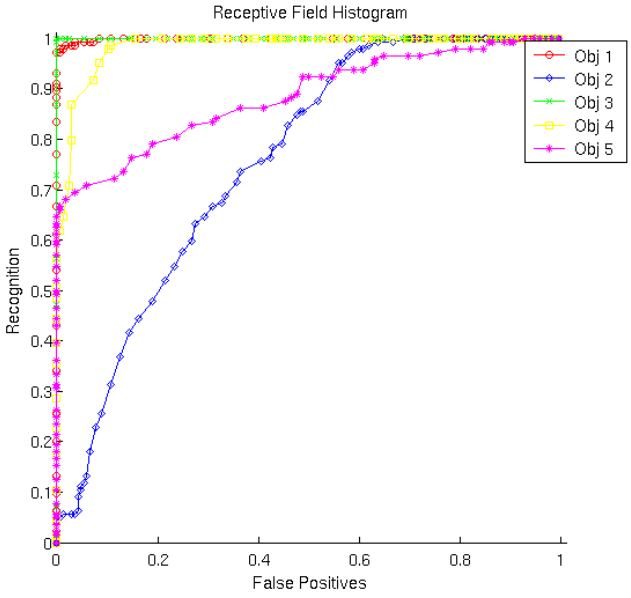

Figure 130: ROC for receptive field histograms when the objects have been turned 35 degrees.

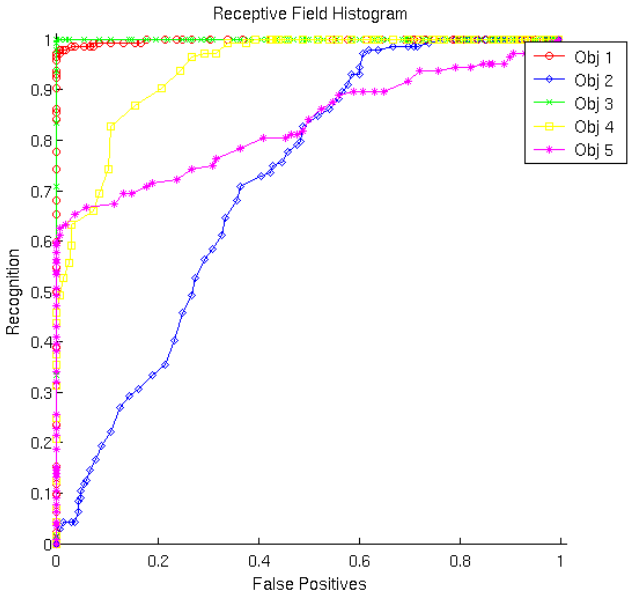

Figure 131: ROC for receptive field histograms when the objects have been turned 45 degrees.

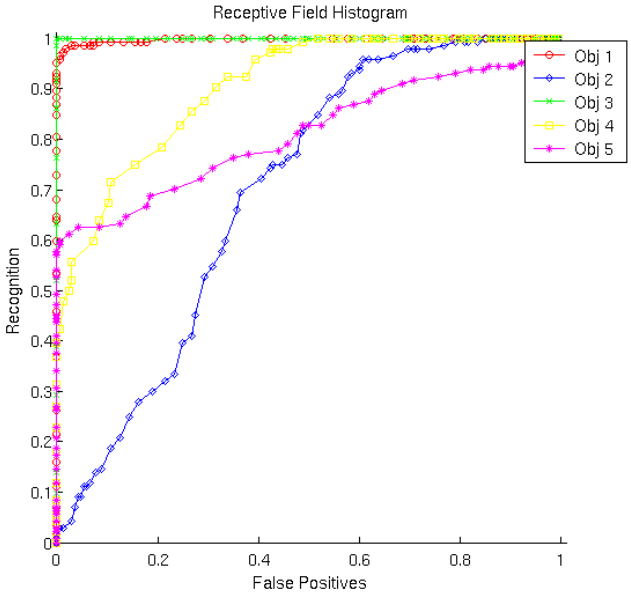

Figure 132: ROC for receptive field histograms when the objects have been turned 55 degrees.